FINAL REPORT

Next Generation Helimag UXO Mapping Technology

ESTCP Project MM-0741

OCTOBER 2009

Dr. Stephen Billings
Sky Research, Inc.

Mr. David Wright
Wright Research and Design

Environmental Security Technology Certification Program

REPORT DOCUMENTATION PAGE

Form Approved
OMB No. 0704-0188

PLEASE DO NOT RETURN YOUR FORM TO THE ABOVE ORGANIZATION.

1. REPORT DATE *(DD-MM-YYYY)*	2. REPORT TYPE	3. DATES COVERED *(From - To)*
10-23-2009	Demonstration Report, Final	1/2009-10/2009

4. TITLE AND SUBTITLE

Next Generation HeliMag UXO Mapping Technology Demonstration Report

5a. CONTRACT NUMBER

W912HQ-07-C-0041

5b. GRANT NUMBER

5c. PROGRAM ELEMENT NUMBER

6. AUTHOR(S)

Dr. Stephen Billings, Sky Research, Inc.
David Wright, Wright Research and Development

5d. PROJECT NUMBER

MM-0741

5e. TASK NUMBER

5f. WORK UNIT NUMBER

7. PERFORMING ORGANIZATION NAME(S) AND ADDRESS(ES)

Sky Research, Inc.
445 Dead Indian Memorial Rd.
Ashland, OR 97520

8. PERFORMING ORGANIZATION REPORT NUMBER

9. SPONSORING/MONITORING AGENCY NAME(S) AND ADDRESS(ES)

SERDP/ESTCP Program Office
901 North Stuart Street
Suite 303
Arlington, VA 22203

10. SPONSOR/MONITOR'S ACRONYM(S)

11. SPONSOR/MONITOR'S REPORT NUMBER(S)

12. DISTRIBUTION/AVAILABILITY STATEMENT

Unlimited

13. SUPPLEMENTARY NOTES

14. ABSTRACT

Technical innovations were made to an existing helicopter magnetometry platform to improve performance in WAA. Wireless telemetry was implemented to remove the sensor operator from the helicopter. Based on a survey design study , the number of magnetometers was increased from 7 to 13, decreasing the across line sensor spacing from 1.5 to 0.75 m and allowing full sampling of the magnetic field at heights 1.5 m or greater, enabling the accurate calculation of horizontal and vertical gradients. Enhanced noise suppression filtering algorithms were developed. Performance testing was performed at a site in New Mexico and demonstrated significant performance improvements, including higher SNR, greater detection probabilities and improved characterization capabilities. All 81 mm mortars seeded in one area were detected within a 1.0 m halo and classified as sm-med ordnance. Only 23% of seeded 60 mm mortars were detected due to a higher than anticipated flying height. In a geologically challenging environment, 106 of 109 seeds were detected within a 1.0 m halo and classified as high-probability UXO.

15. SUBJECT TERMS

UXO, HeliMag, airborne geophysics

16. SECURITY CLASSIFICATION OF:			17. LIMITATION OF ABSTRACT	18. NUMBER OF PAGES	19a. NAME OF RESPONSIBLE PERSON
a. REPORT	b. ABSTRACT	c. THIS PAGE		101	Dr. Stephen Billings
					19b. TELEPHONE NUMBER *(Include area code)* 541.552.5185

Reset

Standard Form 298 (Rev. 8/98)
Prescribed by ANSI Std. Z39.18

EXECUTIVE SUMMARY

A number of technical innovations were made to an existing helicopter magnetometry (HeliMag) platform to improve performance in wide-area-assessment applications. The HeliMag technology was originally developed by the Naval Research Laboratory, for deployment of 7 total-field magnetometers on a Kevlar reinforced boom mounted on a Bell 206L helicopter. The objectives of this demonstration were too:

- Improve data acquisition speeds through implementation of advanced data sampling and noise suppression methodologies;
- Enhance HeliMag detection by optimizing sensor configurations (to ensure that the magnetic field is fully and optimally sampled), and by improving noise suppression techniques (to maximize the signal to noise ratio [SNR] of targets of interest);
- Enhance HeliMag data interpretation using automated detection and characterization algorithms to improve productivity and produce objective, repeatable results; and
- Implement real-time data telemetry to remove the requirement to have a systems operator on board the aircraft, thereby increasing productivity, expanding applicability and reducing risk.

A design study was conducted to select the telemetry components and decide on the deployment configuration. We determined that any operational advantage achieved by real-time telemetry of the actual sensor data were not significant enough to warrant the complexity of a telemetry system that would allow that goal to be achieved. The ability to transmit information on the state of the system to the ground-crew was determined to be a more realistic and mission-critical requirement. For this task, an omni-directional HD Communication Corp antenna was selected for mounting on the helicopter. A MP-Tech puck sector antenna, which needs to be manually pointed towards the helicopter during operation, was selected as the ground station antenna. A Tranzeo TR-600 radio, which meets both 802.11b and 802.11g communication standards, was selected for the broadcast and receive tasks. To monitor the data quality and allow remote interaction with the computer on the helicopter we used virtual network computing (VNC) viewer software.

A sensor optimization study was conducted to determine if additional sensors were needed, and if so where they should be placed for optimal detection and characterization performance. It was found that the optimal configuration was to decrease the sensor spacing from 1.5 m to 0.75 m, thus increasing the number of sensors from 7 to 13. Full-sampling of the magnetic field occurs whenever the sensors are greater than 1.5 m above the ground. Potential field theory can then be used to calculate the magnetic field at any higher elevation, so that vertical gradients can be calculated rather than measured as in competing systems.

We mounted the modified sensor boom on a Hughes MD530F helicopter. The dominant noise source in the system was found to originate from the rotor hub and resulted in a largely sinusoidal signal with a frequency of about 7.8 Hz. When flying low and fast, the frequency band of the rotor noise overlaps with that of the signals of interest and the noise can't simply be eliminated by a notch filter. A new technique for rotor noise suppression was developed as part of this project. It uses data collected during a high-altitude aeromagnetic compensation flight to

provide a model of the amplitude of the rotor-noise as a function of helicopter attitude. The phase of the rotor-noise varies as a function of helicopter attitude and is calculated along short segments. The algorithm can successfully suppress the rotor noise without distorting the spatial signature of the underlying anomalies of interest.

A demonstration study was conducted over 586 acres at the Former Kirtland Precision Bombing Range (KPBR) in New Mexico. The area covered overlapped a previous survey with the original system along with a number of ground-based surveys. Two areas were blind seeded with a number of ordnance with calibers ranging from 60 to 155 millimeters (mm).

Three different locations were used as base-stations for the telemetry. During the demonstration the telemetry system worked extremely well, with connectivity maintained for between 70 to 100% of the time during each survey event. On average, connectivity was maintained for greater than 95% of the time. With this type of performance, removing the sensor operator from the helicopter is a viable option, with associated reduction in the risk and cost of the technology.

Detection performance was evaluated on two seeded sites. The first in the Central North Area comprised forty 60 mm mortars and forty 81 mm mortars. With a halo of 1 meter (m), 23% of the 60 mm mortars and 100% of the 81 mm mortars were detected. The poor detection performance on the 60 mm mortars occurred because the sensor ground clearance was too high (~1.8 m) compared to our intended ground-clearance (1.0 m). Previous operational experience with the precursor system had revealed considerable variability in the flying heights achieved by different pilots, and for this survey we were unlucky to have selected a pilot who was not comfortable flying (very) low to the ground. In addition, it's more difficult to get the MD530 helicopter close to the ground than the Bell-206. For future surveys we will mount the modified sensor boom on the Bell-206.

In the Western seed area the Program Office emplaced 110 seeds in a geologically "challenging" environment. These comprised a mix of 81 mm and 4.2" mortars, 105 mm HEAT-rounds, and 105 mm and 155 mm projectiles. With a detection halo of 1.0 m, all items except 3 of 12 81 mm mortars were detected. Each detected anomaly was fit with a dipole model and an apparent remanence metric was calculated and used to rank the anomalies by unexploded ordnance (UXO) likelihood. When using this ranking scheme 99% of the detected seed items occurred in the top 50% of the target declarations.

Signal to noise ratio was improved by a factor of about 18% compared to the previous generation system. The improvement occurred because of increased signal from the denser sampling of the magnetic field and reduced distortion in the signal and superior noise rejection from the new rotor-suppression algorithm.

TABLE of CONTENTS

LIST OF FIGURES

LIST OF TABLES

ACRONYMS

3D	Three-Dimensional
agl	Above Ground Level
Am^2	Ampere-meters squared
AMTADS	Airborne Multisensor Towed Array Detection System
ASR	Archive Search Report
CERCLA	Comprehensive Environmental, Response, Compensation, and Liability Act
cm	centimeter
CRADA	Cooperative Research and Development Agreement
Cs	Cesium
CSM	Conceptual Site Model
DAS	Data Acquisition System
dB	Decibel
DC	Direct Current
DEM	Digital Elevation Model
DGM	Digital Geophysical Mapping
DoD	Department of Defense
EE/CA	Engineering Evaluation and Cost Analysis
ESTCP	Environmental Security Technology Certification Program
FLBGR	Former Lowry Bombing and Gunnery Range
FUDS	Formerly Used Defense Sites
GPO	Geophysical Proveout
GPS	Global Positioning System
HE	High Explosive
HEAT	High Explosive Anti-tank
HeliMag	Helicopter Magnetometry
HR	HEAT-round
Hz	Hertz
IDA	Institute for Defense Analyses
IMU	Inertial Measurement Unit

km	kilometer(s)
KPBR	Kirtland Precision Bombing Range
lb	pound
LiDAR	Light Detection and Ranging
m	meter
MD	McDonald Douglas
µs	micro Second
mm	millimeter
MMRP	Military Munitions Response Program
MTADS	Multi-sensor Towed Array Detection System
m/s	meters per second
mW	milliWatt
NDIA	New Demolitions Impact Area
NOTAM	Notice To Airmen
NRL	Naval Research Laboratory
nT	nanotesla
OB/OD	Open Burn/Open Detonation
Pd	Probability of Detection
Pfa	Probability of False Alarm
PI	Principal Investigator
PRTG	Paessler Router Traffic Grapher
QC	Quality Control
ROC	Receiver Operating Characteristic
rpm	revolutions per minute
RSSI	Received Signal Strength
RTK GPS	Real-time Kinematic Global Positioning System
SKY	Sky Research, Inc.
SNR	Signal to Noise Ratio
SO	Sensor Operator
SORT	Simulated Oil Refinery Target
TMF	Total Magnetic Field
USACE	US Army Corps of Engineers
USEPA	US Environmental Protection Agency

UXO	Unexploded Ordnance
V	volts
VNC	Virtual Network Computing
VSEMS	Vehicular Simultaneous Electromagenetic Induction and Magnetometer System
W	Watts
WAA	Wide Area Assessment

ACKNOWLEDGEMENTS

This *Next Generation HeliMag UXO Mapping Technology Technical Report* documents HeliMag system modifications implemented to improve system productivity and performance, and testing conducted to assess the system performance. The testing was conducted at the Former Kirtland Precision Bombing Range near Albuquerque, New Mexico. This report documents the system modifications, data acquisition, processing, analysis, and interpretation, and overall performance assessment. The work was performed by Sky Research, Inc. of Oregon, with Dr. Stephen Billings serving as Principal Investigator and Mr. David Wright of Wright Research and Design serving as co-Principal Investigator.

Funding for this project was provided by the Environmental Security Technology Certification Program Office. This project offered the opportunity to examine advanced airborne methods as part of the Department of Defense's efforts to evaluate wide area assessment technologies for the efficient characterization and investigation of large Department of Defense sites.

We wish to express our sincere appreciation to Dr. Jeffrey Marqusee, Dr. Anne Andrews, Dr. Herb Nelson, and Ms. Katherine Kaye of the ESTCP Office for providing support and funding for this project.

1 INTRODUCTION

1.1 BACKGROUND

Unexploded ordnance (UXO) contamination is a high priority problem for the Department of Defense (DoD). Recent DoD estimates of UXO contamination across approximately 1,400 DoD sites indicate that 10 million acres are suspected of containing UXO. Because many sites are large in size (greater than 10,000 acres), the investigation and remediation of these sites could cost billions of dollars. However, on many of these sites only a small percentage of the site may in fact contain UXO contamination. Therefore, a number of wide area assessment (WAA) technologies, including Helicopter Multi-sensor Towed Array Detection System (MTADS) Magnetometry (HeliMag) technology, have been demonstrated and validated, both as individual technologies and as a comprehensive approach to WAA (Nelson et al., 2008; Nelson et al., 2005, Foley and Wright, 2008 a, b, c.).

HeliMag technology provides efficient low-altitude digital geophysical mapping (DGM) capabilities for metal detection and feature discrimination at a resolution approaching that of ground survey methods, limited primarily by terrain, vegetation, and structural inhibitions to safe low-altitude flight. The magnetometer data can be analyzed to extract either distributions of magnetic anomalies (which can be further used to locate and bound targets, aim points, and open burn/open detonation [OB/OD] sites), or individual anomaly parameters such as location, depth, and size estimate. The individual parameters can be used in conjunction with target remediation to validate the results of the magnetometer survey.

Developed by the Naval Research Laboratory (NRL), HeliMag technology was transferred to Sky Research (SKY) via a Cooperative Research and Development Agreement (CRADA) in 2005. Since then, SKY has used the technology to characterize more than 100,000 acres at more than twenty sites, including the Environmental Security Technology Certification Program (ESTCP) Wide Area Assessment Pilot Program demonstration sites. During this technology transition process, several technical innovations were identified as having the potential to provide greater efficiency, broader applicability, and greater UXO detection capabilities. These innovations were completed, integrated with the HeliMag technology, and demonstrated at former Kirtland Precision Bombing Range (KPBR), Albuquerque, New Mexico, as part of ESTCP project MM-0741: Next Generation HeliMag UXO Mapping Technology. This report documents the project activities, demonstration results and performance evaluation for the project.

1.2 OBJECTIVES OF THE DEMONSTRATION

The objectives of this demonstration were to improve HeliMag productivity and to expand HeliMag applicability. Specifically, these improvements were to be gained by a series of interconnected innovations:

- Improve data acquisition speeds through implementation of advanced data sampling and noise suppression methodologies (i.e. remove the sampling-based and filter-based limitations on survey speed);
- Enhance HeliMag detection by optimizing sensor configurations to ensure that the magnetic field is fully and optimally sampled, and improving noise suppression

techniques (e.g. implementation of the McDonald Douglas [MD]530F helicopter platform, revised filtering approaches) to maximize the signal to noise ratio (SNR) of targets of interest;

- Enhance HeliMag data interpretation using automated detection and characterization algorithms (e.g. equivalent layer modeling, automatic magnetic dipole analysis/classification) to improve productivity and produce objective, repeatable (thus defensible) results; and
- Implement real-time data telemetry to remove the requirement to have a systems operator on board the aircraft, thereby increasing productivity (less weight provides an opportunity for more fuel and longer flight duration), expanding applicability (less weight provides a greater operational altitude range at existing fuel load conditions) and reducing risk (any aviation activity has an element of risk, removing the operator reduces the risk exposure accordingly).

1.3 REGULATORY DRIVERS

United States Army Corps of Engineers (USACE) is the lead federal agency under the Formerly Used Defense Site (FUDS) program. USACE administers the FUDS Military Munitions Response Program (MMRP) program using DoD investigation/cleanup methods based on the U.S. Environmental Protection Agency (USEPA) Comprehensive Environmental, Response, Compensation, and Liability Act (CERCLA) process.

2 TECHNOLOGY

2.1 TECHNOLOGY DESCRIPTION

The next generation HeliMag system includes a helicopter-borne array of magnetometers (Figure 1), hardware, and software designed specifically to process data collected with this system and perform physics-based analyses on identified targets (Table 1).

Table 1. Sky Research Next Generation HeliMag Technology Components.

Technology Component		Specifications
Geophysical Sensors		14 Geometrics 822 cesium (Cs) vapor magnetometers, 0.001 nanotesla (nT) resolution
Global Positioning System (GPS) Equipment		2 Trimble MS750 GPS receivers, 2-3 centimeter (cm) horizontal precision
Altimeters		1 Optech laser altimeter and 4 acoustic altimeters, 1 cm resolution
Magnetic Attitude		Applied Physics 3-axis flux-gate
Data Acquisition System (DAS)		SKY DAS capable of data collection up to 400 Hertz (Hz), 10 microsecond (μs) timing precision
Telemetry System	Ground Antenna	MP-Tech Single Sector WFP0200508 120 Degrees Coverage
	Vehicle Antenna	HD Communication Corp 5 dBi Omni HD24115
	Radio	Tranzeo TR600
	Amplifier	Luxul 1 W
Aircraft		Hughes MD530F helicopter

Figure 1. SKY next generation HeliMag system. The sensor boom holds a linear array of 13 magnetometers spaced 0.75m apart. A 14th sensor is temporarily mounted above the middle sensor to provide measured vertical gradient test data. The system is operated with an 'Experimental' category airworthiness certification.

2.1.1 Helicopter Platform

The MD530F helicopter is used to deploy the geophysical sensors, GPS equipment, altimeters, inertial measurement unit (IMU), DAS, and telemetry technologies listed in Table 1 and shown in Figure 1. Because the magnetic signal falls off quickly with distance, the helicopter is typically flown at survey altitudes of 1-3 meters (m) above ground level (agl). Onboard navigation guidance displays provides pilot guidance, with survey parameters established in a navigation computer that shares the real-time kinematic GPS (RTK GPS) positioning data stream with the DAS. Survey courses are plotted for the pilot in real time on the display. The sensor operator monitors presentations showing the data quality for the altimeter and GPS (along with the magnetometer data). Following each survey, the operator has the ability to determine the need for surveys of any missed areas before leaving the site.

2.1.2 Sensors and Sensor Configuration

The MTADS magnetic sensors are Geometrics 822A Cs vapor full-field magnetometers (a variant of the Geometrics 822). An array of 13 sensors is interfaced to the DAS and are evenly spaced at 0.75 m intervals at the same elevation on a 9 m Kevlar boom mounted on the helicopter. A 14th sensor is mounted 0.5 m higher and directly above the middle sensor.

2.1.3 Positioning Technologies

As in the initial Airborne Multisensor Towed Array Detection System (AMTADS) design, all data are positioned using 2 Trimble RTK GPS receivers with nominal accuracy of 2 cm horizontal and 4 cm vertical. Ancillary instrumentation records aircraft height above ground and attitude. A fluxgate magnetometer is used to allow for aeromagnetic compensation of the data as well as to provide redundant attitude information.

2.1.4 Telemetry System

Two antennas are used for the telemetry system. An omni-directional antenna, HD Communication Corp antenna (referred to as the ‘whip’) is mounted on the helicopter and transmits data indicating the operational status of system components. A MP-Tech puck sector antenna, a multi-polarity diversity antenna with a vertical radiation pattern of 35 degrees and a gain of 10 decibels (dB), is the ground station antenna and is manually pointed toward the helicopter during operation.

A Tranzeo TR-600 radio, which meets both 802.11b and 802.11g communication standards, puts out 200 milliWatts (mW), 23 dBm, of power (dBm is an absolute unit expressing the power ratio in decibels of the measured power referenced to one mW). The amplifier is a Luxul 1 Watt, capable of amplifying both 802.11g and 802.11b signals. In addition to output amplification, the Luxul units amplify the incoming signal by 18 dB.

To monitor the link and test the remote link capabilities, computers on either end use virtual network computing (VNC) viewer software to allow remote computer control and to utilize the available bandwidth and data rates. Two laptops are used at the ground station, one for VNC to see the shared desktop in the helicopter and the other to monitor the signal strength of the wireless telemetry connected via a 12 volt (V) network switch.

2.1.5 Data Acquisition System

The SKY DAS uses a Linux operating system and logs magnetometer data at 400 Hz.

2.1.6 Data Processing

Data are downloaded via computer disks and uploaded via the Internet after each survey mission. SKY's custom in-house software SkyNet is used to transcribe, filter, decimate and position the airborne geophysical data. The output from SkyNet is either an ASCII xyz file or a Geosoft Oasis Montaj compatible database. Oasis is used to visualize the data and apply advanced processing where required. The SkyNET/Montaj combination facilitates data review, merging, correction, filtering, interpolation and target picking while also providing an industry-standard data management system. A rotor noise suppression algorithm, described in a white paper by Billings and Wright (2008), suppresses rotor noise in the data without distorting the spatial response of any magnetic anomalies with overlapping frequency content.

2.1.7 Data Analysis

The gridded total magnetic field (TMF) image is used as a basis for selection of magnetic anomalies. Automatic target selection has the advantage of being objective, repeatable and more efficient than manual selection. However, automatic target pickers are not yet sophisticated enough to reliably detect closely spaced targets or targets that are at or below the same amplitude as local geologic signal and are not able to differentiate between targets of interest and local geologic anomalies. Therefore, automatic target selection routines must only be used to select targets with response amplitudes significantly above the nominal geologic noise, otherwise an inordinate number of false targets are selected. Furthermore, the automatic routines do not perform well in areas of high target density.

For the purposes of WAA where the main goal is to delineate target density throughout the survey site, the limitations of automatic target selection are not as detrimental as they would be if we were concerned with detecting every possible UXO target. The challenge is to calibrate the automatic target selection routine so that the number of valid targets of interest selected is maximized, while minimizing the number of targets selected due to geologic noise or other noise sources (geologic noise is usually the predominant noise source). In some cases, the geology of the site may dictate that automatic target selection is augmented or even replaced by manual target selection.

The final product of a HeliMag site characterization survey is an anomaly density map. In order to aid in visualizing the distribution of metallic items across the areas, a density grid is computed using a 100 m radius neighborhood kernel that assigns anomaly densities in anomalies per hectare (1 hectare = 2.47 acres) to each cell in the grid i.e., we sweep through a 100 m radius and count the number of targets and determine the area covered (in hectares). We then calculate the density in anomalies/hectare and assign that value to the grid node. A radius of 100 m is suitable for detecting/delineating high-density areas that are indicative of UXO contaminated impact areas. These grids are presented for visualization using a standard color stretch of 0-250 anomalies per acre. This color stretch has been found to be ideal for recognizing and delineating 'high concentration' areas that are indicative of extensive UXO contamination. 'High concentrations' indicative of UXO contamination generally have anomaly densities greater than 200 anomalies/hectare.

2.2 TECHNOLOGY DEVELOPMENT

Development and testing of the first generation of helicopter magnetometry technology in general was supported by ESTCP (Nelson et al. 2005). The primary development objective was

to provide a UXO site characterization capability for extended areas, while retaining substantial detection sensitivity for individual UXO items. The system included data collection hardware in the form of a helicopter-borne array of magnetometers, and software designed to process data collected with this system and to perform physics-based analyses on identified targets. The original NRL AMTADS sensor configuration is a linear array of 7 sensors positioned using two GPS receivers as described in Wright et al (2002). The initial sensor spacing was designed for nominal survey elevations of 3 to 5 m agl. Subsequent testing and demonstrations showed that nominal survey elevations of 1.5 to 2 m agl are regularly achievable.

2.2.1 System Component Development and Updates

2.2.1.1 Helicopter Platform

For the next generation HeliMag system, the Bell 206 Long Ranger (206L) was replaced with the MacDonald Douglas 530F (MD530F) helicopter to provide better power and maneuverability capabilities. The MD530F has the best power/lift ratio of any small form-factor helicopter. For example, both the Bell Long Ranger and MD530F use the same Rolls Royce C-30 engine, but the MD530F is over 1,000 pounds lighter and is therefore much more powerful. This capability provides the pilot with better handling performance and allows for deployment in higher altitude settings[1]. The MD530F also has 5 blades (versus 2 for the Bell system), which provides increased operator control and lower vibration characteristics to support flying low-altitude missions. The rotor speed of the MD530F is also slightly higher than that of the 206L, providing some extra separation between the frequency of the magnetic rotor noise response and that of discrete UXO targets.

2.2.1.2 Sensors and Sensor Configuration

The modified sensor configuration of the next generation system represents a design optimized to achieve the objectives of this project through modeling and analysis conducted on existing data as discussed in the white paper by Billings & Wright (2007). This study evaluated the effects of geology and cultural features, coherent noise suppression alternatives, and dipole characterization processing to determine the optimal sensor spacing.

In addition, data were collected around the helicopter to determine the noise environment of the system itself. This noise characterization allowed us to better understand the spatial characteristics of the noise generated from the helicopter and to compare a vertical gradient with a "reference corrected" total-field system. In this latter system, a reference total-field sensor was placed relatively high up on the helicopter near the dominant noise source (the rotor hub) and used to suppress rotor noise recorded by the sensors on the boom. The results of the study were reported in Billings and Wright (2007) and showed that for every advantage of a vertical gradient system, there is an equal or better advantage with a denser array of magnetometers at the same vertical elevation. In particular:

- Horizontal gradients are as effective or better than vertical gradients at suppressing the impact of geology or large distant magnetic anomalies;
- Rotor noise can be mitigated with advanced noise removal techniques that result in lower noise levels in the total-field than the vertical gradient system;

[1] The increased maneuverability can result in larger heading errors so is not always an advantage.

- The optimal sensor configuration for dipole characterization has all sensors at the same level at a spacing of 0.4 x height (or less).

Note that the horizontal gradients are intended to augment (and not replace) the total-field system. The horizontal gradients would be particularly effective at enhancing detection in geologically complex environments or when there are significant magnetic anomalies caused by cultural infrastructure features.

Based on the design study results, the following sensor configuration modifications were implemented:

- Modification of the existing boom to accommodate 13 sensors spaced 0.75 m apart;
- Move the boom 0.5 m closer to the helicopter to reduce the amount of ballast required to offset the weight of the sensors;
- Inclusion of a "reference" sensor close to the rotor-hub for coherent noise suppression. Following a shakedown test at the Former Lowry Bombing and Gunnery Range (FLBGR), the need for a reference sensor was obviated after the development of an intelligent noise-suppression algorithm.

2.2.1.3 Noise Suppression Algorithm

Rotor noise in the MD530F manifests itself at approximately 7.9 Hz (Billings and Wright, 2007). We could choose to suppress that using a low-pass filter with a cutoff of around 5 Hz. However, this places significant constraints on the survey velocity as a function of survey altitude: in particular, it is not possible to fly low and fast. To avoid these speed constraints, we apply a low-pass filter with a much less aggressive cut-off and rely on suppression of the rotor noise using one of two methods. For measured gradients we rely on the coherent noise rejection capabilities of vertically offset sensors. For the calculated gradients we could use a reference sensor as per our previous analysis in Billings and Wright (2007). However, we have developed a more effective technique that does not require the reference sensor (see appendix B). Essentially, the method calculates the period of the rotor noise and then computes a moving average of the rotor noise. The method accounts for small variations in the rotor noise period and fluctuations in the rotor noise amplitude. Additionally, this method is logistically less complex as it does not require an additional sensor, and is not susceptible to errors due to competing signals measured at the reference sensor that are not due to the rotor.

2.2.1.4 Telemetry System

The telemetry system design was described in detail in a white paper by O'Connor & Wright (2008) and includes the components described in Section 2.1.4. Incorporation of telemetry into the data collection process provides real-time wireless communications between a ground-based sensor operator and the helicopter data system, enabling remote control of data acquisition without an on-board operator.

2.2.2 Shakedown Tests

Following the design study and initial telemetry system development and testing, the system components were assembled and installed. A shakedown test was conducted at the FLBGR near Denver, Colorado, in early June, 2008, to demonstrate the functionality of the technical changes made to the HeliMag system and empirically confirm the findings of the sensor configuration

optimization design study. The performance of the telemetry system components was also tested during the shakedown flights.

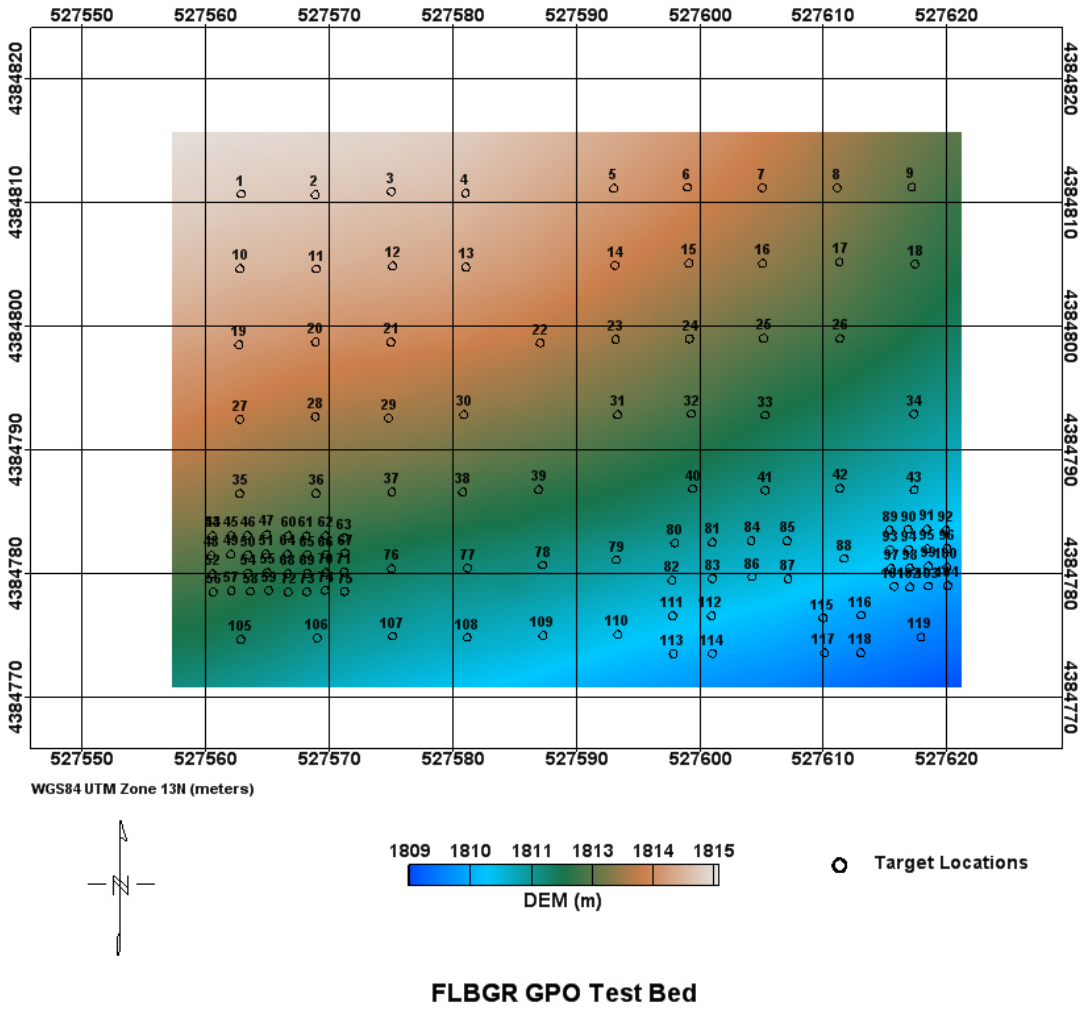

Figure 2. DEM and emplaced target locations at the GPO site at FLBGR.

The FLBGR site was selected for the shakedown test flights because of its accessibility, and because the original NRL AMTADS system was flown over the geophysical proveout (GPO) site established at FLBGR and the results were available for comparison. The FLBGR GPO was initially constructed to support ground-based UXO remediation surveys. It covers 0.7 acres on gently sloping terrain and is seeded with 119 targets (Figure 2). Many of these targets are too small and/or spaced too closely together to be detected with the HeliMag system. The results of the tests of the original system were used to help define the limitations of the HeliMag system prior to deployment as a site characterization tool at a selected number of 'live sites' at FLBGR. Figure 2 shows the digital elevation model (DEM) and target locations at the GPO.

A detailed analysis of the results was presented in the white paper "Project MM-0741, Shakedown Test Results", dated September 15, 2008 (Billings and Wright) and is summarized here.

2.2.3 Detection/Analysis Comparison

The design study results predicted improved performance with respect to anomaly detection/characterization when the sensor spacing is less than approximately 0.4 to 0.5 of the sensor altitude survey, as was the case for the shakedown test flight. The data from previous surveys over the GPO were compared to evaluate the relative performance of the modified system. As noted, three datasets collected over the FLBGR GPO were available for comparison with data collected using the new sensor configuration. The shakedown test flight and a previous flight using the original NRL AMTADS configuration were collected at a height of 1.75 m agl and the results were directly compared. The other data set was collected using the NRL AMTADS system at 1.0 m agl. These data were used to assess the relative merits of flying lower vs. flying with tighter sensor spacing. For this assessment we selected 55 targets to perform dipole fit analyses using data from each of the three surveys.

The magnetic dipole fit analysis was performed with UXOLab. This analysis produces the dipole model that best fits the observed magnetic response in the localized region surrounding each target. This is achieved by iteratively modifying the seven model parameters representing position (3 dimensions), dipole moment (3 components) and a direct current (DC) shift term to correct for any residual background field. Of these parameters, we have independent knowledge of the position information (the 'true' dipole orientation cannot be determined independently of the magnetic data) and the fit correlation coefficient provides a measure of how well the observed results fit the final model. So we can compare the horizontal position estimates, depth estimates and fit correlations from each survey to infer the relative quality of each of the surveys.

The position estimates for all three surveys demonstrated a similar bias (Figure 3), attributed to small base station position errors or similar systematic error between the ground truth and airborne surveys. Because this bias implies some uncertainty in the position accuracy, we used the standard deviation of the position errors as the comparison metric. The results of this comparison showed that the survey flown at 1.5 m spacing and 1 m agl was clearly superior to the other two surveys with respect to the accuracy of the fit positions and the quality of the dipole fit. This advantage is greatest when all targets are included and diminishes as the sample is reduced to include increasingly larger targets only. In Figure 4 we compare the position (horizontal and depth) errors and the fit quality for three cases; all targets, large and small only (very small excluded), and large only (small and very small excluded). We also present the detection performance of the two 1.75 m agl surveys relative to the 1.0 m agl survey. For this comparison, a target was declared 'detected' if the dipole fit horizontal position error was less than 1 m. Note that very small targets were targets that were only detected in the 1 m agl survey, small targets were targets where detection and interpretation was difficult at 1.75 m agl, while large targets were targets that were easily detected and analyzed at 1.75 m agl.

Of the surveys flown at 1.75 m agl, the 0.75 m spacing configuration shows definite improvement over the 1.5 m sensor spacing survey with respect to detection and anomaly characterization. From these results we can surmise that survey altitude is one of the prime determinants of survey efficacy. However, the lowest attainable survey altitude for a given site is determined by factors that are mostly extrinsic to the system configuration (such as topography, vegetation, wind conditions and pilot skill), thus there is little room for improvement in this regard. We can also surmise that the tighter sensor spacing provides improved results with respect to detection and characterization of smaller targets. These findings are congruent with the

sensor configuration design study prediction of improved performance for this combination of altitude and sensor spacing.

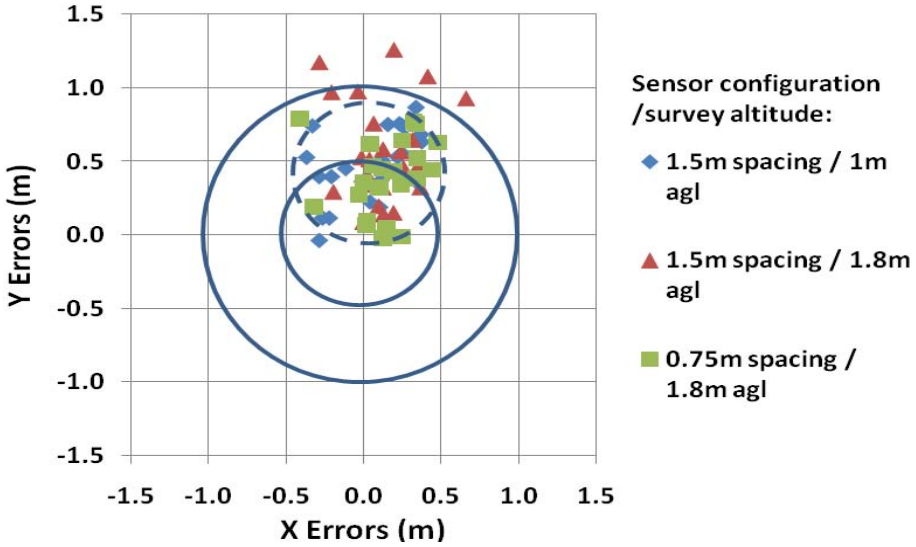

Figure 3. Horizontal position bias for HeliMag surveys collected over the FLBGR GPO test site. Solid circles delineate 0.5 and 1 m position error (centered at x=0, y=0), while the dashed circle delineates an 0.5 m positional error when adjusted for bias (circle centered at x=0.02m, y=0.46m).

Figure 4. Comparison of dipole fit analyses results for three surveys and three classes of target sets.

2.2.4 Noise Suppression and Calculation of Gradients

The sensor configuration design study recommendation of a linear array of sensors was predicated on the assertion that the advantage of coherent noise cancellation inherent to a vertical gradient configuration may be achieved through alternate noise reduction schemes. If this assertion is true, then we can calculate the vertical gradient from the properly spaced/sampled linear array data. We can determine the relative advantage of the vertical gradient noise suppression by comparing the noise levels of the measured vertical gradient relative to the calculated vertical gradient.

Our measurements and calculations in Billings and Wright (2007) demonstrated that the rotor hub contributed the most noise and that the noise was not quite coherent between two vertically offset sensors. Furthermore, by placing a reference sensor close to the rotor-hub and appropriately lagging and scaling the data, more noise could be suppressed in the total-field data than from the gradient data alone. These tests were conducted with the helicopter stationary. To provide a more realistic test of noise suppression capabilities we installed a vertically offset sensor on the boom during the shakedown tests conducted at FLBGR. The sensor (#14) was placed 0.5 m above sensor 7 which is in the middle of the boom. Here we compare measured and calculated gradients from (1) a high-altitude test; and (2) a survey over the test plot.

Measured gradients were obtained by:

- Low-pass filtering sensors 7 and 14 with a 20 Hz cut-off;
- Applying a non-linear detrend filter; and
- Forming the gradient as (sensor14-sensor7)/0.5. The division by 0.5 converts the value to nanoTesla/meter (nT/m) where 0.5 m was the sensor separation.

We also constructed a “calculated” gradient using the magnetic data after application of the de-noising filter. The calculated gradients were obtained by:

- Low-pass filtering sensors 1 to 13 with a 20 Hz cut-off;
- Application of our new noise suppression method to sensors 1 to 13;
- Overlap removal (keeping lowest elevations);
- Gridding and upward continuation by 0.5 m; and
- Forming the gradient by subtracting the original grid from the upward continued grid, dividing by 0.5, and then sampling the grid at the locations of sensor 7.

Note that the calculated gradient was obtained through a 2-dimensional gridding procedure and has some limitations with regard to the grid cell size. In particular, after gridding and upward continuation the data are sampled back at the original locations. We expect some discretization error to contribute to the noise in the calculated gradient. Once we implement the equivalent layer procedure this problem should be eliminated.

Figure 5 compares the 20 Hz low-pass filter and noise suppressed data in a 12 second period of high altitude data. The de-noised data has a standard deviation of 0.08 nT compared to 1.9 nT for the 20 Hz low-pass filter. The measured gradient has a standard deviation of 0.42 nT/m without

de-noising, and 0.08 nT/m with de-noising, compared to 0.12 nT/m for the calculated gradient. Thus the calculated gradient noise floor is comparable to but larger than the measured gradient **after** denoising. The advantage of the calculated gradient is that it can be estimated every 0.75 m (the sensor spacing) compared to 1.5 m for the measured gradient (if we were to distribute our sensors vertically). In addition, because the magnetic field is fully sampled, other quantities such as the total gradient (often mistakenly called the analytic signal) can be more accurately calculated when the sensors are all at the same level. In summary, the high-altitude test indicates that a de-noising filter is an essential requirement for low-noise gradients. In addition, use of the de-noising filter obviates the advantage of coherent noise suppression through vertical gradient subtraction techniques.

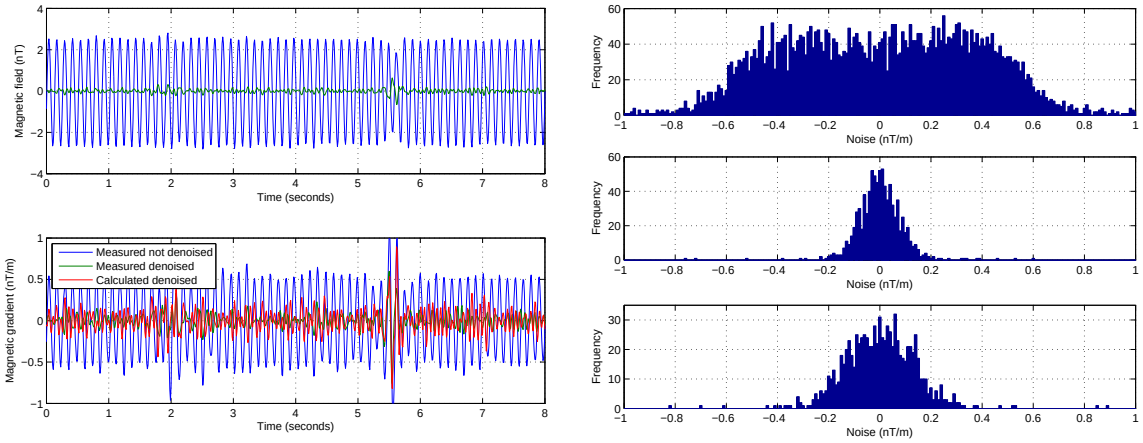

Figure 5. High altitude noise test with data high-pass filtered with a cutoff of 5 Hz. (Left-top) Comparison of de-noised magnetic data against data filtered with a lowpass cutoff of 20 Hz; (Left-bottom) Comparison of measured (with and without de-noising) and calculated gradients (de-noised). At right, top is measured gradient, middle is measured gradient after denoising and bottom is calculated gradient with de-noising.

In Figures 6 and 7, we compare 6 low-altitude traverses over the test plot. The measured (20Hz lowpass and de-noised) and calculated gradients over most of the test plot anomalies correspond quite closely. Inspection of the data to the north of the test plot (the first 5 seconds in each traverse) demonstrates that the measured gradients obtained without de-noising still have a significant amount of rotor noise present. The noise floor appears to be a factor of 2-4 times larger than either the measured or calculated gradients obtained from the de-noised data. It's difficult to determine whether the measured or calculated gradient data are better. Standard deviations in the lead-up to the test-plot are comparable at around the 0.5 nT/m level. However, this number most likely represents the background geological noise which is higher than the 0.1 to 0.15 nT/m noise evident in the high-altitude test.

In conclusion, the FLBGR shakedown test results demonstrate that a noise-suppression algorithm is more important and more effective than the 'stand alone' coherent noise rejection capabilities of a vertically offset gradient measurement. Furthermore, use of the noise rejection algorithm obviates the need for noise rejection through implementation of noise subtraction methods such as reference sensors or vertical gradient configurations.

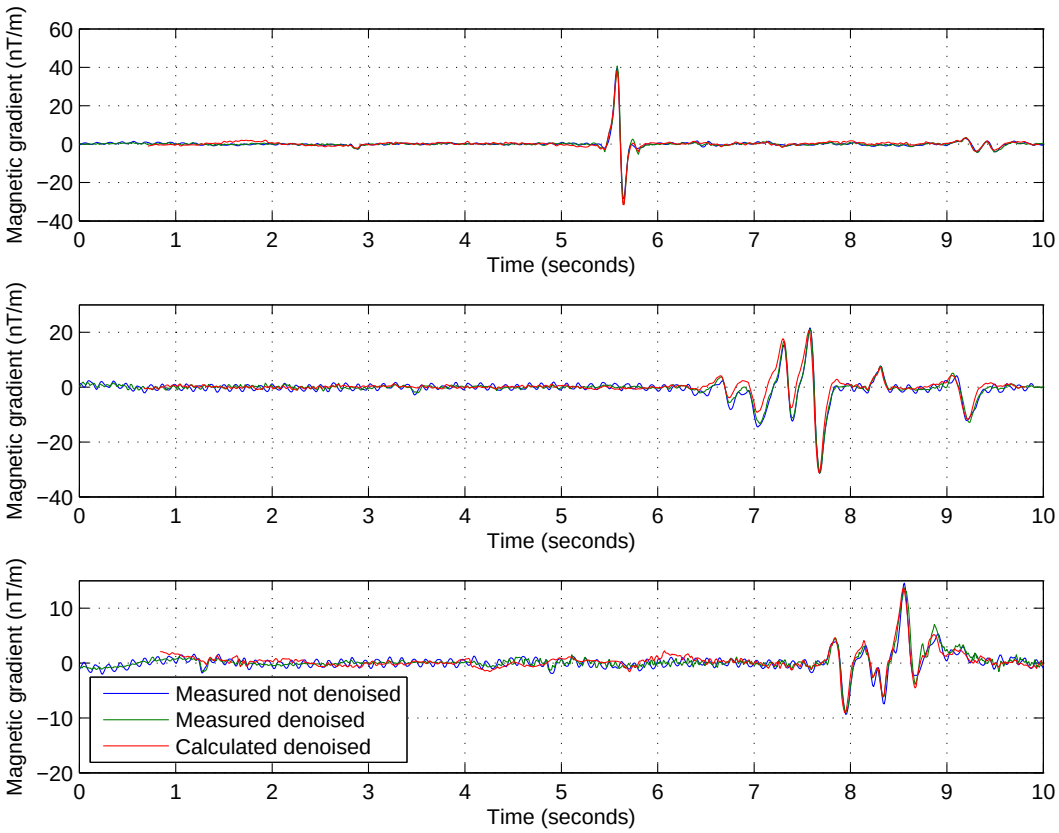

Figure 6. Comparison of measured and calculated magnetic gradients for 3 lines over the FLBGR testplot (the first 5 seconds were collected to the North of the test plot where there are no magnetic items).

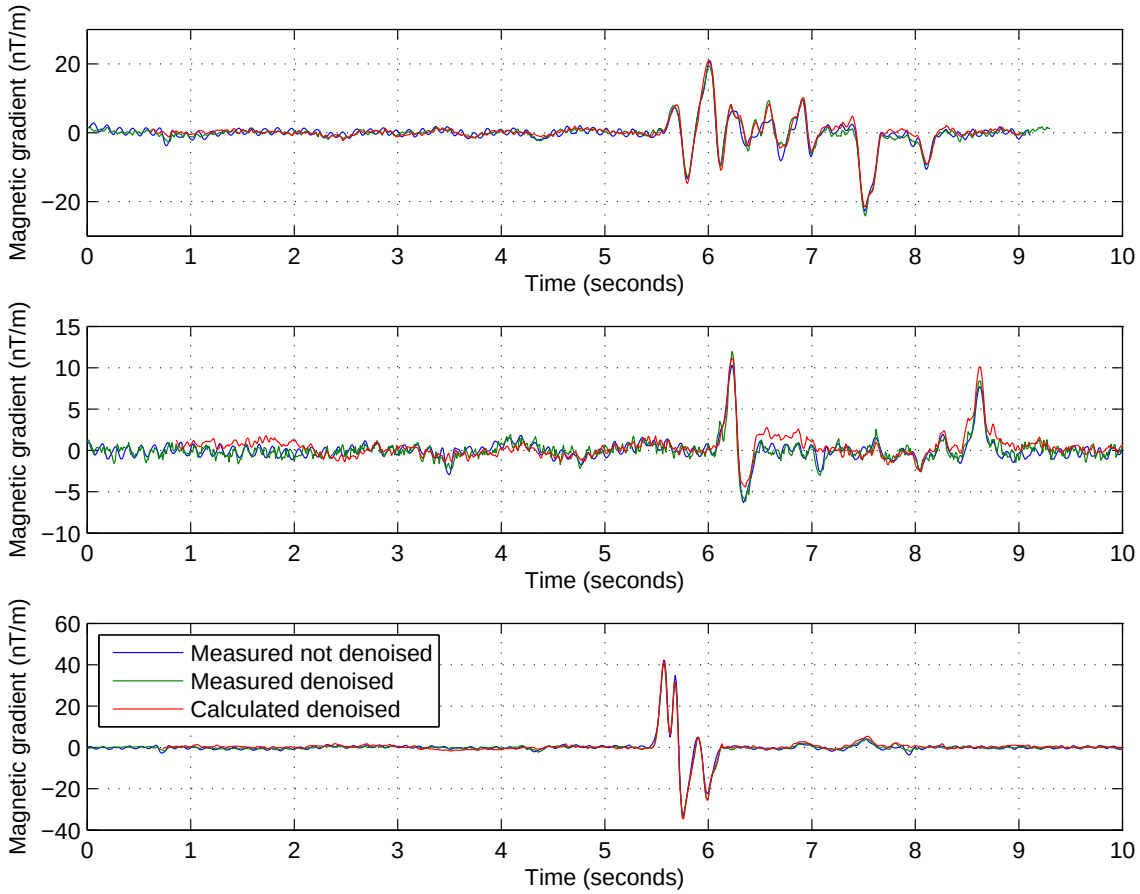

Figure 7. Comparison of measured and calculated magnetic gradients for another 3 lines over the FLBGR test plot (the first 5 seconds were collected to the North of the test plot where there are no magnetic items).

2.2.5 Telemetry Implementation Results

For the telemetry system tests, the base station was set up within line of sight of the survey area at a distance of between 3 to 5 kilometers (km) away. In order to measure telemetry performance, Paessler Router Traffic Grapher (PRTG) software was used to monitor the average received signal strength (RSSI) and average noise with the various combinations of vehicle antennas and the ground based antennas. The puck antenna on the vehicle performed very poorly, having signal strength less than the noise floor. This was unexpected and may have been related to the location of the antenna in the helicopter. The whip antenna performed acceptably well. Although they were both mounted in the same location, one reason for the superior performance of the whip antenna is that the vertical extent of this antenna may be less prone to signal occlusion by components of the aircraft. The two ground antennas performed similarly to each other with respect to signal strength while the puck has a slightly lower noise floor.

With an acceptable radio link, the VNC performance was suitable for monitoring all aspects of the DAS computer in the helicopter except for the pilot navigation display. VNC could not keep pace with the navigation control's refresh rate. This is not considered a serious problem because the system operator has no control over the left-right steering of the aircraft and constant real-time feedback regarding the pilot's performance is not critical to the success of the survey (in

reality, the on-board operator also has little control or input regarding the performance of the pilot in real-time – the pilot is either good at this type of flying or if not, should be replaced).

Several times during the survey flights, operation of the flight computer via the remote station VNC connection was attempted. Some of these attempts were done simply to test this ability, while others were done to respond to a request by the operator on board the helicopter. As expected, the data link was not robust enough to dependably control the DAS and navigation functions consistently during a survey flight. Operational control of the system from the ground will always depend upon the robustness of the data link. The requirement to maintain such a robust data link places significant logistical constraints on the survey process.

2.3 ADVANTAGES AND LIMITATIONS OF THE TECHNOLOGY

As with all characterization technologies, site specific advantages and disadvantages exist that dictate the level of success of their application.

Advantages of HeliMag technologies include:

- The ability to characterize very large areas; and
- Lower cost as compared to ground based digital geophysical mapping (DGM) methods.

Limitations of HeliMag technologies include:

- As a WAA tool, not intended to detect individual UXO items;
- Site physical factors, such as terrain, soils, and vegetation, can constrain the use of the technology.

3 TEST DESIGN

3.1 SITE DESCRIPTION

The Former KPBR is a WWII-era former military training facility located about 2 miles west to 18 miles northwest of the western city limits of Albuquerque, New Mexico. Within the 15,246 acre FUDS, ESTCP established a 6,500 acre demonstration plan sub-area for the WAA Pilot Program (Figure 8). Results from the data analysis for the WAA Pilot Program confirmed the presence of three precision bombing targets (N2, N3 and New Demolitions Impact Area [NDIA]) and a simulated oil refinery target (SORT), and several additional areas of interest (also shown on Figure 8).

Currently the study area is undeveloped. Portions are planned for commercial or industrial development within the next decade, and airport expansion into these lands is possible.

3.1.1 SITE SELECTION/EXPERIMENTAL DESIGN

For this demonstration, the next generation HeliMag system was used to survey approximately 586 acres configured to encompass a subset of the areas surveyed as part of the Pilot Program. The extent of the planned survey area shown in Figure 8 and comprises the following six areas:

- North-central survey area (118 acres) covering three full-coverage ground-based grids and part of the SORT area. The area covered with the ground-based grids was used for seeding.
- South-central survey area (79 acres) covering two full-coverage ground-based grids. The area covered with the ground-based grids was used for seeding.
- Northeast 1 survey area (190 acres) covering three full-coverage ground-based grids and part of the NDIA area.
- Northeast 2 survey area (58 acres) covering two full-coverage ground-based grids.
- Western seed area (105 acres) established for testing of Battelle's EM helicopter array.
- Western ground-coverage area (36 acres) overlying a full-coverage grid collected by SAIC.

All of the areas surveyed for this demonstration also overlapped with areas surveyed using the AMTADS helicopter system in 2005 (Nelson et al., 2005) and most overlapped with 10 areas that were surveyed on the ground in full coverage mode by the Vehicular Simultaneous Electromagenetic Induction and Magnetometer System (VSEMS) (Seigel, 2008). The Program Office blind-seeded part of the area with 60 and 80 mm mortars. The area reserved for seeding overlapped three of the full-coverage grids. In addition, a 100-acre seeded area was surveyed that had already been established by the Program Office for testing of the Battelle EM array. This area was seeded with 81 mm and 4.2" mortars, 105 mm and 155 mm projectiles, and 105 mm High-explosive Anti-tank (HEAT) rounds.

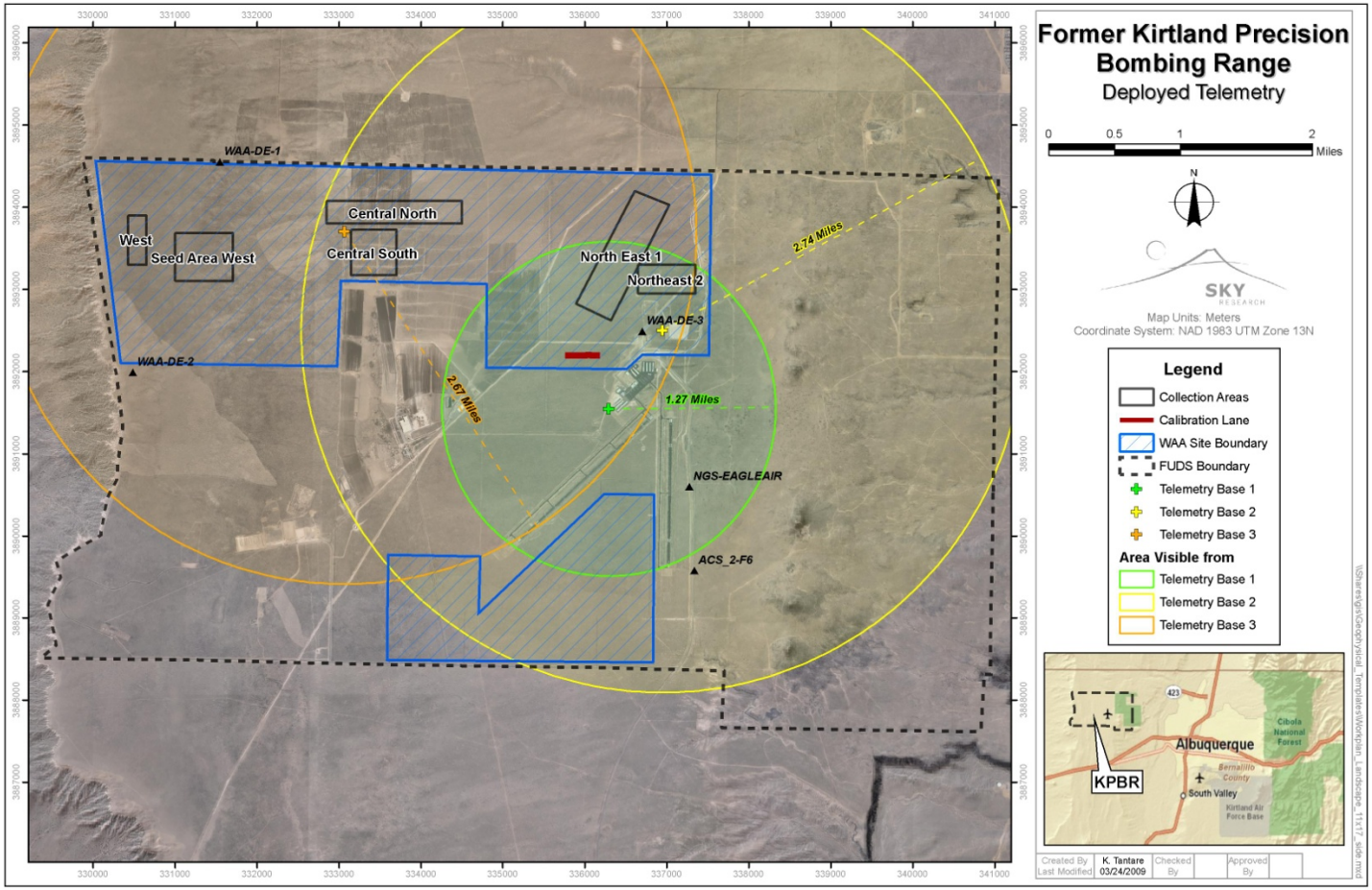

Figure 8. Former Kirtland Precision Bombing Range with HeliMag 2009 test data (opaque palette) superimposed upon HeliMag data collected in 2005 (semi-opaque palette). The HeliMag areas flown in 2009 are labeled with black typeface and the areas where VSEMS (ground-based) data were collected are shown with brown borders and typeface.

Because previous HeliMag, AMTADS and ground-based systems have been demonstrated at the site, overlap of survey areas allows for comparison of the datasets as an effective mechanism for evaluating the next generation system performance.

3.1.2 SITE HISTORY

The Former KPBR is a WWII-era former military training facility located. A summary of the site history is as follows:

- 1940s – US Army leased 15,135 acres from the City of Albuquerque, Santa Pacific Railroad and Dept. of Interior
- 1940s – The leased property was used for precision bombardier training during World War II
- 1947 – The ranges were declared surplus and the lease was canceled
- 1953 – Certificates of Clearance issued for all ranges except for N-4 and the New Demolition Range
- 1955 – 1988 the City of Albuquerque acquired 13,868 acres. The State of New Mexico retains 898 acres, and 480 acres are privately owned.
- 1994 – USACE generated an Archive Search Report (ASR) (USACE, 1994)
- 2007 – Engineering Evaluation and Cost Analysis (EE/CA) was completed in January 2007 by USACE Albuquerque District (EODT, 2007)

3.1.3 SITE GEOLOGY

The demonstration survey area is on a relatively flat terrace at about 6,000 feet mean sea level atop the Rio Puerco Escarpment which falls away to the west of the site. The soils within the former KPBR are described as Deep Soils on Alluvial Fans, Mesas and Piedmonts. The soils in this area are the Madurez-Wink association and are deep, well-drained homogeneous sandy loams formed on loess parent material with low magnetic mineral content.

3.1.4 MUNITIONS CONTAMINATION

Munitions known or suspected to have been used on the site include 100 pound (lb) practice bombs and 250 lb high-explosive (HE) bombs. Target N2 is documented as a 160-acre quarter-section containing a circular night bombing target including power plant, underground cables, floodlights and target circle. Target N3 is documented as being within a 320-acre half-section near the northwest corner of the study area. This target was cleared in 1952, and large pits within the area have been hypothesized as OB/OD areas. The NDIA target area is a target circle. The SORT area was documented in the ASR with the location unknown in the first conceptual site model (CSM) prepared as part of the WAA Pilot Program (Versar, 2005). The surveys conducted under the WAA Pilot Program confirmed its presence.

Documented ordnance present on the site surface within the study area includes the following:

- M38A2 100 lb practice bombs and spotting charges
- M85 100 lb practice bombs and spotting charges
- 250 lb General Purpose HE bombs.

The primary aircraft in use at the Former KPBR was the AT-11 bomber trainer which carried up to ten 100 lb practice bombs. The B-18 bomber was also reportedly used, which could carry a 4,000 lb payload of bombs. Aircraft flares also were reportedly dropped. Information in the ASR indicates that a single 250 lb HE bomb was dropped "unofficially" by each trainee bombardier upon graduation from the training course, probably at the NDIA target area east of the N2 target area.

3.1.5 SITE PREPARATION

No site preparation (i.e. vegetation removal, site clearance, etc.) was required.

ESTCP emplaced blind seeded targets in the north-central survey area and south-central survey area where ground-based grids were located. The ground truth data was protected from the performers until after the data analysis was complete.

3.2 SYSTEM SPECIFICATION

The Next Generation HeliMag system was deployed as described in Section 2.1 of this report. Flight parameter specifications for data collection were as follows:

Table 2. Flight Parameters for Data Collection

Parameter	Specifications
Flight Speed Average	40 knots (20 m/second [m/s])
Flight Speed Range	20 to 60 knots (10 to 30 m/s)
Altitude	1 to 3 m agl
Across Track Spacing	0.75 m
Flight Line Separation	7.0 m separation to provide 40% overlap between adjacent passes
Along Track Density	0.2 m (at 100 Hz sample rate, 20m/s ground speed)

Data processing and analysis was conducted using UXOLab, SkyNet and Geosoft as follows:

- UXOLab, SkyNET and Geosoft for initial surface interpolation and for target picking and classification;
- Frequency domain notch filters to suppress 60 Hz noise and other harmonic noise sources (implemented within SkyNET).
- Non-linear rotor noise suppression algorithm (implemented within SkyNET)
- Aeromagnetic compensation (implemented within SkyNET)
- Equivalent source code in Fortran from Colorado School of Mines
- Dipole fits and apparent remanence (within UXOLab).

3.3 PERFORMANCE OBJECTIVES

The performance objectives provide the basis for evaluating the performance and costs of the technology. For this demonstration, both primary and secondary performance objectives were established. Table 3 lists performance objectives, criteria and metrics used for evaluation.

Table 3. Performance Objectives

Performance Objective	Metric	Data Required	Success Criteria
Ease of Use	Efficiency and ease of use meets design specifications	Feedback from technician and pilot on usability of technology and time required	System efficient and easy to use
Geo-reference position accuracy	Comparison of validation target dipole fit analysis position estimates (in 3 dimensions) to ground truth.	Location of seed items surveyed to accuracy of 1 cm Validation target dipole fit analysis position estimates (in 3 dimensions)	Target location estimates within 0.25 m radial horizontal error and 0.5m vertical position error
Detection performance on seeded items	Percent detected (Pd) of blind-seeded items	Location of seeded Items Prioritized dig list	Pd > 0.9 for 60 mm and above
Detection performance compared to ground-based system	Comparison of target list with target lists generated from the full coverage data	Target lists of next generation system and ground based systems for 60 mm mortar	Pd > 0.9 for 0.03 ampere- meter squared (Am^2) anomalies (60 mm mortar) with probability of False Alarm (Pfa) < 0.5 (from ground-based)
Detection performance compared to AMTADS	Comparison of target lists from next generation HeliMag to that of the original AMTADS	Target lists of next generation system and original AMTADS Inflection point for both systems	Pd for next generation > Pd from AMTADS Inflection point (in total targets vs. detection threshold graph) for next generation lower than AMTADS

Performance Objective	Metric	Data Required	Success Criteria
Telemetry link	Percentage of survey time during which the operator can view the DAS interface through VNC	Operator log	Maintain link with helicopter for >80% of the data acquisition. Interruptions limited to 15 minute durations.
Noise level (combined sensor/platform sources, post-filtering)	Accumulation of noise from sensors and sensor platforms calculated as the standard deviation of a 20 sec window of processed data collected out of ground effect.	20 second sample of data collected at high altitude (out of 'ground effect')	<1 nT and < 0.1 nT/m for calculated gradient
SNR Improvement	Improved SNR relative to baseline HeliMag system	SNR of original and next generation sensor systems	Average SNR > original 7 sensor system for selected common anomalies
Accuracy and noise of calculated vertical gradients	Gradients calculated by potential field operations on the total-field data and compared to the gradient measured by the one vertically offset sensor	Magnetic data over validation line.	Noise level of calculated gradient $\leq$ measured gradient Better than 0.99 correlation between measured and calculated gradients

Performance Objective	**Metric**	**Data Required**	**Success Criteria**
Accuracy of equivalent layer	Comparison of data predicted by equivalent layer at 2 m altitude compared to data predicted by upward continuation of ground-based data	Magnetic data over a portion of the site.	Better than 0.95 correlation between equivalent layer and upward continued ground-based data at 2 m elevation
UXO parameter estimate repeatability	Size and dipole angle estimates of the calibration items consistent	Daily calibration data	Size <50% (standard deviation) Angle relative to Earth's field < 20º (standard deviation)
Operating parameters (altitude, speed, production level)	Values calculated using average and mean statistical methods to compute each parameter.	Statistics are extracted from the databases (altitude/speed) and field data logs (production level)	1-3 m AGL; 10-30 m/s (20-60 knots); 300 acres/day
Rotor noise suppression algorithm at high speed	Comparison of high and low-speed results over validation line targets to verify correct operation of rotor noise suppression algorithm when the signal frequency overlaps the rotor noise frequency	Data acquired over validation line.	Fit error of dipoles on validation-line survey collected at high-speed within 5% of low-speed data

Performance Objective	**Metric**	**Data Required**	**Success Criteria**
Data density/point spacing	Along track: (# of sensor readings/second) / airspeed. (Across track: sensor line spacing = 0.75m)	Statics are derived from the survey databases (along track density) and sensor configuration (cross-track sensor spacing)	0.1 -0.3 m along-track (0.2 m at 100 Hz sample rate, 20 m/s ground speed) 0.75 m cross track
Survey coverage	Surveyed acres / Planned survey acres	Actual # acres surveyed Planned # of survey acres	>0.95 of planned survey area

3.3.1 EASE OF USE

Technology usage is a qualitative assessment of the ease of use to operate the technology to accomplish survey objectives. As such, the field experience of the lead on-site geophysicist is the basis for this qualitative metric. In general, meeting this objective depends upon successful completion of the project objectives within the budgeted time frame.

3.3.2 GEO-REFERENCE POSITION ACCURACY

Position accuracy is critical to proper interpretation/analysis of total magnetic field data. Unlike ground surveys, HeliMag data are collected in three dimensions and at relatively high speeds. Position accuracy on a dynamic platform is very difficult to measure precisely. Therefore, we are able to infer the position accuracy of the sensor data by using the position estimates derived from dipole fit analysis of data collected over known validation targets, and also over any seeded items. The data collected over each target from the validation line passes that are assumed to be valid (i.e., target positions are stable and data positioning quality is good) were analyzed with the Sky Research UXOLab dipole fit algorithm. This analysis derives the parameters for a model dipole that best fits the observed data. These parameters include horizontal position, depth, size, and solid angle (i.e., the angle between the Earth's magnetic field vector and that of the dipole model). The derived parameters were examined for accuracy, (determined as the average error or 'bias' where relevant), and repeatability (indicated by the standard deviation). Although the positioning of the helicopter data are assumed to be accurate to < 0.1m in the horizontal plane, and <0.2m in the vertical plane, additional measurement/computational errors will result in higher target position errors. With this in mind, the performance objectives for positioning of targets was set at 0.25m (horizontal) and 0.5m (vertical).

3.3.3 DETECTION PERFORMANCE

For performance confirmation of metrics, related Pd and false alarm (Pfa), three types of validation information were available:

1. A small subset of data where there was overlapping next generation HeliMag, vehicular, and existing AMTADS data. The vehicular data can be used as ground truth and Pd and Pfa derived assuming the vehicular data are perfect (Pd=1, Pfa = 0). Note, since HeliMag is a WAA tool, we did not try to discriminate UXO from clutter so false alarms are defined as picks where there are no metal targets detected by the ground vehicular data.
2. For regions with only AMTADS and next generation HeliMag data, we conducted a similar analysis. We used an automated target picking algorithm (Geosoft's 'peak detection' routine) on both versions of the HeliMag data and plotted the number of targets versus threshold – this plot has an inflection point where we start to pick into the noise (i.e., at lower thresholds the number of targets selected increases radically). Once the inflection point was determined for both systems we compared the following:
    - Number of targets detected to generate relative detection performance of the systems. All detections above the defined threshold(s) were assumed to be legitimate (after manual review to ensure realistic thresholds were used). Anomalies were correlated between systems and reviewed to identify systematic difference between the systems (e.g. improved performance for low amplitude targets);

- The threshold of the actual inflection point for comparison of system performance with respect to base noise levels (the assumption being that a lower inflection point is indicative of lower system noise levels). We recognize that a number of items have been removed since the original AMTADS survey. Therefore, when we obtained a list of these items from the Program Office we excluded them from the analysis described above.

3. The detection performance of the system against small UXO types was evaluated with a blind seed test. ESTCP Program Office had a set of 80 targets emplaced with their positions unknown to SKY. Based upon SKY target list submissions, the Program Office developed a Pd for each of the ordnance types. A Pd of 0.9 for detection of 60mm mortar and larger targets was set as the pass criterion for this objective.

3.3.4 TELEMETRY LINK

Previous demonstrations of this technology required that a sensor operator (SO) remain on board during data acquisition to monitor data quality as the survey progresses. All aviation involves some risk. Removal of the SO allows us to reduce the overall risk and improve productivity by increasing the available aircraft payload. To maintain real-time data quality oversight we implemented a telemetry system to allow the SO control of the on board data acquisition from a ground station. The system was designed so that momentary lapses in coverage did not compromise the data quality. The primary purpose of the real-time oversight is to ensure that we do not spend expensive helicopter time collecting poor quality data. In practice, small delays and interruptions in the quality control (QC) activity carry relatively low risk, so it was determined that gaps in coverage of up to 15 minutes duration and an %80 coverage rate were acceptable. Other than delaying the initial QC of the data, lapse in telemetry coverage has no effect on the final quality of the data.

3.3.5 NOISE LEVEL

Detection performance is based upon maximizing the SNR of UXO-like targets. Unwanted signal or ‘noise’ is due to external sources (e.g. localized geology and anthropogenic infrastructure) as well as intrinsic sources such as the rotor or changes in orientation of the airframe relative to the Earth’s field. While we cannot control the extrinsic noise, we endeavor to minimize the intrinsic noise to ensure that it is not the limiting factor in the detection performance of the system. The performance criterion for this objective was to maintain intrinsic noise less than 1nT, measured as the standard deviation of a 20 second window of processed high altitude data.

3.3.6 SNR IMPROVEMENT

We anticipate an improvement in the SNR performance of the next generation HeliMag relative to the original 7 sensor system. Improvements in the SNR are achieved by increasing the amplitude of the signal and/or reducing the noise of the system. Because we are passively measuring the total magnetic field, the amplitude of the signal is determined primarily by the sensor-target offset distance. Control of this distance is dominated by the local site conditions and pilot skill/comfort levels. However, for sites where the boom can be flown relatively low ($\leq$2m agl), the decreased sensor spacing should result in increased signal levels for a significant number of targets that would have passed between two of the wider spaced sensors in the 7 sensor boom. This advantage is not as definite as one may assume: Due to the swath overlap

required to ensure complete coverage (7m line spacing with a 9m boom), only the middle 3/7 of any given survey line the area is flown at 1.5m spacing by the 7 sensor system. The remaining 4/7 of the line is covered at a tighter (though inconsistent) sensor spacing.

We have achieved improvements in system noise reduction by implementation of both an advanced rotor noise removal process and aeromagnetic compensation routine to remove maneuver-induced magnetic responses. Although the dominant noise source continues to be local geologic response, the improved noise rejection process obviates the requirement for aggressive filtering of the blade noise. The low-pass filter employed for the original 7 sensor system potentially had a deleterious effect of the target signal amplitude, depending upon the speed and altitude of the data acquisition. The advanced noise removal process demonstrated with the next generation HeliMag system does not have this effect on signal amplitude, regardless of the flight envelope characteristics.

3.3.7 ACCURACY AND NOISE OF CALCULATED VERTICAL GRADIENTS

One of the predictions of the configuration design study discussed in section 2.2.1.2 was that a linear array of sensors at 0.75m spacing could be used to accurately calculate the vertical gradient, thus there was no advantage to a measured gradient configuration. For the survey, there were 13 magnetometers distributed along the boom with a horizontal spacing of .75 m. A 14th magnetometer was placed in the center of the boom at 0.5 m higher to make a single vertical gradient measurement. This measured gradient was compared to that obtained by upward continuation and differencing of the data from the 13 magnetometers. Noise comparisons were made using high altitude calibration flights as well as short-segments of data that didn't transect selected anomalies. The correlation between the measured and calculated gradient was obtained using the daily validation data.

3.3.8 ACCURACY OF EQUIVALENT LAYER

For this deployment we had intended to test an equivalent source algorithm developed by Colorado School of Mines. It allows HeliMag data collected at different sensor altitudes to be calculated at a fixed elevation above the ground. We did not evaluate any metrics associated with the equivalent layer as we were only able to apply the methodology to a limited 30 m by 30 m section of data.

3.3.9 UXO PARAMETER ESTIMATE REPEATIBILITY

In addition to the position data, the dipole fit analysis provides a measure of the apparent dipole size and orientation with respect to the Earth's field. The dipole fit size estimate for any given ordnance will vary considerably depending upon the alignment of the object with the Earth's magnetic field. Therefore, the size can only be used as a coarse estimate of the object size. For this reason, the accuracy of the size estimate of the calibration items is not of particular import when discussing the system performance, other than simply verifying that the estimate falls within the expected range for a given target. Because the calibration data consists of repeated flights over the same stationary targets, the repeatability of the derived size estimates can be used as an indication of consistent system performance.

Similarly, the accuracy of the dipole angle derivation is unimportant (and it cannot easily be determined) but the repeatability of this parameter, when derived from a series of validation flights over the same targets, can be used as an indicator of the stability of the system.

Historical experience indicates that a standard deviations of < 50% for size and <20° for dipole angle are indicative of proper performance of the system.

3.3.10 OPERATING PARAMETERS

The ultimate success of an airborne survey for UXO detection depends upon our ability to fly according to a set of operating parameters including survey altitude, speed and production level. Because of the 1/(distance)^3 fall-off in discrete dipole response amplitude, survey altitude is the primary determinant of the effectiveness of the system. In any survey we attempt to fly as low as possible without compromising the safety of the aircraft and crew. The objective for this parameter is to maintain survey altitude between 1 and 3m. (ideally we would like to see data collected below 2m, however our ability to do this is very site specific). Survey speed is related to survey altitude in that most pilots will slow down as they fly lower to the ground. Survey speeds of 10 – 30m/s (20 – 60 kts) are sufficient to ensure adequate down-line data density (0.1 - 0.3m at 100Hz sample rate) and maintain productivity. Productivity is a function of survey speed and site conditions (e.g. weather, ferry distance, access issues). Although on very large scale surveys, the average production rate can be as high as 800 acres/day a production rate of 300acre/day for this demonstration was considered reasonable

3.3.11 ROTOR NOISE SUPPRESSION ALGORITHM

By replacing the previously used low-pass filter with the new rotor noise suppression algorithm we remove speed/altitude restrictions from the flight envelope as described in Billings and Wright (2008). We tested this algorithm and verified that it can effectively suppress rotor noise without distorting the spatial response of near-surface survey anomalies. We collected data along the validation line at a speed low enough that there was little or no overlap between the frequencies of the rotor-noise and near-surface metallic anomalies, as well as a speed fast enough so that there was significant overlap. The dipole fit model parameters derived from the de-noised data at both speeds should match those derived from the low-speed, low-passed data.

3.3.12 DATA DENSITY/POINT SPACING

The cross-track data density is essentially static and is a function of the system geometry. With the exception of isolated data gaps that can arise during a survey, the ‘worst case’ spacing is our sensor spacing of 0.75 m. The effective density is much higher than this due to the significant overlap required to eliminate (or at least minimize) data gaps due to the inevitable cross-track variation of the helicopter flight path. Down-track data density is much higher than the cross-track density and is a function of survey speed. Based upon the survey speed objectives and 100 Hz sample rate, we expected the down track density to be between 0.1 and 0.3 m.

3.3.13 SURVEY COVERAGE

The spatial extent of a magnetic anomaly (from our targets of interest) is a factor of two times greater than the sensor offset distance. Based upon our minimum survey height of 1 m, we can conservatively define gaps in survey coverage as areas where the distance to the nearest sensor reading is greater than 2 m. Gaps in survey coverage are generally related to navigation (a combination of pilot skill, topography/vegetation, and wind conditions) or data integrity (primarily GPS fix quality). The objective set for this criteria is that the total coverage is >0.95 of the planned coverage.

4 DATA ACQUISITION ACTIVITIES

4.1 AEROMAGNETIC COMPENSATION CALIBRATION

High altitude noise characterization and aeromagnetic compensation flights were conducted on the first day. The high altitude noise fight was conducted at high elevation with the helicopter traversing a box of about 1000 m per side. For aeromagnetic compensation, a compensation flight was carried out at as high an altitude as was feasible (~1000 feet) with the helicopter hovering in a fixed location. The helicopter nose first was pointed east, then north, then west and then south. At each heading approximately 30 seconds of data were acquired while performing each of yaws of at least 5 degree amplitude, pitches of at least 5 degree amplitude, and rolls of at least 10 degree amplitude. The magnetic field data in each sensor, along with the aircraft attitude and altitude, was continuously recorded. A well known 18 term model was then fit to the observed data and defined the maneuver noise characteristics of the helicopter.

4.2 GROUND CONTROL

RTK GPS provided centimeter-level accuracy real time positioning and was used to generate positions for ground fiducials and for positioning ground validation data. The GPS base-stations at KPBR were established on existing survey monuments (Table 4).

Table 4. Locations of Survey Monuments at KPBR in UTM, NAD-83

Name	Northing	Easting	Elevation
WAA-DE-3	3892488.676	336703.269	1771.262
ACS 2-F6	3889573.947	337337.344	1768.569
WAA-DE-5	3893029.178	333713.290	1793.518
NGS EAGLEAIR	3890596.422	337278.521	1767.998
NGS Q424	3882321.542	337925.050	1715.482

4.3 VALIDATION LINE

A system validation line was established at the base of field operations at the Double Eagle Airport. To confirm its suitability for the validation line placement, background noise data were collected and reviewed before the validation line was established. The validation targets were placed on the ground surface at a spacing of 50 m at the orientations as listed in Table 5. The locations of all validation items were surveyed to verify positional accuracy. Validation line surveys were conducted twice each day and the resulting signatures compared to calculated responses to confirm correct system operation. No targets were buried and no attempt was made to measure a probability of detection from the validation data.

Table 5. Validation Targets

Item and Orientation	Depth	Easting (m)	Northing (m)
37mm vertical	Ground level	3892310.99	336214.99
37mm E/W	Ground level	3892310.45	336202.72
37mm N/S	Ground level	3892310.20	336191.59
3 pound bomb E/W	Ground level	3892309.79	336181.83
3 pound bomb N/S	Ground level	3892309.31	336167.62
Ammo Box Sim.	Ground level	3892308.20	336142.44
2.75 rocket E/W	Ground level	3892307.42	336122.59
100# Bomb E/W	Ground level	3892305.95	336097.17
155mm E/W	Ground level	3892305.31	336078.97
Ammo Box Sim.	Ground level	3892304.19	336055.00
2.75 rocket N/S	Ground level	3892302.80	336027.384
100# Bomb N/S	Ground level	3892301.98	336001.85
155mm N/S	Ground level	3892301.17	335978.21
37mm vertical	Ground level	3892310.99	336214.99

4.4 DATA COLLECTION

The field data collection program ran from initial mobilization on March 14th to demobilization on March 20th. Daily data collection activities for the demonstration are provided in Table 6, and Figure 9 shows the areas surveyed in reference to the previous surveys. Initial testing began on March 16th and data acquisition occurred from the 17th to the 20th. There were minor delays on each of the first two data acquisition days due to reconfiguration of the boom mounting hardware. Additionally, poor GPS quality on March 18th resulted in more reflies than are typically required for HeliMag surveys. Discounting time lost for these delays, a total of 586 acres were surveyed in approximately 2 survey days.

The helicopter was based virtually on site at Double Eagle airport. Double Eagle has just become a tower-controlled airport so close coordination of low altitude airborne activities in the direct vicinity of the airport was required.

Table 6. Data Collection Schedule.

Date	Activity
March 14	• Helicopter mobilized to Double Eagle Airport
March 15	• Crew mobilized to Albuquerque, NM
March 16	• Assembled boom on helicopter • Established validation lane • Set-up telemetry base-station • Validation lane survey • High altitude and compensation flights
March 17	• Began surveying
March 20	• Completed survey
March 20	• Demobilized helicopter, equipment and personnel

During the data acquisition process, the data quality was monitored via real-time telemetry of the survey data to a ground station. This system provided for monitoring of the quality of the position data, survey coverage, and magnetometer data as the survey progressed.

There were three different set-up locations used for the telemetry system (Figure 8). The sensor operator kept track of how often the telemetry link was maintained (Table B1 in Appendix B). On average, the link was maintained for over 95% of the survey time. The telemetry system operated satisfactorily while the aircraft was within line of sight up to a little over 2.5 miles away.

Telemetry Base 1 had only 'end of line' connection for site North East 1 due to obstructions at the airport (control tower, hangars). Telemetry Base 2 had connection out to 2.74 miles and coverage included sites Central North, Central South, North East 1 and North East 2. Telemetry Base 3 had connection out to 2.67 miles and covered virtually all of the survey sites. This location was the highest in elevation of the 3 base locations. A small hill separated this location from sites West and Seed Area West, telemetry link was only occasionally lost during the survey of these sites.

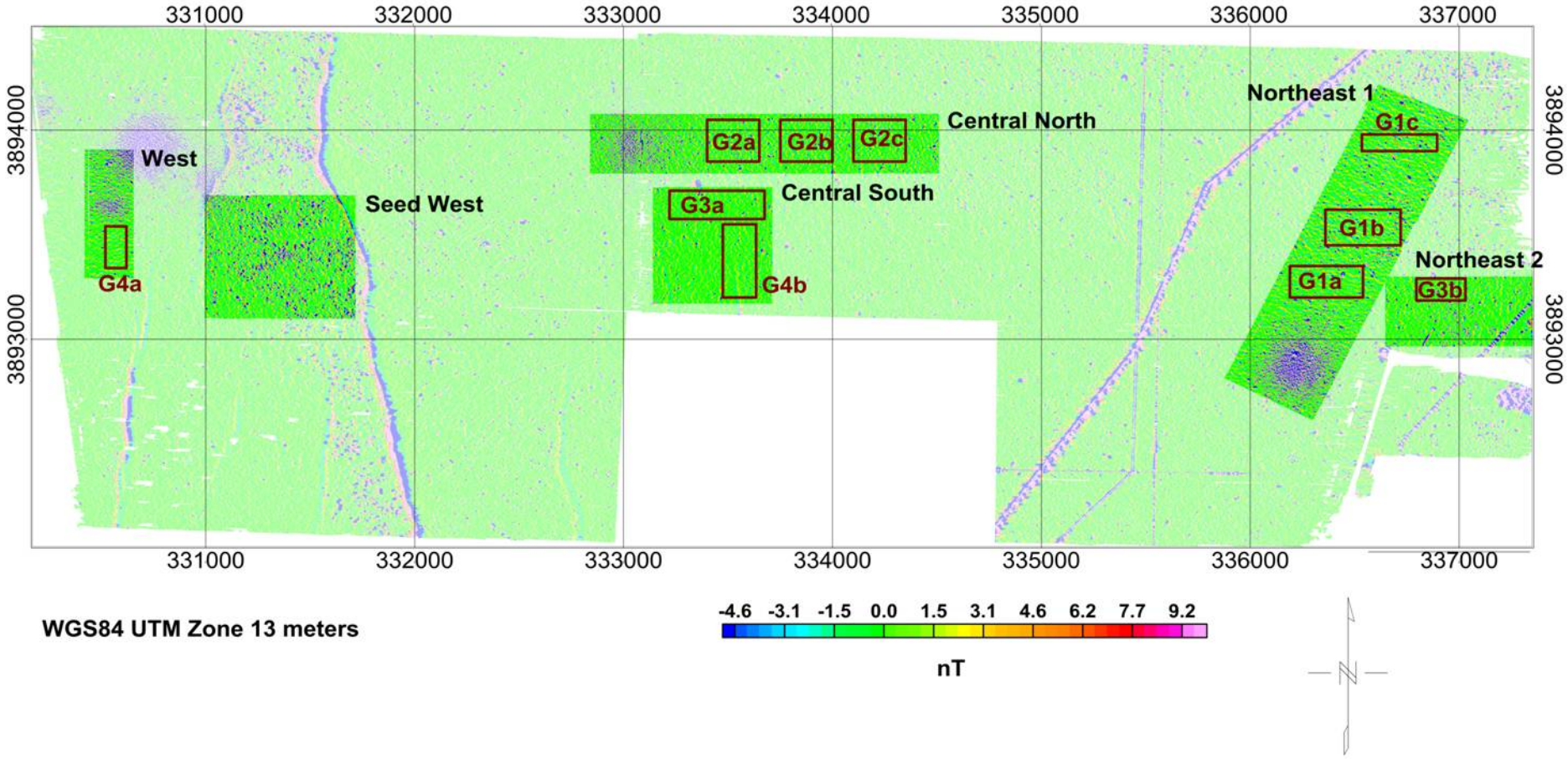

Figure 9. Overview of survey data collected: The areas with opaque palettes were collected with the 13 sensor HeliMag configuration, The large semi-opaque palette is the AMTADS 2005 data set and the boxes outlined in red represent area that were surveyed with a ground-based towed magnetometer array in 2005.

4.5 DATA ANALYSIS AND PRODUCTS

4.5.1 PREPROCESSING

The raw data were transcribed from their native data file formats into ASCII xyz files using SkyNet. At this point, the geophysical data were subjected to a lowpass/notch filter and decimated to a sample rate of 100 Hz and assigned three-dimensional (3D) positions based upon the GPS master antennae position, aircraft attitude and the system geometry. Because the geophysical and position data were collected asynchronously, they were aligned with respect to their time of applicability. This was performed automatically during the merge process based upon highly precise time stamps associated with each data channel.

For this demonstration, the rotor noise suppression algorithm was used to suppress the 7.8 Hz rotor noise without distorting the spatial response of any magnetic anomalies with overlapping frequency content. See the discussion in the section below for more details about the rotor-suppression method.

The Data Processor performed the initial review of the geophysical data following each survey day. As needed, adjustments were made to the field operations or data processing to ensure quality data collection.

The initial review of geophysical (magnetometry) data was performed to ensure that the data were within a reasonable range (35,000 – 75,000 nanotesla [nT]), free from dropouts/spikes, and timing errors and otherwise appear to be valid. Invalid data were removed and, where appropriate, requests for re-flights passed to the acquisition team.

The initial review of positional data involved checking line profiles for position dropouts/spikes. A GPS fix quality indication was recorded as part of the GPS data string. Any data tagged with a fix status that indicated the GPS was not operating in 'RTK-fix' mode (nominally 2 cm level accuracy) were rejected automatically.

After the initial data review described above, the data underwent a site-specific processing procedure for sensor data filtering, gridding, and visualization that was developed based on preliminary analysis of the validation and initial survey results.

4.5.2 ROTOR NOISE SUPRESSION

We expended significant effort understanding and mitigating the dominant intrinsic noise source of the system which originates in the rotor-hub. It is an especially problematic noise-source because, when flying fast and low, the frequency range of the noise (7.8 Hz) overlaps with the frequency content of near-surface metallic items. Thus, it can't be suppressed with a low-pass or notch filter, without distorting the spatial structure of the underling signals of interest. The rotor-suppression algorithm that was developed and applied to the FLBGR test-data often failed when applied to the Kirtland data. We thus sought to develop a more reliable algorithm by studying the characteristics of the rotor-noise. We summarize our findings here and expand on the main issues in the text that follows.

(1) Noise source has a frequency of 7.8 Hz, corresponding to a period of 0.128 s.

(2) Source of noise fits a dipole located at the approximate position of the rotor hub;

(3) Amplitude of rotor noise varies as a function of magnetic attitude;

(4) The phase delay between each sensor is a function of magnetic heading.

We contemplated developing a rotor-suppression algorithm that took account of the coherent nature of the rotor-noise, and an expected fixed phase difference between the noise at each sensor. However, it turns out that the relative amplitudes of the rotor-noise and the phase-delay between each sensor are a function of helicopter attitude (Figures 10 and 11). In Figure 10 we track the peak-to-peak amplitude of the rotor-noise during an aeromagnetic compensation flight flown on day 78. For the central sensor (number 7) to peak-to-peak amplitude of the rotor noise varies from less than 1 nT to almost 4 nT. For one of the outer sensors (number 13), the peak-to-peak noise ranges from 0.1 nT to 1.7 nT. Notice that the variation in amplitude for sensors 7 and 13 are not always correlated. For both sensors, a Leliak (1961) model can be used to accurately predict the variation in the peak-to-peak amplitude as a function of helicopter attitude. Figure 11 plots the phase-difference between sensors 7 and 13 during that same compensation flight. For the first part of the flight, which encompasses a fairly wide range of headings, the phase difference remains fairly constant at -0.02 seconds. At about 95 seconds into the flight, there is a rapid change in the phase-difference and it varies quite significantly as the aircraft executes pitch/roll maneuvers at a fixed heading.

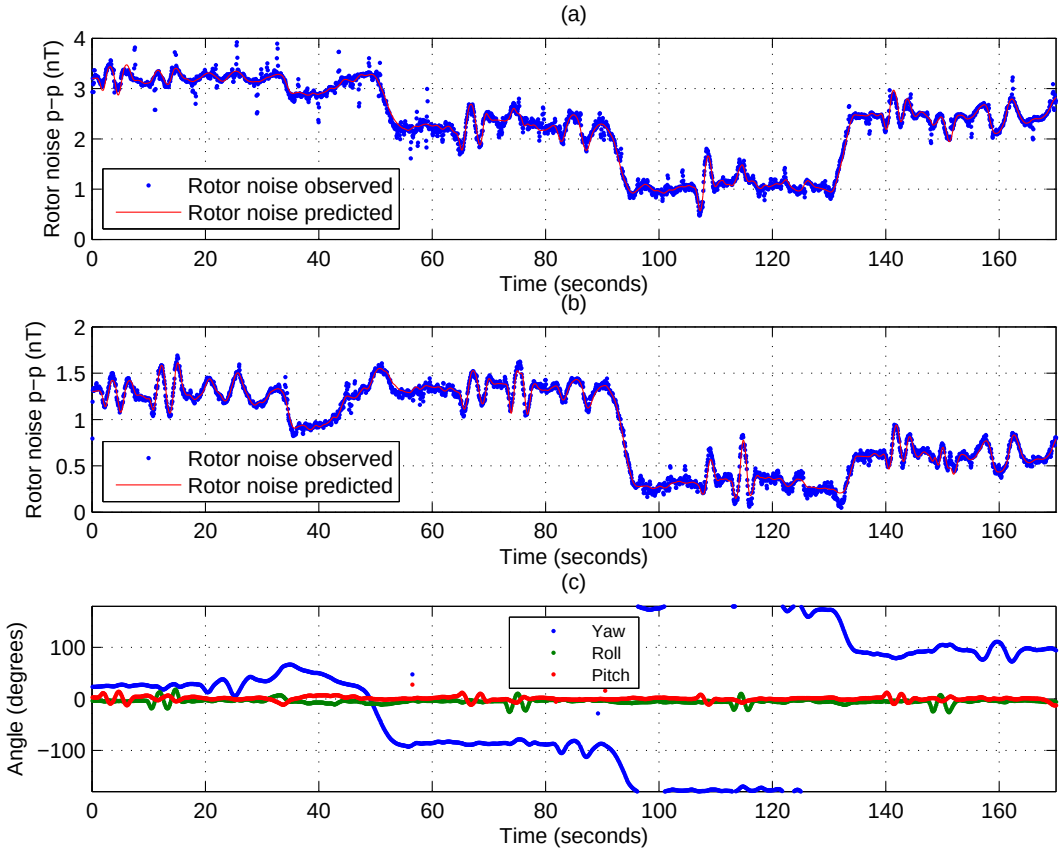

Figure 10. Amplitude of rotor noise during compensation flight on day 078 for (a) sensor 7 (middle sensor) and (b) sensor 13 (sensor on far right of boom). The helicopter attitude is shown in (c).

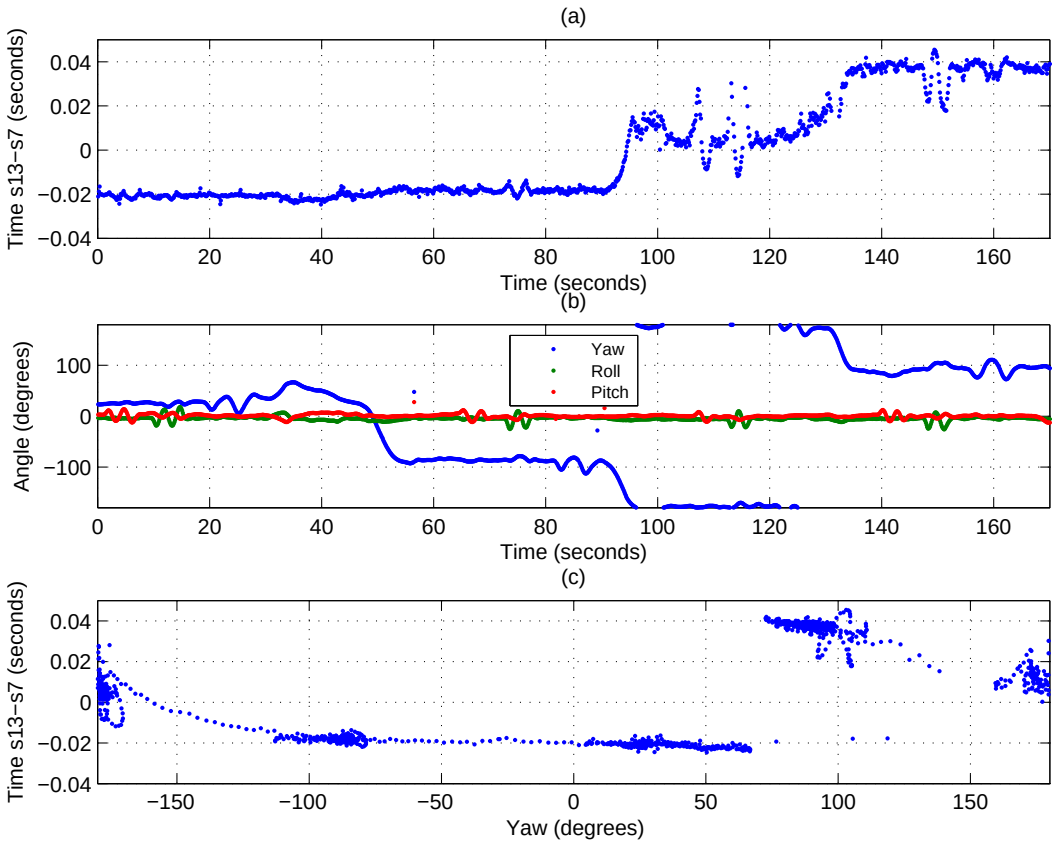

Figure 11. Time delay between sensors 13 and 7 (a) as the helicopter attitude changes (b) during the compensation flight on day 78. The time-delay is largely correlated with the helicopter yaw (c).

A two-dimensional analysis of a rotating dipole can be used to understand why the peak-to-peak amplitude and phase-difference vary as a function of magnetic attitude. Assume that the rotor-hub is located at [0, 0] and that a sensor is located at $r = [\sin\phi, \cos\phi]$, with the moment of the rotor-hub noise varying as $m(t) = [\sin\omega t, \cos\omega t]$. In the helicopter frame of reference the earth's field vector is $B_o = [\sin D, \cos D]$ and the measured total-field is then proportional to:

$$[3\sin^2\phi\sin D + 3\cos\phi\sin\phi\cos D - \sin D]\sin\omega t + [3\cos^2\phi\cos D + 3\cos\phi\sin\phi\sin D - \cos D]\cos\omega t$$

After differentiating this equation with respect to *t*, setting the result to zero and rearranging terms we find that extrema occur when:

$$\tan\omega t = \frac{3\sin^2\phi\sin D + 3\cos\phi\sin\phi\cos D - \sin D}{3\cos^2\phi\cos D + 3\cos\phi\sin\phi\sin D - \cos D}$$

We consider a sensor inline with the center of the helicopter (so ϕ=0) and one at the outer edge of the boom (so ϕ=45) and then calculate ωt as a function of declination for both sensor positions. Figure 12 shows the phase and amplitude of the two sensors as a function of the magnetic declination. The amplitude is a maximum at each sensor when D=ϕ (declination parallel to the line between dipole and sensor) and is at minimum when D=ϕ ±90 (declination

perpendicular to the line between dipole and sensor). It is evident that there is a significant variation in phase difference and ratio of amplitudes depending on the declination.

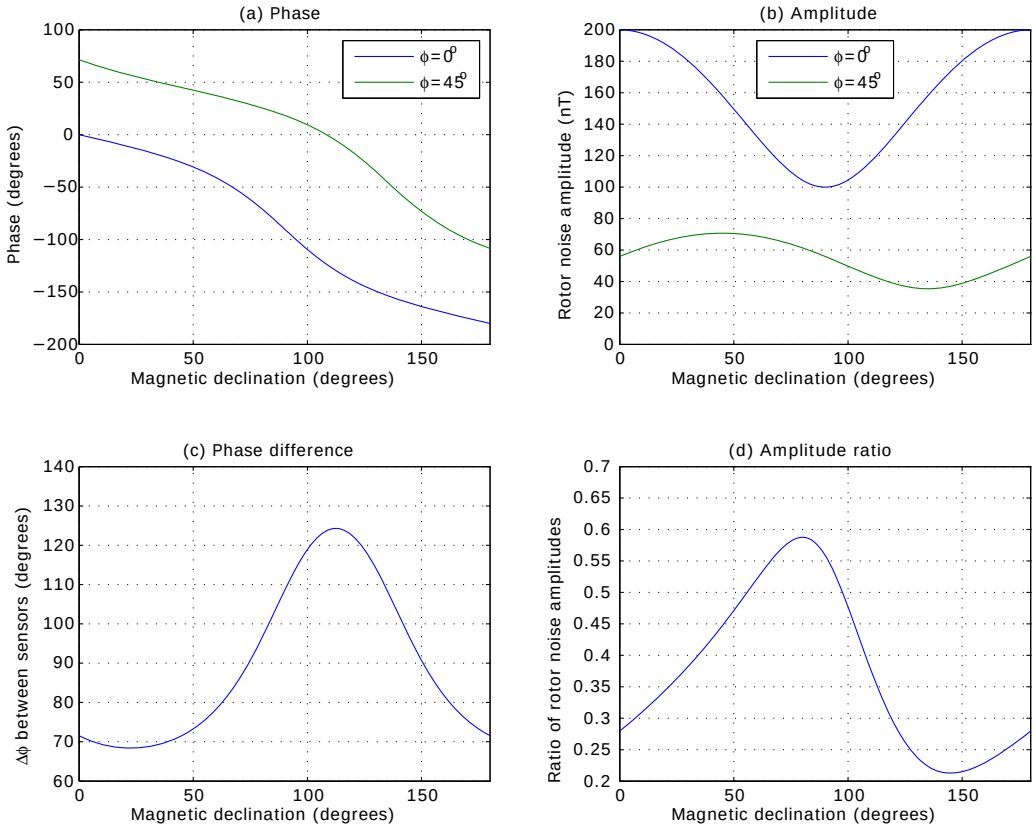

Figure 12. The phase (a) and maximum amplitude (b) of rotor-noise at two sensor locations (ϕ=0 & 45) as a function of declination angle (helicopter heading) are shown for a 2-D model of a rotating dipole. The phase difference between sensors (c) and ratio of amplitudes (d) depend strongly on the magnetic declination.

Next we investigated the spatial structure of the rotor-noise by fitting a dipole model to all 13 sensors at each instant in time. We fixed the location of the dipole at the rotor-hub so that this calculation was very fast (as it turns into a linear inverse problem). Figure 13 shows the amplitude of the rotor noise on the central (sensor 7) and far right sensors (sensor 13) during the compensation flight, as well as the residuals from the dipole model fit. The residuals are generally very small (< 0.1 nT) indicating that the rotor-noise is described very well by the dipole model. The y-component of the dipole model is also shown, and varies sinusoidally as evident in the expanded view of the first 5 seconds of the compensation flight in Figure 14. The maximum amplitude of the fitted moment does not change significantly with helicopter heading indicating that the strength of the rotor-noise is largely invariant to magnetic attitude. The variation in amplitude evident in Figures 13 and 14 is due to variations in the angle between noise-source and sensor and that of the Earth's magnetic field. Note that for most of the compensation flight the component of the moment in the z-direction is generally very small indicating that the rotor-noise can mostly be described by a dipole rotating in the horizontal plane. The vertical moment is non-zero during some of the heading maneuvers, particularly around the 95 second mark. At those times, the rotor hub is rotating at an angle to vertical, hence the z-component to the moment.

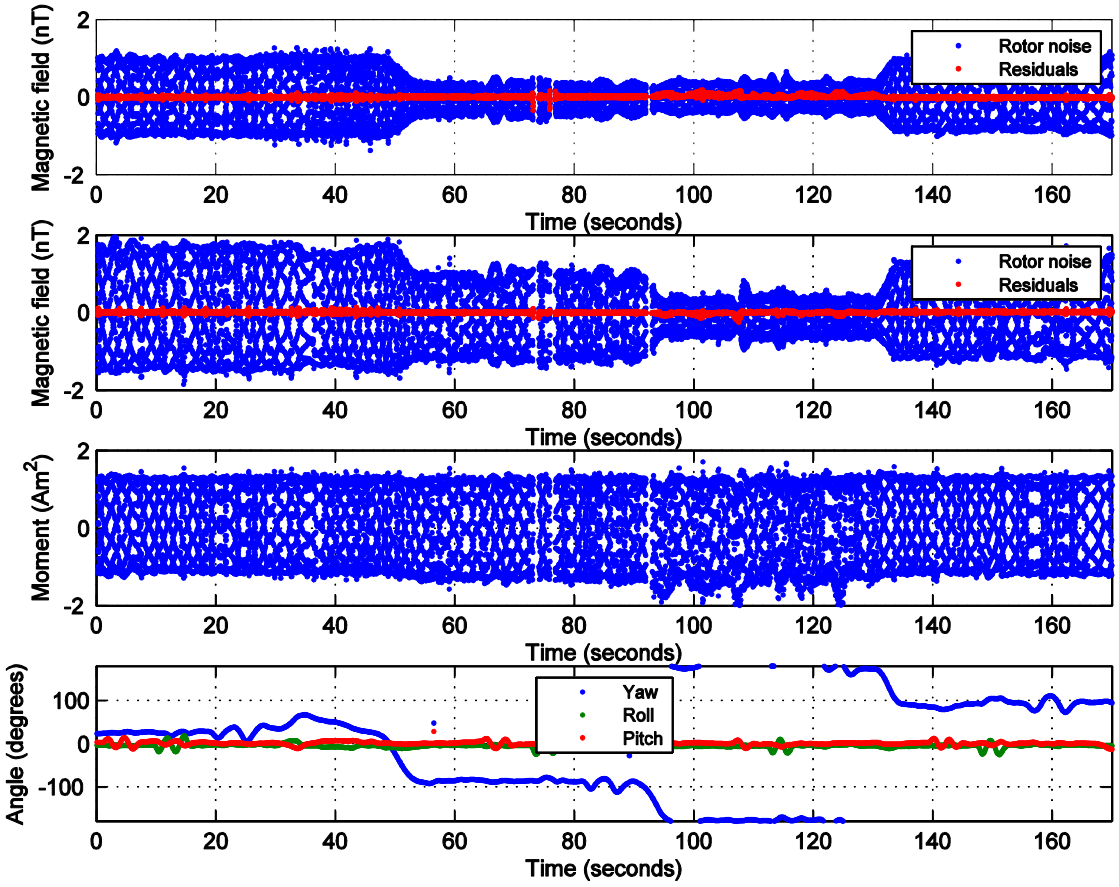

Figure 13. Rotor-noise during the compensation flight on day 78 for sensors 7 (top row) and 13 (second row). The red dots represent the residuals from a dipole moment fit to all 13 sensors on the boom. The y-component of the dipole moment is shown in the third-row.

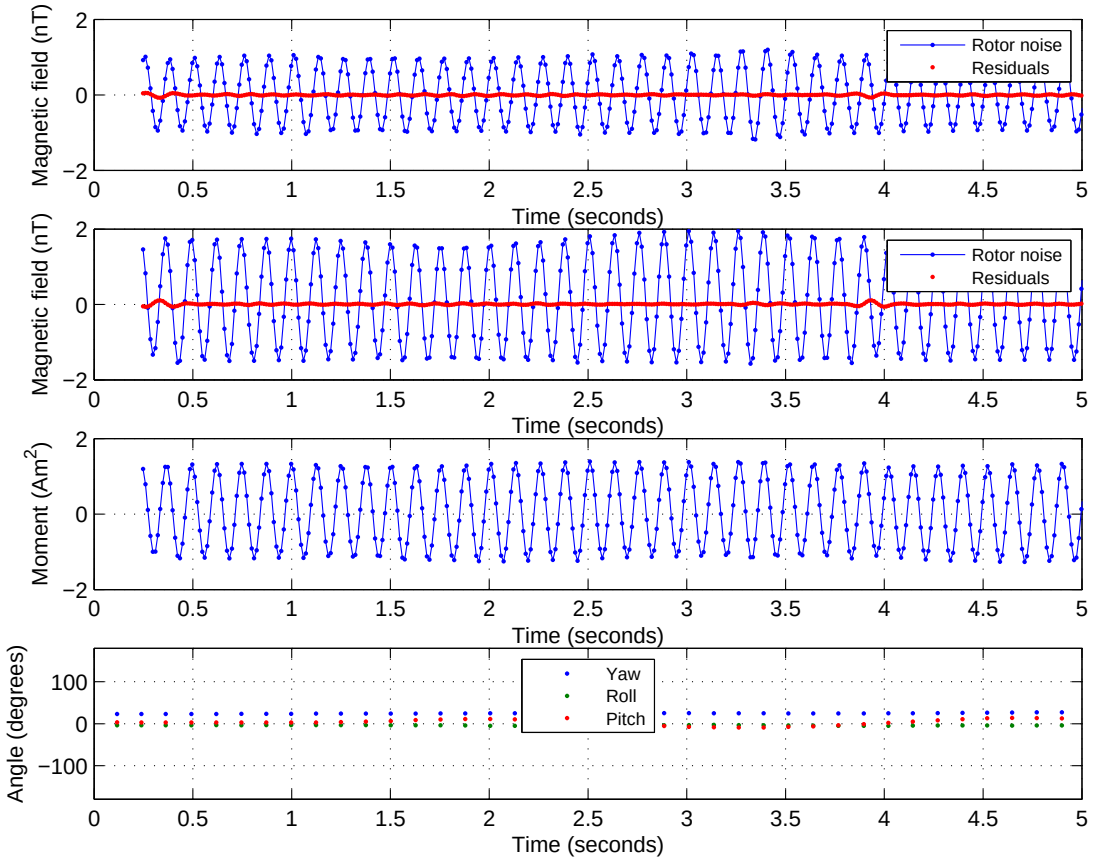

Figure 14. The first 5 seconds of the data shown in Figure 14.

We didn't feel that the dipole fitting method could be used effectively to model the rotor-hub noise when the helicopter was close to the ground. Therefore, we decided to concentrate on developing a rotor-noise suppression algorithm using the magnetic compensation flight. The algorithm works as follows:

(1) Break the sensor data up into 10 second segments;

(2) Accentuate the response from the rotor by filtering each sensor with a notch filter with lower cutoff of 5 Hz and upper filter of 10 Hz;

(3) Find the positive and negative peaks for each sensor;

(4) Determine the average offset between the phase of each sensor and sensor 7;

(5) Apply a phase adjustment to each sensor so that the sensor data is in phase with sensor 7;

(6) Identify clusters of peaks and use these to estimate the time of occurrence of each positive and negative peak in sensor 7;

(7) Discard peaks that are not clustered and fill-in any missing peaks;

(8) Use the flux-gate data and compensation calibration to estimate the magnitude of the peak-to-peak rotor noise at each peak location;

(9) For each sensor fit and then remove a cosine function between each positive and negative peak with a magnitude determined by the previous step.

4.6 ANOMALY SELECTION

The gridded TMF image as well as the 'analytic signal' (i.e. total gradient) were used as the basis for selection of magnetic anomalies. Geosoft's peak detection routine was applied to the analytic signal grids to automatically select targets with response amplitudes significantly above the nominal geologic noise. The SKY analyst used a cut-off threshold of 4 nT/m (SNR = 8) for the auto-detection process and augmented the target list by selecting and de-selecting anomalies based upon the TMF image.

Recently, SKY has developed analysis techniques to extract more information from the data and improve delineation of potentially hazardous areas. These techniques involve refining the target lists based upon parameters derived from the dipole fit analysis.

4.7 PARAMETER ESTIMATES

Each selected anomaly is subjected to a dipole fit analysis to derive features (e.g. dipole size, orientation and position). The analysis software extracts sensor data points associated with each selected target. Each sensor reading is an input datum used in a seven-parameter, iterative calculation to derive the parameter values that describe a dipole model that best fits the observed data. These parameters include dipole position (3 dimensions), dipole angle (2 dimensions), dipole magnitude (size) and an offset parameter to account for any bias in the magnetometer data.

4.8 CLASSIFIER AND TRAINING

The dipole parameters derived from the target picking step are then classified using the apparent magnetic remanence metric (Billings, 2004). Items used to calculate apparent remanence were a 60 mm and 81 mm mortars (small ordnance), 105 and 155 mm projectiles (medium ordnance) and a 100 pound bomb (large ordnance). If the apparent remanence was less than 70% then the item was assigned to the corresponding class (e.g. small ordnance), whereas if larger it was placed in a low confidence UXO class (e.g. low confidence small ordnance). Any items with a depth greater than 3.95 m are assigned to a "low confidence metallic" class, while items with failed fits are placed in a "can't analyze category". The target list is then ordered by apparent remanence, with smaller values representing items with a higher likelihood of being a UXO. Final outputs from this step are an ASCII formatted target list providing target ID, refined position and associated dipole parameters and target classification declarations.

4.9 DATA PRODUCTS

There were two main data products produced (target list and magnetic data), with additional products derived from these two items (e.g. images, target density estimates).

Raw data: The raw data is supplied in Geosoft XYZ format, which comprises an ASCII file with individual data collection lines delineated by a line header NNNNNNN.s, where s is the sensor number. The columns are:

- Time (seconds): The GPS time of the magnetometer measurement;
- Easting (meters): Easting of measurement in NAD83 datum.

- Northing (meters): Northing of measurement in NAD83 datum.
- Elevation (meters): Height above ellipsoid of the measurement in NAD83 datum.
- h_agl (meters): Estimated height of measurement above the ground.
- Sensor_Number: Sensor number, 1 is far left up to 13 on the far right and with 14 the central sensor that is 0.5 meters higher.
- Mag_Raw (nT): Raw magnetic data (after application of rotor suppression algorithm, but before aeromagnetic compensation and geology removal).
- mag_full_fin (nT): Compensated magnetic data
- Mag_demedian_fin (nT): Compensated and high-pass filtered magnetic data.

Target lists: These were provided in Microsoft Excel format with the following columns:

- Target: A unique label identifying the anomaly number.
- X (meters): Easting in NAD83 datum.
- Y (meters): Northing in NAD83 datum.
- Depth (meters): Estimated depth below the ground of the anomaly.
- Elevation (meters): Estimated height above ellipsoid of the anomaly.
- dx (meters): Difference between the original estimated of the easting and the refined estimate returned by the dipole model;
- dy (meters): As for dx but for the Northing.
- MagMin (nT): Minimum value of magnetic data about anomaly.
- MagMax (nT): Maximum value of magnetic data about anomaly.
- MagAmp (nT): Difference between anomaly maximum and minimum.
- Moment (Am^2): Magnitude of fitted dipole moment.
- Azimuth (degrees): Azimuth of dipole moment measured clockwise from Magnetic North.
- Dip (degrees): Dip of dipole measured below the horizontal (0 for a horizontal dipole).
- CorrCoeff: Correlation coefficient between observed and predicted data.
- NumData: Number of data points that constrain the dipole fit.
- Angle (degrees): Angle between the Earth's field and the fitted dipole moment.
- Fit: Indication of whether the fit is acceptable or not.
- Comment: Comment regarding the fit (typically auto-generated).
- Best Item: Item with lowest magnetic remanence.
- Remanence (%): Apparent remanence of the fitted dipole moment.

5 PERFORMANCE ASSESSMENT

Table 3 lists performance objectives, criteria and metrics used for evaluation, with **Table 7** summarizing the performance achieved.

Table 7. Performance Objective Results

Performance Objective	Confirmation Method	Expected Performance	Performance Achieved
Ease of Use	Efficiency and ease of use meets design specifications	System efficient and easy to use	Met with qualifications (see text)
Geo-reference position accuracy	Comparison of validation target dipole fit analysis position estimates (in 3 dimensions) to ground truth.	Target location estimates within 0.25 m radial horizontal error and 0.5m vertical position error	Met: standard deviation of location error was 23 and 24 cm for Central and West seed areas and 7 cm for validation line objects. Vertical error standard deviations for Central and West were 29 and 21 cm and for validation line were < 23 cm
Detection performance on seeded items	Pd of blind-seeded items	Pd > 0.9 for 60 mm and above	Met for 81 mm on Central seed area but not on 60 mm Pd = 100% for 81mm Pd = 23% for 60mm Met for all projectiles on Western seed area except 81 mm Pd = 98% for all (except 81 mm), Pd = 58% for 81 mm
Detection performance compared to ground-based system	Comparison of target list with target lists generated from the full coverage data	Pd > 0.9 for 0.03 Am^2 anomalies (60 mm mortar) with Pfa < 0.5 (from ground-based)	Not evaluated as ground-based data were high-pass filtered using significantly different parameters than the airborne data.

Performance Objective	Confirmation Method	Expected Performance	Performance Achieved
Detection performance compared to AMTADS	Comparison of target lists from next generation HeliMag to that of the original AMTADS	Pd for next generation > Pd from AMTADS Inflection point (in total targets vs detection threshold graph) for next generation lower than AMTADS	Pd < 2005 AMTADS data due to altitude differences, but >simulated AMTADS data (7 sensors, low-pass filtered) Pd against seeded targets > for simulated AMTADS data Inflection points comparable (when presented in terms of SNR)
Telemetry link	Percentage of survey time during which the operator can view the DAS interface through VNC	Maintain link with helicopter for >80% of the data acquisition. Interruptions limited to 15 minute durations.	Met, telemetry link maintained for > 95% of the time. Worst performance had telemetry link maintained for 70% of a flight (< 5 minute interruption)
Noise level (combined sensor/platform sources, post-filtering)	Accumulation of noise from sensors and sensor platforms calculated as the standard deviation of a 20 sec window of processed data collected out of ground effect.	<1 nT and < 0.1 nT/m for calculated gradient	Met Noise standard deviation < 0.42 nT on all sensors (probably closer to 0.1 to 0.2 nT). Standard deviation for both calculated and measured gradients < 0.1 nT/m
SNR Improvement	Improved SNR relative to baseline HeliMag system	Average SNR > original 7 sensor system for selected common anomalies	Met: factor of 1.17 improvement over 2005 AMTADS data and 1.68 over simulated AMTADS data (same altitude)
Accuracy and noise of calculated vertical gradients	Gradients calculated by potential field operations on the total-field data and compared to the gradient measured by the one vertically offset sensor	Noise level of calculated gradient ≤ measured gradient Better than 0.99 correlation between measured and calculated gradients	Met, correlation coefficient 0.997

Performance Objective	Confirmation Method	Expected Performance	Performance Achieved
Accuracy of equivalent layer	Comparison of data predicted by equivalent layer at 2 m altitude compared to data predicted by upward continuation of ground-based data	Better than 0.95 correlation between equivalent layer and upward continued ground-based data at 2 m elevation	Not evaluated due to limited data fit with an equivalent layer
UXO parameter estimate repeatability	Size and dipole angle estimates of the calibration items consistent	Size <50% Angle relative to earth's field < 20º	Met. Size < 30% Angle < 10º.
Operating parameters (altitude, speed, production level)	Values calculated using average and mean statistical methods to compute each parameter.	1-3 m AGL; 10-30 m/s (20-60 knots); 300 acres/day	Altitude = 1.6 – 2.0m (depending upon survey area); speed = 15 – 25m/s (depending upon survey area); production rate = 290 acres/day
Rotor noise suppression algorithm at high speed	Comparison of high and low-speed results over validation line targets to verify correct operation of rotor noise suppression algorithm when the signal frequency overlaps the rotor noise frequency	Planed: Fit results of dipoles on validation-line survey collected at high-speed within 5% of low-speed, low-pass filtered data After survey: Used visual assessment of low-pass and rotor noise suppressed data on validation lane	Met, using semi-quantitative criteria
Data density/ point spacing	Along track: (# of sensor readings/second) / airspeed. (Across track: sensor line spacing = 0.75m)	0.1 -0.3 m along-track (0.2 m at 100 Hz sample rate, 20 m/s ground speed) 0.75 m cross track	0.15 – 0.25m along track, 0.75m cross track (worst case)
Survey coverage	Surveyed acres / Planned survey acres	>0.95 of planned survey area	Met, 0.99

5.1 EASE OF USE

'Ease of use' is a qualitative performance metric that we assume is met when the survey is performed with satisfactory results in the time period predicted as was the case for this demonstration. With the exceptions of the new helicopter platform (MD350F) and the implementation of a telemetry system to remove the system operator from the aircraft, this deployment was very similar to previous demonstrations of the HeliMag technology.

Although the telemetry system worked well, there were some software glitches that made the utilization of this system less than seamless, necessitating occasional rebooting of the data acquisition system. These problems were non-critical and will be resolved prior to any subsequent deployments.

SKY has performed a number of surveys with the MD350F. However, this was the first opportunity to test and compare the performance of this aircraft with that of the original Bell 206L platform. During the survey the pilot experienced difficulty flying as low as the previous survey. After modifications were made to the boom mounting system, a satisfactory survey altitude was achieved. (discussed in greater detail in section 5.10)

5.2 GEO-REFERENCE POSITION ACCURACY

The positions estimated from the validation lane are shown in Figure 15. The maximum position error is 28 cm in Easting and 34 cm in Northing, with a mean-square error of 9.7 cm Easting and 12.7 cm Northing. Several of the items appear to be consistently biased (e.g. the 100 pound bomb is about 20 cm biased in both easting and northing). Because this bias is consistent for each target, (and not consistent for each survey pass) we assume that the error is related to the ground truth measurement of the target position. After correcting for the bias in each validation item, the mean-square error falls to 4 cm in Easting and 5.6 cm in Northing, with maximum errors of 11 cm in Easting and 19 cm in Northing.

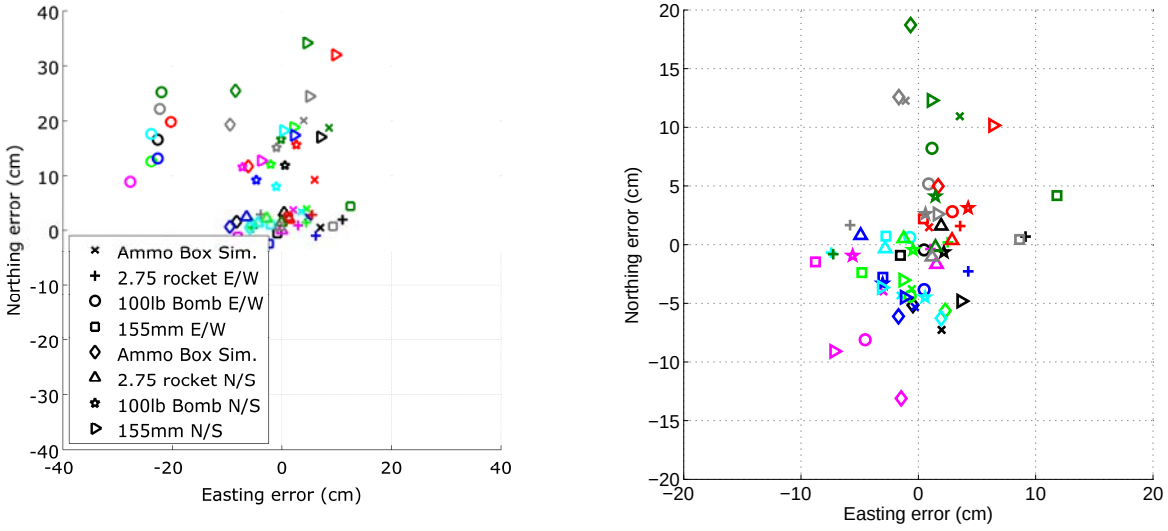

(a) Raw comparison (b) After adjusting for bias

Figure 15. Estimated locations of items on the validation lane for all 4 days with the lane flown twice per day. In (a) the raw results are shown while in (b) the results are shown after adjusting for bias. The results are shown in different colors for each pass over the validation line.

5.3 DETECTION PERFORMANCE

The detection performance was assessed by analysis of three scenarios. Where available, we used vehicular towed magnetic array (ground) as ground truth to compare and contrast the 'old' HeliMag (AMTADS) data set collected in 2005 with the data collected as part of this demonstration. In areas where we only have the 2005 and 2009 airborne data we compare and contrast the relative performance of the two systems. Finally, we report the detection performance of the next generation HeliMag system against blind seeded targets.

5.3.1 Scenario 1: Ground Vehicle, 2005 AMTADS and 2009 HeliMag data.

For the small subset of data where there was overlapping next generation HeliMag, vehicular and existing AMTADS data we upward continue the ground data by 1.5m to approximate the same data acquisition altitude of the airborne data sets. We used an automated target picking algorithm, (Geosoft's 'peak detection' routine) on each of the data sets and plotted detection performance as a function of detection threshold. On the left panel of Figure 16 we show that the ground data set displays the lowest number of detections and has the lowest inflection point of all of the data sets, and the next generation system displays a highest number of detections and highest inflection point. This result implies that the 2009 HeliMag data are noisier than the 2005 data. However, this result does not account for the differences in filtering of the two data sets. Because the 2005 data have been subjected to a more aggressive low-pass filter than the 2009 data, it follows that the total number of detections and the inflection point are lower. After normalizing the detection thresholds using the derived noise for each data set, there is no apparent difference between the two sets. On the right panel of Figure 16 we plot the number of detections as a function of SNR threshold. We calculated the noise as the standard deviation of the AS sampled at 100 points in the survey area that were visually non-anomalous. The noise

values obtained for the ground, AMTADS 2005, and HeliMag 2009 data were 0.1, 0.4 and 0.5 nT/m respectively.

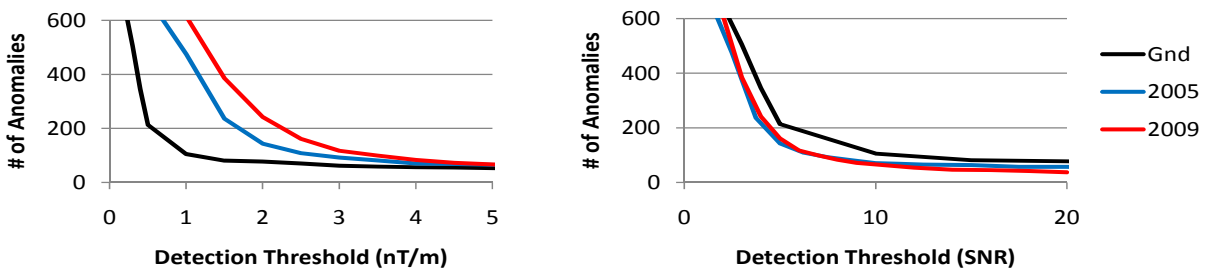

Figure 16. Total detections in Area 2a as a function of detection threshold for ground-based towed array, AMTADS (7 sensors, low-pass filtered) collected in 2005, and HeliMag (13 sensors, de-noised) collected in 2009. The right panel shows results for thresholds that have been normalized by the sampled noise of each system (0.1, 0.4, and 0.5 nT respectively)

Using the ground detections as our 'ground truth' we compared the detection perfomance of the two systems. For this analysis we determined that all ground anomalies with a signal higher than 1nT/m are considered our 'ground truth' anomalies. Valid detections are declared when an airborne anomaly falls within a 2m halo around the ground truth position. We relaxed our halo constraint to 2m because of inaccuracies inherent in simple peak detection due to spatial sampling and grid cell size limitations. As we lower our detection threshold for the airborne systems, the number of ground truth detections increases along with the total number of detections. We derive the probability of detection (Pd) as the number of detected ground truth anomalies divided by the total number of ground truth anomalies. We plot this value as a function of the total number of anomalies detected to derive the simulated Receiver Operating Characteristic (ROC) curves shown in Figure 17.

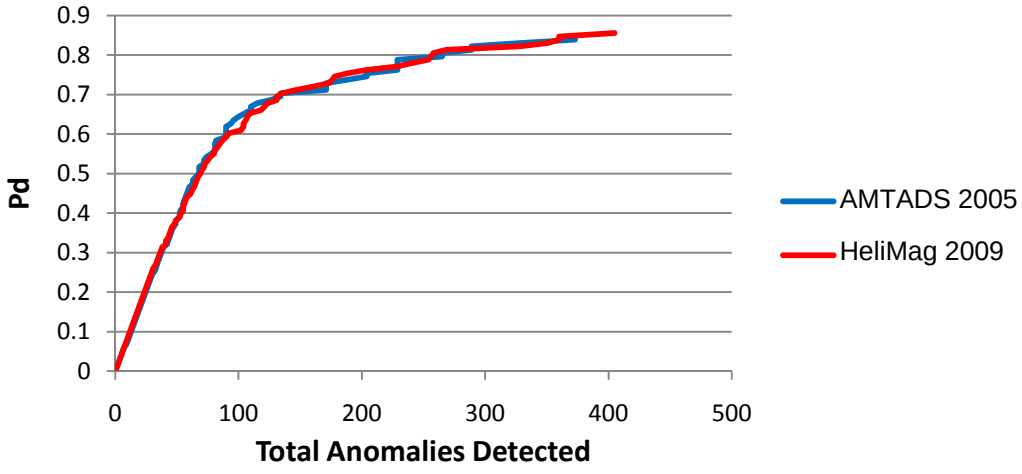

Figure 17. Pseudo ROC curves for detection performance of the AMTADS 2005 and HeliMag 2009 data against upward continued ground vehicle targets.

These results show no apparent improvement in the 2009 data set relative to the 2005 data set. However, there are a couple of factors which must also be considered before we can draw this conclusion. When we visually compare the three data sets (Figure 18) we notice that the background geologic response (as well as the anomalous responses) in the upward continued

data is suppressed relative to the airborne data sets. The circles on this figure highlight an example of geologic response that is common to both of the airborne data sets but is not visible on the ground data. This would indicate that the many 'false alarms' in the airborne data are due to detection of features that have been removed from the ground data that we are using as 'ground truth'. Furthermore, because of the different filter approaches, the 2005 AMTADS data appear muted relative to the 2009 HeliMag data or conversely the 2009 data set appears to be more sensitive than the 2005 data.

This observation holds true if we plot the number of detections vs detection threshold (Figure 19). We also present the same results after normalizing the detection threshold by the background noise of both systems to account for the different filter regimes of each system.

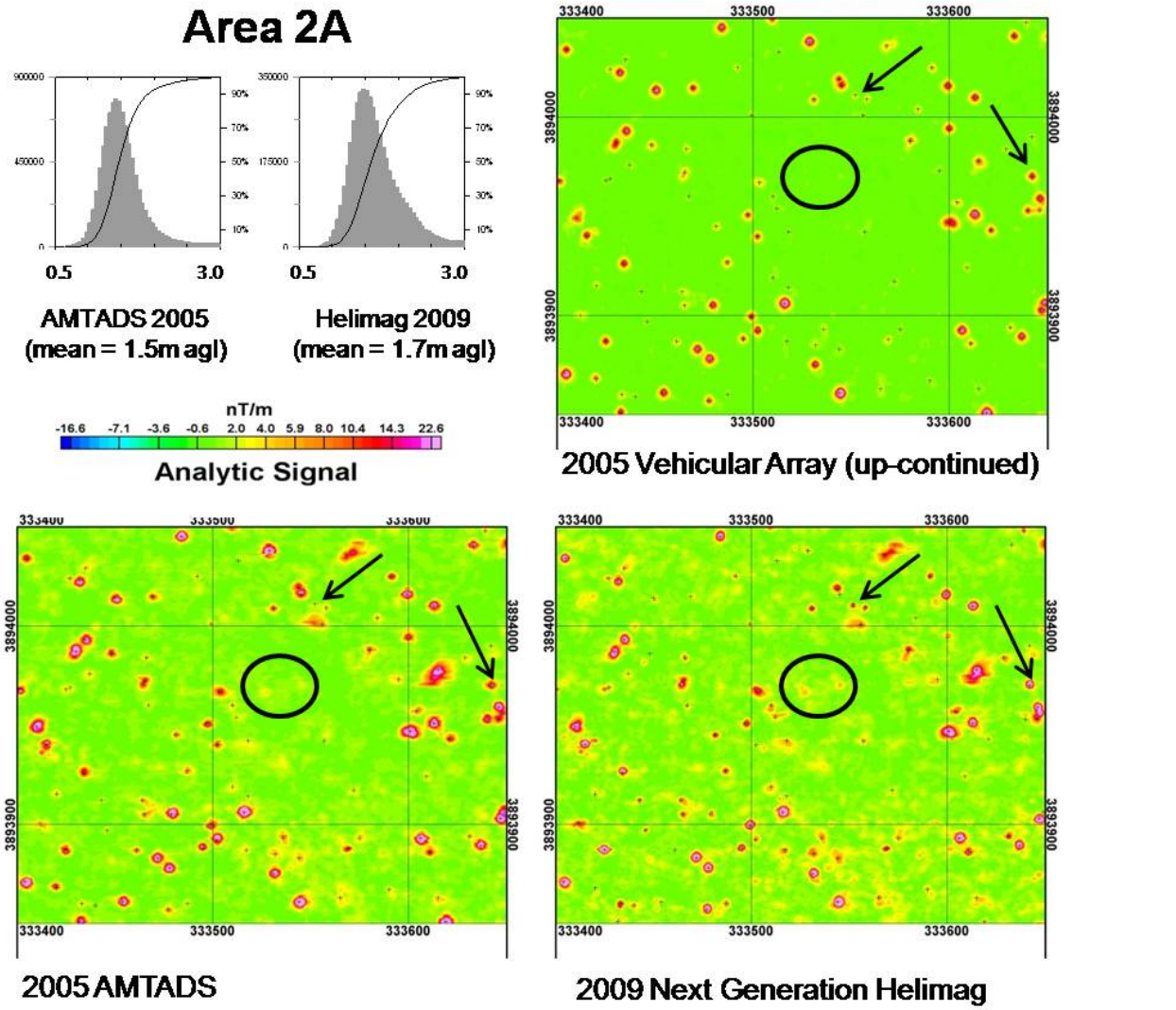

Figure 18. Qualitative comparison of upward-continued ground-based, AMTADS (7 sensors, low-pass filtered), and HeliMag (13 sensors, de-noised) data sets. The AMTADS data were collected at a lower survey elevation but the anomaly amplitudes appear muted due to the low-pass filter. Anomalies and background noise in the upward continued ground data appear suppressed.

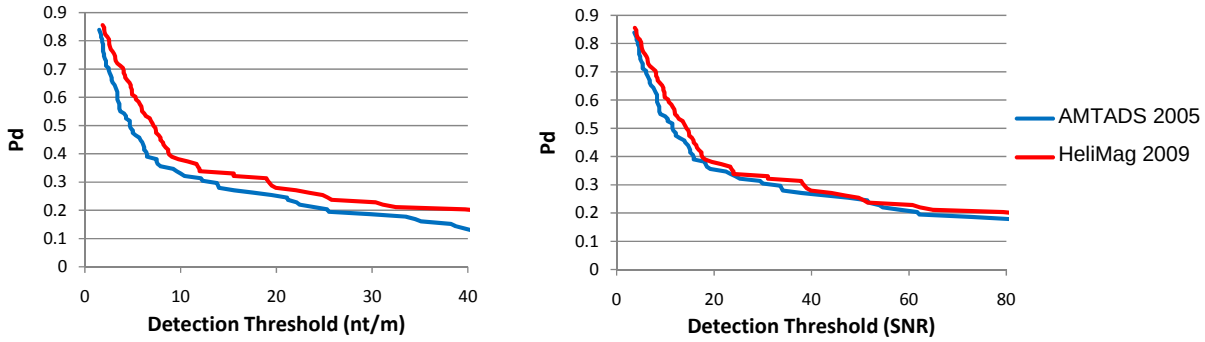

Figure 19. Pd (vs upward continued ground data) for AMTADS 2005 and HeliMag 2009 data. Note that the HeliMag data performs better at a given detection threshold in spite of the fact that these data were collected at a higher survey elevation.

A second factor that must be taken into account when comparing the performance of the 2005 AMTADS data with the 2009 HeliMag is the difference in survey altitude. As discussed in section 5.10, the 2009 mean survey altitude for the Central North area was 1.66m agl. This is a little more than 10% higher than the mean survey altitude of the 2005 AMTADS survey. As previously noted, survey altitude is the most dominant determinant of detection performance. It follows then that the comparison of the two systems performance is significantly affected by the difference in survey altitude. In an effort to remove this as a factor in the comparison of the systems, we can use the 2009 data to simulate the 2005 survey configuration and filtering methodologies. We created comparison data sets and analyzed these data sets using the same approach as described above. In Figure 20 we present the results of this comparison for 4 data sets:

1) 13 sensors and de-noised data (the current 2009 HeliMag configuration);
2) 13 sensors and low-pass filtered data;
3) 7 sensors and de-noised data; and
4) 7 sensors and low-pass filtered data (simulating the 2005 AMTADS configuration and filter methodology).

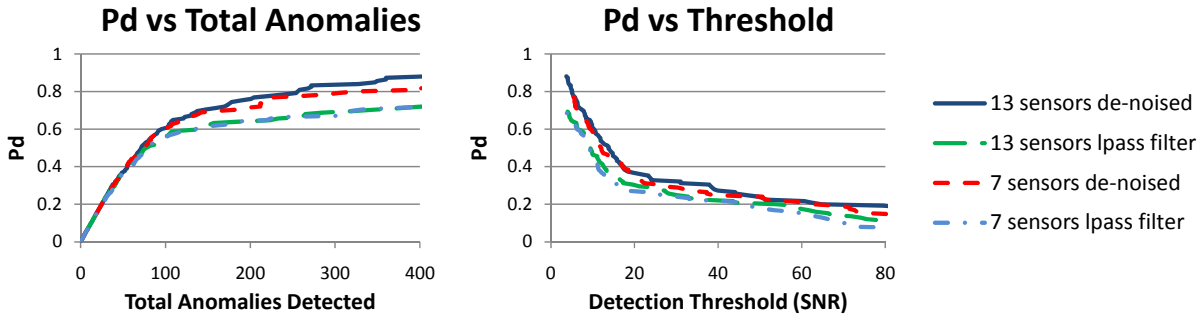

Figure 20. Pd performance against upward continued ground-based towed array data with various sensor spacing/ blade noise filtering configurations. The current HeliMag configuration is 13 sensors, de-noised. The 7 sensor, low-pass filter configuration simulates the 2005 AMTADS system.

A comparison of the relative SNR performance of the simulated AMTADS data with the actual AMTADS data indicates that the SNR of the simulated data are on average only 87% of the 2005 AMTADS responses (Figure 21). Assuming a 1/(distance)^3 fall off, this is consistent with the expected reduction in signal strength due to a 5-10% increase in survey altitude. A more detailed SNR discussion is presented in section 5.6.

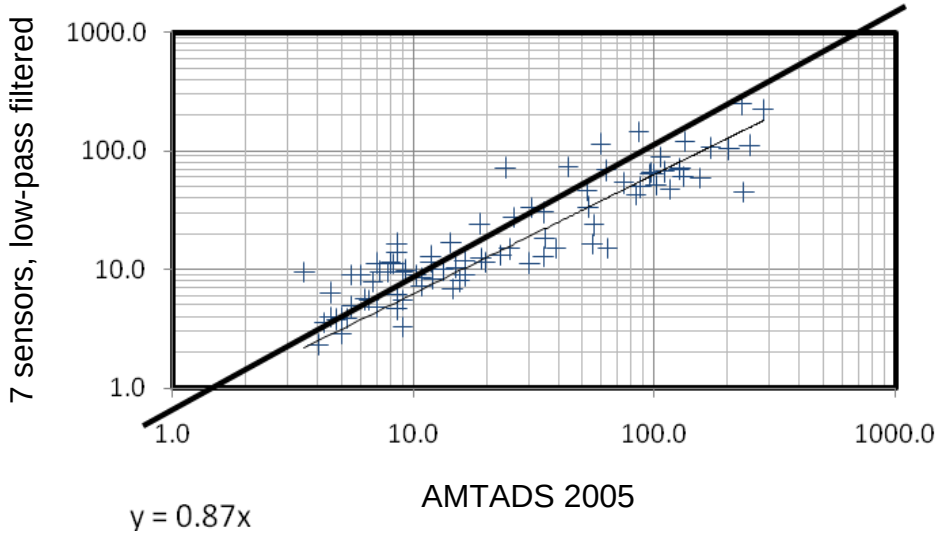

Figure 21. Signal/Noise comparison of simulated AMTADS data, flown at 1.7m agl with the 2005 AMTADS data (flown at 1.5m agl), the simulated data SNR are on average 0.87 that of the 2005 AMTADS. This is consistent with the difference in survey elevation.

From these results we can draw a number of conclusions:

- The current configuration and noise removal filter result in significantly improved detection performance.
- The low-pass filter results in an apparently lower noise floor, but the benefits of this lower noise floor appear to be negated because the anomaly amplitudes are also reduced (thus the lower Pd vs. threshold results)
- The low-pass filter also negates the advantages of the finer sensor spacing.

5.3.2 Scenario 2: 2005 AMTADS and 2009 HeliMag data.

For regions with only AMTADS and next generation HeliMag data we conducted a similar analysis. For each data set we perform the same automatic anomaly detection as described above. The SNR for each target was calculated, where the signal is the analytic signal value found at each peak and the noise is the standard deviation of 200 analytic signal values found at randomly selected points across the survey area. The analyst selected these points in areas that were not visually anomalous. In Figure 22 we compare the detection vs. threshold of the two data sets. On the left panel we show the total number of detected targets as a function of the analytic signal detection threshold. On the right the detection threshold is normalized by the noise (calculated as described above) to account for differences in filters and associated base noise levels. In either case, the 2009 data has a higher detection rate but also has a higher inflection point. The higher rate of detection at a given threshold indicates greater signal amplitudes, in spite of the fact that the 2009 data were collected at a slightly higher altitude. This leads us to conclude that the 2005

peaks are slightly smoothed by the low-pass filter, resulting in both the lower detection rates and a lower inflection point.

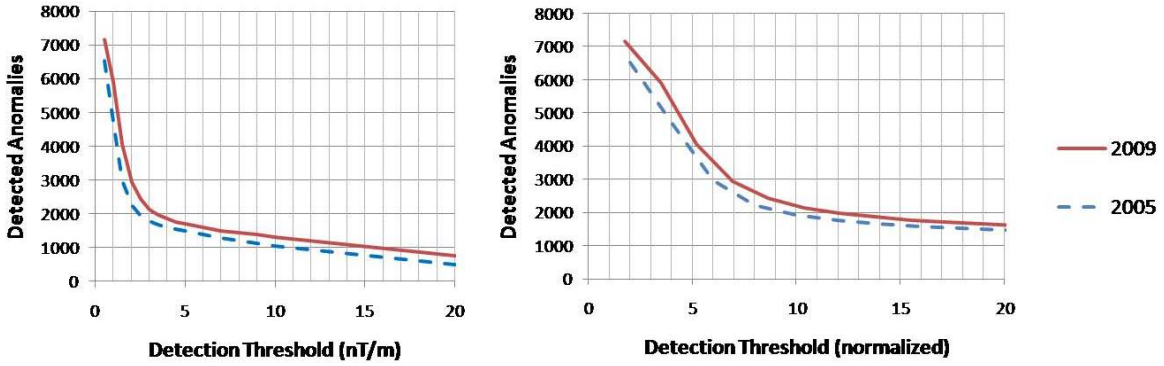

Figure 22. Total detections vs threshold comparison between AMTADS data collected in 2005 and the recently collected HeliMag data. These data are from the Central North area where the mean survey altitude was 1.5m for the 2005 survey and 1.7m for the 2009 survey.

In the absence of independent ground truth, we compared the detection performance of the two data sets by first assuming that the 2005 data are the 'truth' and assessed the performance of the 2009 data against this data set. We then reversed the data sets and performed a similar assessment with the 2009 data assumed as 'truth'. Each assessment was performed by generating pseudo ROC curves plotting the probability of detection (Pd) against the percentage of 'false alarms' (%FA). The Pd is equal to the number of detected anomalies/total number of 'true' anomalies. The %FA is equal to (total number of detections – number valid detections)/ number of valid detections. In each case, the SNR of the 'true' anomalies is limited to 10 to ensure that the anomaly is valid. The results are presented in Figure 23 where we see that the 2009 data performed better against the 2005 data than the 2005 data performed against the 2009 data. It is interesting to note that the detection rates for both systems was less than 90%. This phenomenon is attributed to the presence of spatially large anomalies with small amplitude, poorly defined peaks resulting in imprecise positioning of these peaks by the automatic detection algorithm.

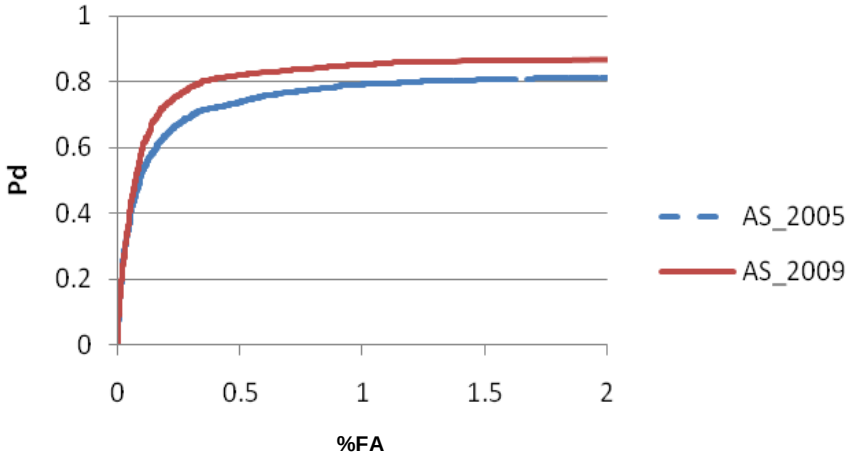

Figure 23. Detection performance of the 2005 AMTADS system against the HeliMag 2005 assumed ground truth (blue line) and the reciprocal analysis showing the detection performance of the HeliMag data vs the AMTADS data assumed as ground truth (red line).

5.3.3 Scenario 3: Detection of Blind Seeded Targets

5.3.3.1 60 and 81 mm mortars in the Central North Seed Area

The ESTCP program office arranged for the blind (to SKY) seeding of 80 targets in the Central North area. These were equally divided between 81 and 60 mm mortars. After processing of the geophysical data, the SKY analyst manually selected targets from the gridded results. Each target was analyzed using the SKY dipole fit algorithm to derive 6 parameters that define the position, orientation, and size of the best fit dipole as well as a 7^{th} parameter that is measure of the goodness of fit of the modeled dipole to the observed data. These parameters were used to refine the target position and classify the target. Each target was assigned one of the classes provided in Table 8.

Table 8. Classes used in the interpretation of the Seed area data.

Class #	Class Name	Classification criterion
1	Potential small UXO	Apparent remanence less than 70% and best matched to a 60 or 81 mm mortar
2	Potential med. UXO	Apparent remanence less than 70% and best matched to a 105 or 155 mm projectile
3	Potential large UXO	Apparent remanence less than 70% and best matched to a 100 pound bomb
4	Low confidence small UXO	Apparent remanence greater than 70% and best matched to a 60 or 81 mm mortar
5	Low confidence med. UXO	Apparent remanence greater than 70% and best matched to a 105 or 155 mm projectile
6	Low confidence large UXO	Apparent remanence greater than 70% and best matched to a 100 pound bomb
7	Low confidence metal	Dipole depth greater than 3.95 m (regardless of apparent remanence)
8	Poor dipole fit	Dipole fit correlation coefficient <.8

A total of 982 targets were classified and submitted to the Institute for Defense Analyses (IDA) via the ESTCP Program Office for scoring. An emplaced target was declared detected if a submitted target position was within a 1.5m halo of the emplaced target position. The scoring results as provided by IDA are presented in Table 9.

Table 9. Scoring results as generated by IDA for the seed targets in the Central North area.

Halo Radius	UXO Type	Total # Seeds	# Seeds Detected	Pd	Mean (Xi)	Mean (Yi)	Sdev (Xi)	Sdev (Yi)	Mean (dist)	Std Dev (dist)
0.5m	All	80	33	0.41	0.03	-0.07	0.23	0.16	0.27	0.10
0.5m	81mm	40	29	0.73	0.01	-0.07	0.23	0.16	0.26	0.10
0.5m	60mm	40	4	0.10	0.14	-0.05	0.28	0.22	0.33	0.12
1m	All	80	49	0.61	0.08	-0.14	0.32	0.30	0.40	0.23
1m	81mm	40	40	1.00	0.11	-0.08	0.32	0.24	0.37	0.21
1m	60mm	40	9	0.23	-0.06	-0.39	0.29	0.38	0.55	0.26
1.5m	All	80	49	0.61	0.08	-0.14	0.32	0.30	0.40	0.23
1.5m	81mm	40	40	1.00	0.11	-0.08	0.32	0.24	0.37	0.21
1.5m	60mm	40	9	0.23	-0.06	-0.39	0.29	0.38	0.55	0.26

All of the targets that were detected were within a 1m halo of the emplaced target position and 67% of the detected targets were within a 0.5m halo. 100% of the 81mm targets were detected with a mean miss distance of 0.37m. Only 23% of the 60mm targets were detected, with a mean miss distance of 0.55m. Overall this performance is better than earlier documented detection performance against 81mm. In 2003 a test was performed with similar site conditions at the Isleta Pueblo. For this test only less than 50% of the 81mm targets and only 20% of the 61mm targets were detected. (Tuley and Dieguez, 2005).

In the left panel of Figure 24 we show the SNR levels of each of the targets. The signal levels are calculated by sampling the AS grid at the ground truth positions of the emplaced targets. The noise was calculated as the standard deviation of 200 randomly positioned AS samples (identified by the analyst as non-anomalous). The solid black horizontal line at SNR=8 shows a reasonable cut off threshold, below which targets become very difficult to detect. As described earlier, we can use the recent HeliMag data to simulate the original AMTADS configuration and filter process. On the right side of Figure 24 we can see that the seeded target SNR values are significantly reduced for the simulated AMTADS data and using the same threshold it is apparent that the detection performance would have been significantly less.

As mentioned above, the target selections were performed manually by the SKY analyst. In practice the analyst uses an auto-detection routine with a conservative cut-off threshold – in this case the threshold was 4 nT/m (SNR = 8). The analyst then augments the auto-detected target list with manual additions and deletions. This explains how we can detect some targets that are apparently below the auto-picker cut-off threshold as well as how some missed targets have significantly greater SNR values than some detected targets.

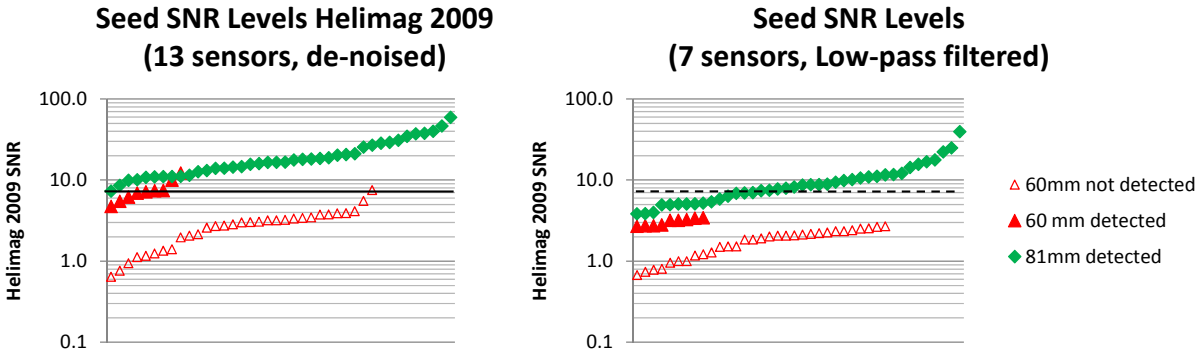

Figure 24. Seeded target SNRs for the HeliMag system (left panel) and simulated AMTADS system (right panel). Signal levels were determined by sampling the analytic signal grids at the seeded ground truth positions, and noise levels were determined as the standard deviation of 200 samples taken in visually quiet positions distributed throughout the Central North area. The horizontal black line mark the auto-picker cut-off threshold used by the analyst.

We can use the automatic target detection routine to sample targets at a series of different thresholds and produce a pseudo ROC curve that shows the detection performance as the threshold moves down into the noise (bottom left panel of Figure 25). Because we are not attempting to discriminate and do not have an independent measure of false alarms, we simply show the number of detected anomalies that are required to attain a given Pd. At a Pd of 0.6 there is a significant inflection point in this curve where the number of detections required to improve the Pd increases dramatically. In the right side of Figure 25 we plot the Pd and the number of detections as a function of SNR threshold for the HeliMag system (upper panel) as well as for

the simulated AMTADS (lower panel). The solid vertical black line on the HeliMag 2009 chart indicates the cut-off threshold of 8 used by the analyst. The dashed black line on the simulated AMTADS chart shows the position of an equivalent cut-off threshold. The tighter sensor spacing afforded by the 13 sensor system, combined with the new de-noising algorithm result in a higher detection rate at similar SNR thresholds.

Although the Pd on these curves reaches 1, in practice the upper Pd limit is constrained by the noise. Below a threshold of 5, the additional number of total detections associated with gains in Pd rises dramatically.

In an attempt to refine target lists and separate targets of interest from targets due to other sources (such as geology, and non-UXO-like metal debris) we use the dipole fit derived features to classify each anomaly. Without an extensive ground truth program, we were not able to assess the performance using standard Pd vs. Pfa ROC curves. However we can infer the efficacy of the classification approach by comparing the classification distribution for the seeded targets that were detected with the distribution for the entire set of anomalies (Figure **26**). All of the detected anomalies were classified correctly as small UXO, and only 16% of these were 'low confidence' declarations. Of all of the anomalies reported, only 36% were declared to be small UXO (22% low confidence). These results imply that dipole fit analysis and classification is a useful tool to reduce the total number of targets and refine the target lists.

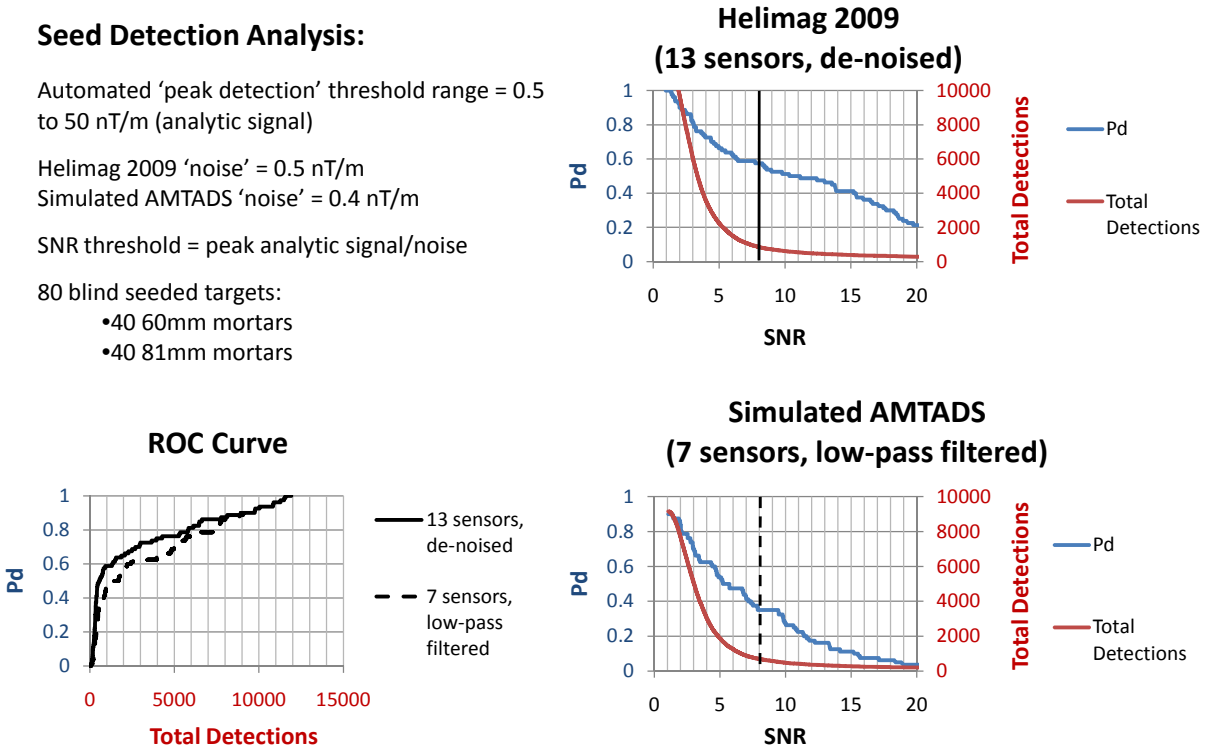

Figure 25. Pseudo ROC curves for seeded targets (bottom left), and graphs of total detections and Pd plotted as a function of SNR cut-off threshold for the HeliMag data (upper right) and simulated AMTADS data (lower right). The vertical black lines mark the auto-picker cut-off threshold.

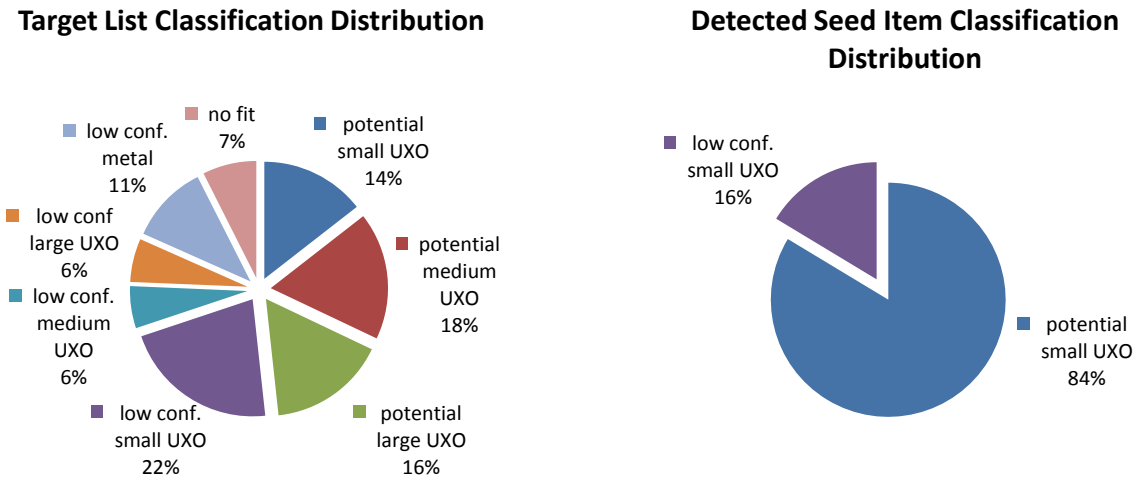

Figure 26**. Comparison of target classification distribution between all 983 targets in the seeded area (left) and the 49 detected seeds (right).**

5.3.3.2 Detection results in the geologically challenging Western seed area.

In the Western Seed Area, the Program Office emplaced 110 seeds in a geologically "challenging" environment. These comprised a mix of 81mm and 4.2" mortars, 105 mm HEAT-rounds (HR), and 105 mm and 155 mm projectiles. Detection results are provided in Table 10. With a detection halo of 0.5 m, 84% of items were detected. Increasing the detection halo resulted in 94% detected at 1.0 m and 96% detected at 1.5 m. At the 1.0 m halo 7 of 12 81 mm mortars, 13 of 14 105 mm HEAT-rounds, all 8 105 mm projectiles and all 52 4.2" mortars plus 23 of 24 155 mm projectiles were detected. When the detection halo is increased to 1.5 m all items except 4 of the 81 mm mortars were detected. Close inspection of the anomalies detected at halos between 1.0 and 1.5 m reveals that the dipole fits were quite poor (Figure 27). The poor fits arise because the default mask is too large and the dipole model is skewed in an effort to fit the underlying geology. In general, we only conduct a cursory and limited QC of the dipole model fits (rather that the full QC that we would conduct when dig/no dig decisions are made). After remasking and inverting each of these anomalies (e.g. Figure 28), the detection results at 1.0 and 1.5 m halo are the same with the exception of one 155 mm projectile. Only part of this anomaly was surveyed at our maximum acceptable ground-clearance of 3.0 meters, with any data above that height eliminated from the data used for interpretation. An anomaly was selected by the analyst at distance of 1.2 meters from the SEED location, but an acceptable dipole fit could not be obtained. Note that there is one additional 81 mm mortar that was originally placed 1.6 m from the seed location that falls within the 1.0 m detection halo after remasking/inversion.

Table 11 lists the number of seed items assigned to each category compared to the total number of detections in each category. 99% of the seed items are placed in the high-probability UXO categories (small, medium and large), which constitute just over 50% of the total detections. Figure 29 plots the number of seeds versus non-seeds recovered when the target detections are ordered by apparent remanence. 105 of the 107 detected items occur within the first 40% of the prioritized target list. Note that we have no information regarding the identity of the non-seed items: many of them may in fact be UXO. These results demonstrate one significant advantage of the decreased sensor spacing in the new boom: an improved ability to estimate dipole parameters and a corresponding improvement in the ability to classify detections as high probability UXO or not.

Table 10. Seed detection results in the Western Seed area. Results are also shown when several poorly fit anomalies are reinverted. Statistics on positions were generated using the original inversion results.

Halo Radius	UXO Type	Total # seeds	# Seeds Detected	Pd	# Seeds Detected reinverted	Pd reinverted	Mean (Xi)	Mean (Yi)	Sdev (Xi)	Sdev (Yi)	Mean (dist)	Std Dev (dist)
0.5 m	81 mm	12	6	**0.50**	7	**0.58**	0.15	0.07	0.16	0.19	0.26	0.13
0.5 m	105 mm HR	14	11	**0.79**	12	**0.86**	0.05	0.06	0.26	0.18	0.30	0.12
0.5 m	105 mm projectile	8	7	**0.88**	7	**0.88**	0.12	0.05	0.14	0.07	0.16	0.12
0.5 m	4.2" mortar	52	45	**0.87**	48	**0.92**	-0.01	0.08	0.15	0.13	0.18	0.11
0.5 m	155 mm projectile	24	23	**0.96**	23	**0.96**	0.01	0.04	0.13	0.14	0.16	0.11
0.5 m	**All**	**110**	**92**	**0.84**	**97**	**0.88**	**0.02**	**0.06**	**0.17**	**0.14**	**0.19**	**0.12**
1.0 m	81 mm	12	7	**0.58**	9	**0.75**	0.14	0.14	0.15	0.25	0.30	0.16
1.0 m	105 mm HR	14	13	**0.93**	14	**1.00**	0.08	0.11	0.29	0.22	0.34	0.15
1.0 m	105 mm projectile	8	8	**1.00**	8	**1.00**	0.08	0.11	0.18	0.19	0.22	0.19
1.0 m	4.2" mortar	52	52	**1.00**	52	**1.00**	0.02	0.09	0.27	0.15	0.25	0.20
1.0 m	155 mm projectile	24	23	**0.96**	23	**0.96**	0.01	0.04	0.13	0.14	0.16	0.11
1.0 m	**All**	**110**	**103**	**0.94**	**106**	**0.96**	**0.04**	**0.08**	**0.23**	**0.16**	**0.24**	**0.18**
1.5 m	81 mm	12	8	**0.67**	9	**0.75**	0.27	0.15	0.39	0.23	0.41	0.35
1.5 m	105 mm HR	14	14	**1.00**	14	**1.00**	0.13	0.16	0.34	0.28	0.40	0.26
1.5 m	105 mm projectile	8	8	**1.00**	8	**1.00**	0.08	0.11	0.18	0.19	0.22	0.19
1.5 m	4.2" mortar	52	52	**1.00**	52	**1.00**	0.02	0.09	0.27	0.15	0.25	0.20
1.5 m	155 mm projectile	24	24	**1.00**	24	**1.00**	0.03	0.09	0.17	0.25	0.20	0.24
1.5 m	**All**	**110**	**106**	**0.96**	**107**	**0.97**	**0.06**	**0.10**	**0.27**	**0.20**	**0.27**	**0.24**

Table 11. Number of seed items and detected items in each category for the Western Seed Area.

Class Name	Number of seeds	Number of detections	% of seeds	% of detections
Potential small UXO	12	88	11.2%	3.2%
Potential med. UXO	63	644	58.9%	23.4%
Potential large UXO	31	705	29.0%	25.6%
Total high probability UXO	**106**	**1437**	**99.1%**	**52.3%**
Low confidence small UXO	0	138	0.0%	5.0%
Low confidence med. UXO	0	450	0.0%	16.4%
Low confidence large UXO	0	510	0.0%	18.5%
Low confidence metal	0	54	0.0%	2.0%
Poor dipole fit	1	161	0.9%	5.9%
Total Number	**107**	**2750**		

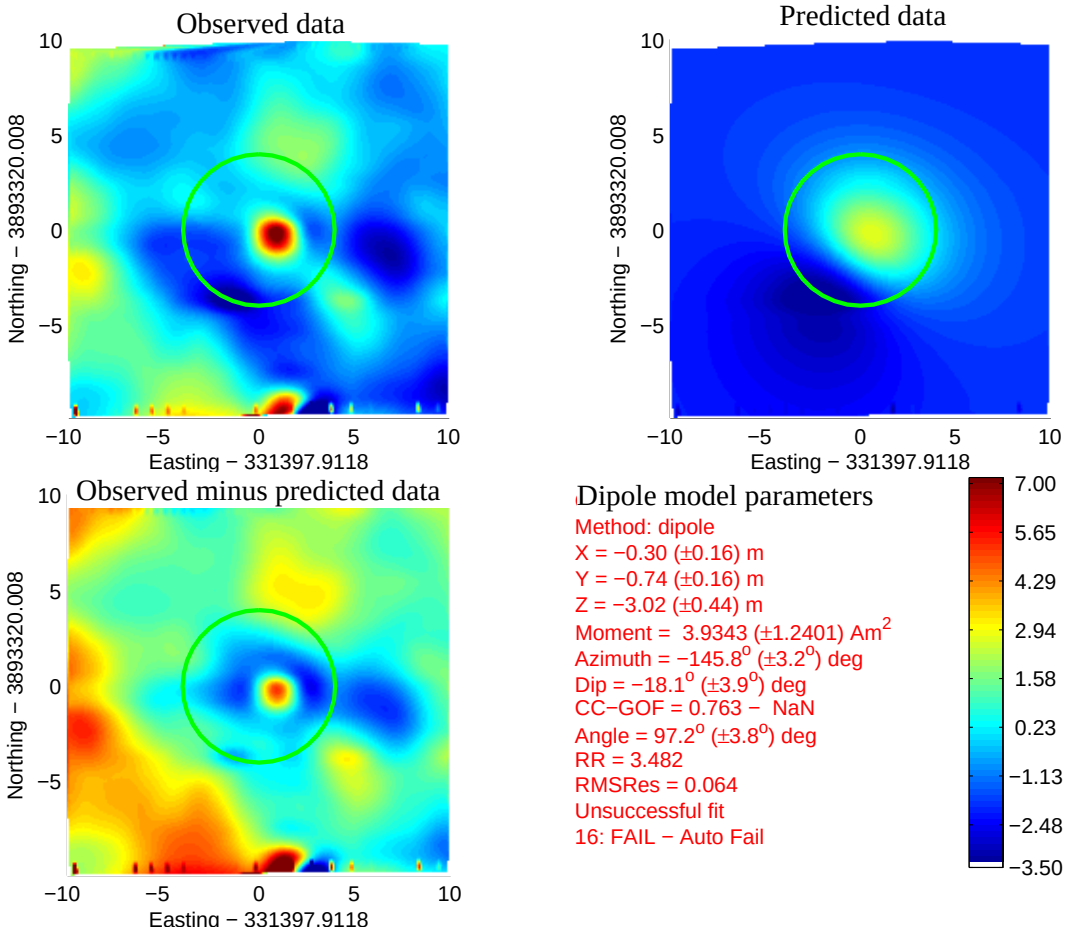

Figure 27. Original dipole fit to anomaly number 1481. The mask is too large and the dipole model is biased by the nearby geological feature.

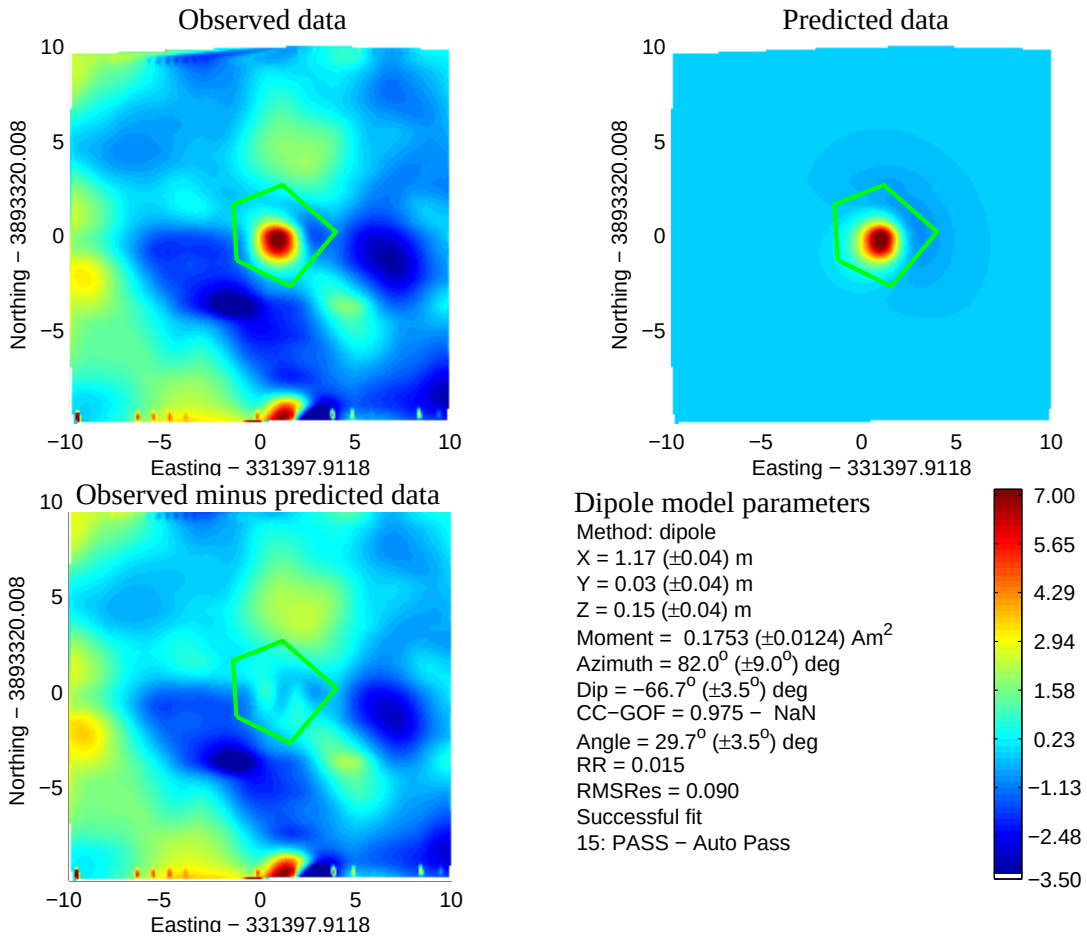

Figure 28. Revised dipole fit to anomaly number 1481.

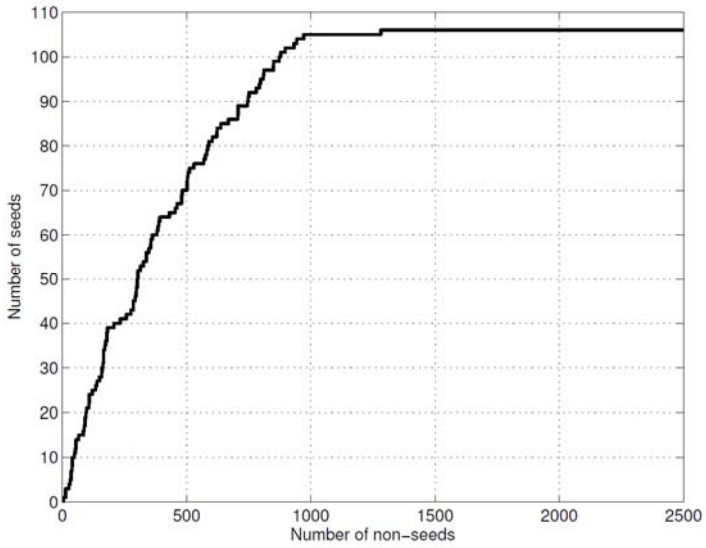

Figure 29. When ordered by apparent remanence, the number of non-seed items detected versus the number of seed items detected (Western Seed Area).

5.4 TELEMETRY LINK

The DAS recorded data from the moment the helicopter took off until landing. The operator monitored the quality of the collected data and maintained a log that recorded the times when the telemetry link was lost and then regained. This log was used to calculate the percentage of time during survey that the link was maintained. There were three different set-up locations used for the telemetry system (Figure 8). As recorded in the file-tracking spreadsheet in Table 19, the telemetry link was maintained for between 70 and 100% of the time during each survey event. For most survey events the telemetry link was maintained all the time. Conservatively, we estimate we maintained the link for 95% of the time.

5.5 NOISE LEVEL

Prior to commencement of the survey we collected high altitude data to determine the intrinsic system noise levels. We applied the same noise removal methodology to the raw data as was used for the survey data. This methodology involves removing the blade noise using the new de-noising algorithm, applying compensation corrections to the data to remove the effect of changing aircraft attitude, then applying a de-median filter to remove long wavelength signals (e.g. diurnal fluctuations and geologic response) from the data. We calculated the standard deviation of the data in each sensor during one of the high-altitude compensation flights (Table 12). This process over-predicts the noise level as the compensated data do contain some artifacts due to uncorrected heading maneuvers. The intrinsic noise was found to be better than 0.42 nT on all sensors. The noise-levels on a 20 second section of data without large changes in helicopter orientation are reduced by about a factor of two from the noise levels calculated using the entire compensation flight (Table 12). For the vertical gradient, the measured and calculated gradients at the central sensor are approximately the same with a standard deviation of 0.1 nT/m. These standard deviations were computed using the whole calibration flight are larger than the effective intrinsic noise level in the gradient component. On the same 20 seconds considered earlier the standard deviations of both calculated and measured are approximately 0.08 nT/m.

Table 12. Standard deviations of the compensated (but not filtered) high-altitude data. The average is calculated over all 13 sensors.

Sensor number	Standard deviation (nT)	Standard deviation 20 s section (nT)	Sensor number	Standard deviation (nT)	Standard deviation 20 s (nT)
1	0.33	0.12	8	0.41	0.30
2	0.37	0.14	9	0.37	0.31
3	0.41	0.15	10	0.34	0.29
4	0.41	0.18	11	0.27	0.26
5	0.39	0.21	12	0.21	0.22
6	0.39	0.24	13	0.20	0.19
7	0.42	0.28			
Average	0.35	0.22			

5.6 SNR IMPROVEMENT

As discussed in section 3.3.6, we anticipate an improvement in the SNR performance of the system. This improvement is due to two factors: the tighter sensor spacing (thus closer sensor-target distances, and increased signal for those targets that would otherwise have been in between the 1.5m spaced sensors) and improved noise rejection techniques. The advantage of increased signal afforded by the closer sensor spacing diminishes with survey altitude and becomes insignificant at survey altitudes that are twice the sensor spacing (Billings and Wright, 2008). Survey altitude is the dominant determinant of target signal amplitude and consequent SNR performance. For those sites flown where the survey altitude achieved in 2009 is significantly higher than that of the 2005 survey, we do not anticipate a significant improvement. However when we compare SNR performance on a site such as the Central North area where the survey altitude was comparable, we are able to obtain a valid comparison. For this site we compare the SNR of the next generation HeliMag to the SNR of the data collected with the original 7 sensor system in 2005.

Because of the dipolar nature of the total magnetic field response we use the Geosoft derived 'analytic signal' (total gradient) grids to simplify the SNR comparisons. For all of the SNR comparisons, the noise was determined as follows: Approximately 200 positions were manually selected by the analyst in a pseudo random manner where the only constraints were to avoid anomalous 'targets' and representatively sample the entire grid. For each grid, the noise was determined to be the standard deviation of the values extracted at these positions. Because of sampling and grid cell size effects, the anomaly peaks between data sets will not necessarily occur in the exact same location, so the peak detector was run on each data set and the anomalies were correlated based upon positions using a 2m halo. The SNR value for each position is then determined to be the peak analytic signal value / noise.

In Figure 30 we plot the 2009 SNR values as a function of the 2005 SNR values. As expected, there is considerable variation between individual values due to the altitude variations common to airborne surveys. In this case, the 2009 SNR values are on average 1.18 times that of the 2005 data.

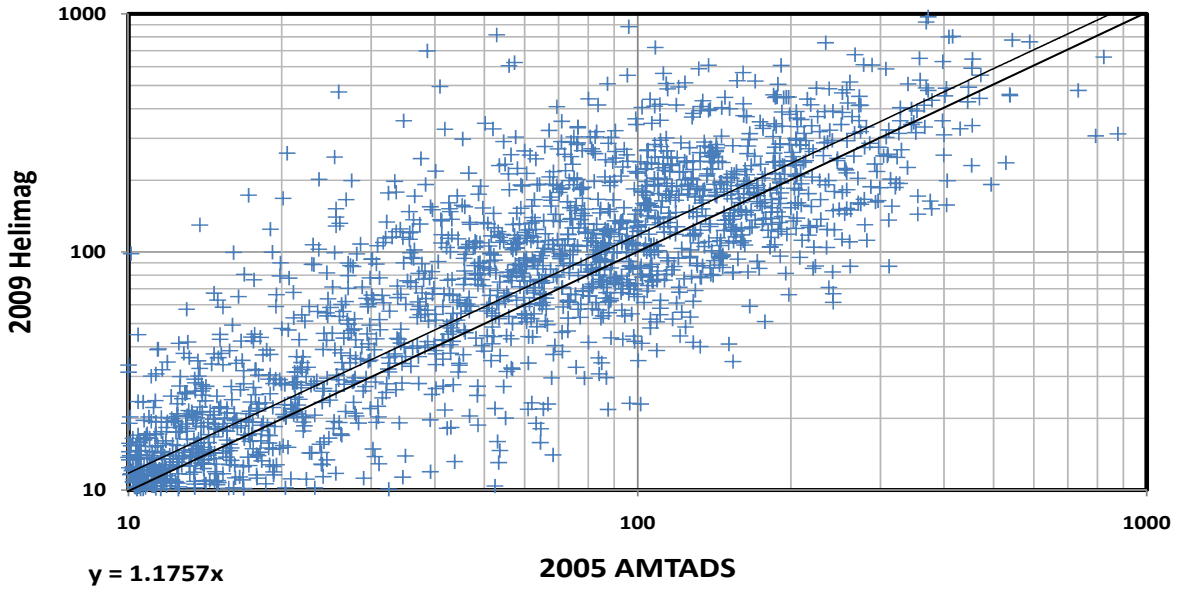

Figure 30. Comparison of the HeliMag 2009 vs the AMTADS 2005 target SNR levels in the Central North Area. At each point the peak analytic signal amplitude was set as the signal level and the noise for each system was calculated separately (because the difference in filter methodologies result in differing geologic noise levels). The background noise was calculated as the standard deviation of analytic signal values sampled at 200 visually quiet points in the Central North survey area. The noise was determined to be 0.5 and 0.4 nT/m for the HeliMag and AMTADS data respectively. The HeliMag data show an 18% improvement in SNR, in spite of the fact that they were collected at a higher mean elevation.

In an effort to validate these findings, as well as isolate the source of any improvements we use the raw data collected in 2009 to simulate the older HeliMag system by processing it with the original filtering methodology and using only 7 sensors at the original line spacing of 1.5m. By comparison of our final data set with each of these improvements in isolation and together, we can quantify the improvements in SNR. Figure 31 presents the results of this analysis performed for area 2A (a subset of the Central North area). In the top left panel of Figure 31 we see that the HeliMag 2009 improvement over the 2005 AMTADS data is consistent with the results shown above. The results in the top left panel indicate that the additional 6 sensors in the HeliMag 2009 configuration result in a marginal improvement of just over 10%. This is not too surprising when we consider the considerable overlap in coverage discussed in section 3.3.6, although presumably this advantage would increase with lower survey elevations. The results in the bottom left indicate a significant improvement of just under 50% in the SNR due to the implementation of the rotor noise removal methodology. Finally, the bottom left panel shows that the modifications made to the HeliMag system result in a 70% improvement in SNR.

The relative agreement of the 7 sensor-low pass filtered SNR with that of the AMTADS 2005 data (discussed above in section 5.3.1) further validates these findings.

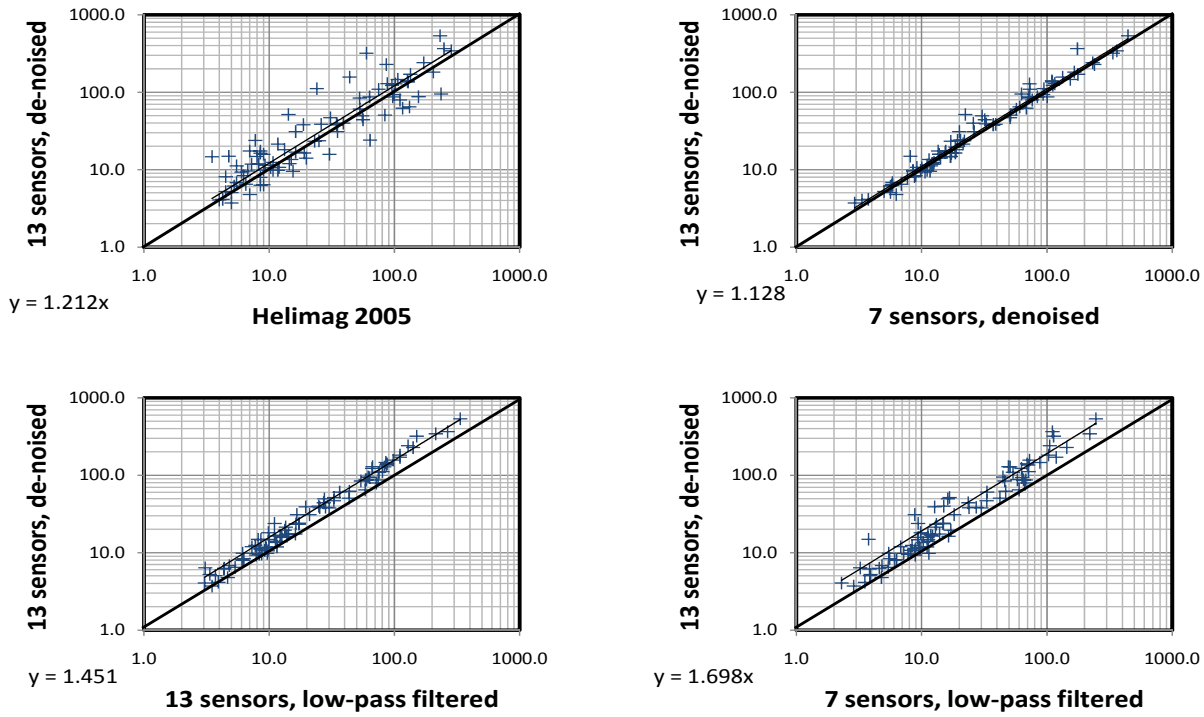

Figure 31. SNR analysis in Area 2A for various configuration/filter schemes. The HeliMag data collected in 2009 were reprocessed using only 7 sensors and with a low-pass filter (together and separately) to determine the effect of each of these modifications under identical survey altitude conditions. The 7 sensor, low-pass filtered data mimic the AMTADS system precisely.

5.7 ACCURACY OF CALCULATED VERTICAL GRADIENTS

The accuracy of the calculated vertical gradient relative to the measured gradient was established during the test-flights at FLBGR (e.g. Figure 6, Figure 7). We verified the accuracy using the last validation flight on day 78 (Figure 32). No high-pass filtering (to suppress geology) was applied to either the calculated or measured gradients, but a DC correction was applied to the measured gradient so that it best matched the calculated gradient. The measured and calculated gradients agree quite closely, with a correlation coefficient of 0.997. There are some minor differences in gradient measurements around some of the larger anomalies.

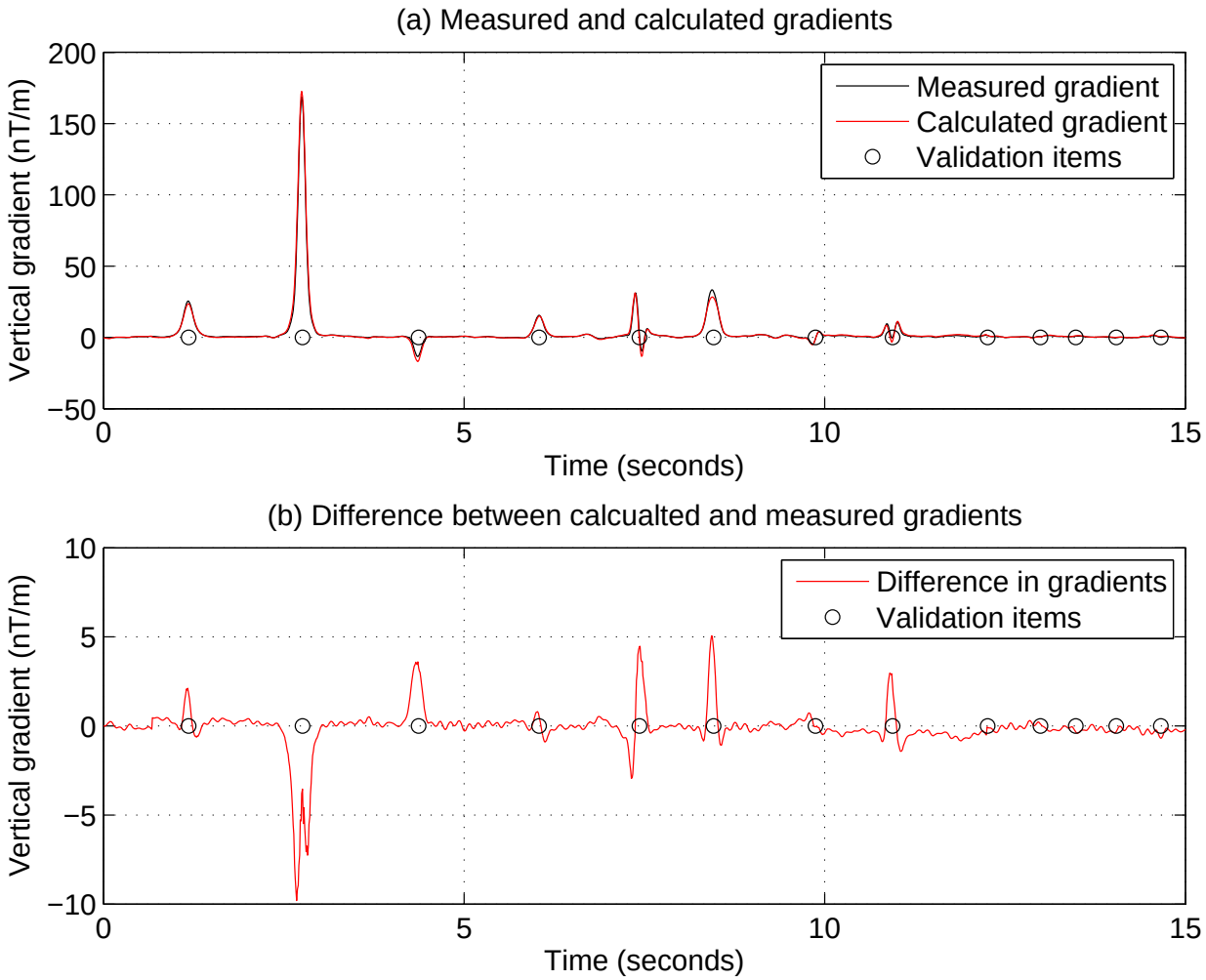

Figure 32. Comparison between measured and calculated gradients over the validation line flown on the last flight of day 78.

5.8 ACCURACY OF EQUIVALENT LAYER

A preliminary code for computing an equivalent layer was tested by Colorado School of Mines on a small portion of the data collected over the central SEED area (Figure 33 and Figure 34). The equivalent layer provided a good fit to the data with residuals generally less than 2 nT over the 30 m by 30 m section of data studied (Figure 33). When computed at a fixed sensor elevation, the equivalent layer is able to remove the obvious sensor elevation artifacts that are present in the usual 2-D minimum curvature image (Figure 34). No metrics were calculated for the equivalent layer as we don't believe we tested the algorithm on enough data. The initial results look promising and further results will be presented in SERDP reports contributed by Dr Yaoguo Li.

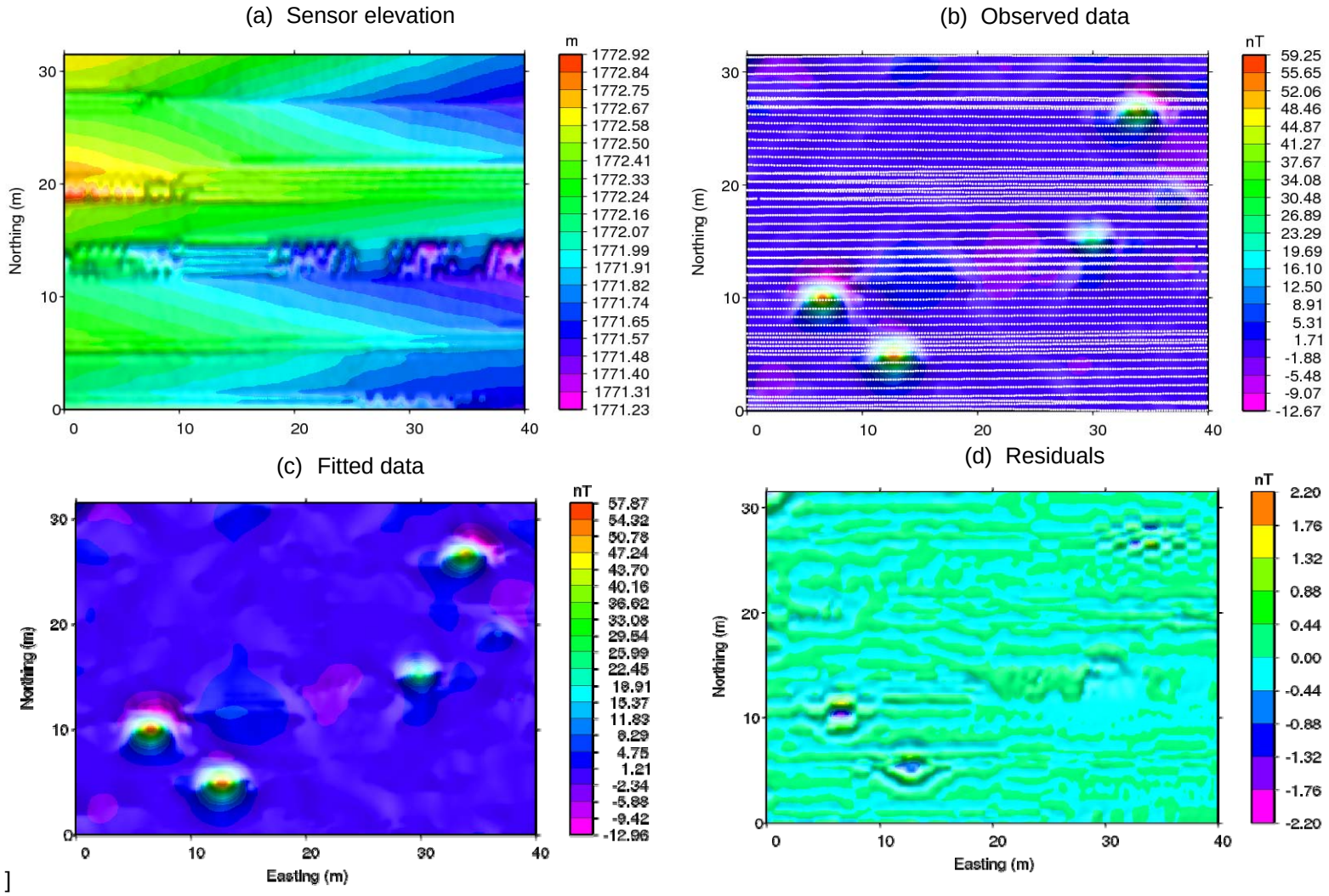

]

Figure 33. Equivalent layer fit over a small section of the Central Seed area.

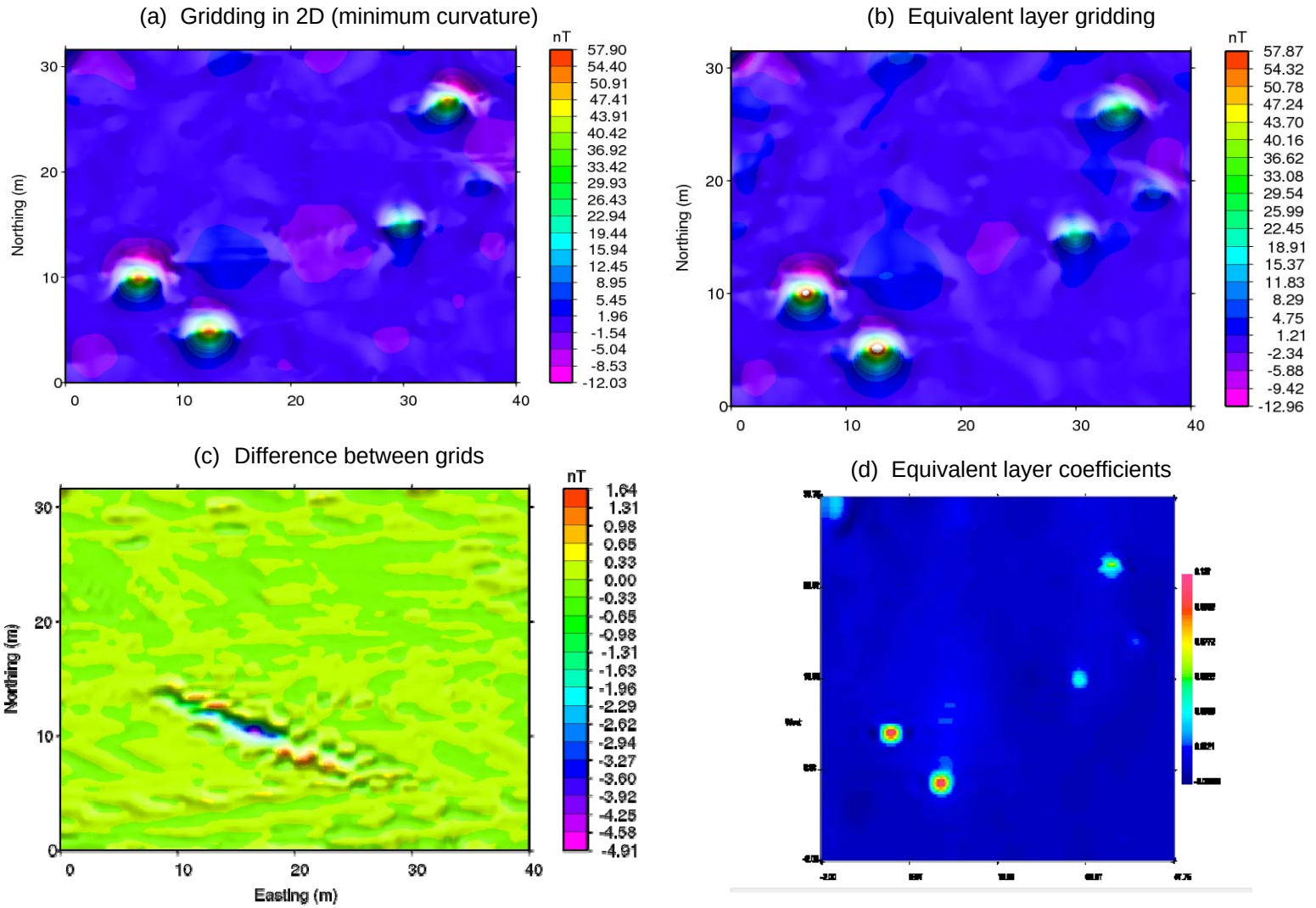

Figure 34. Equivalent layer gridded to a constant sensor elevation compared to minimum curvature.

5.9 UXO PARAMETER ESTIMATE REPEATIBILITY

Plots of the dipole parameters from the validation lane are shown in Figure 35 with the standard deviations provided in Table 13. The estimated dipole depth was obtained by comparing the elevation predicted by the dipole model with a Light Detection and Ranging (LiDAR). There is significant correlated variation day-to-day indicating that there were systematic biases in the GPS elevations.

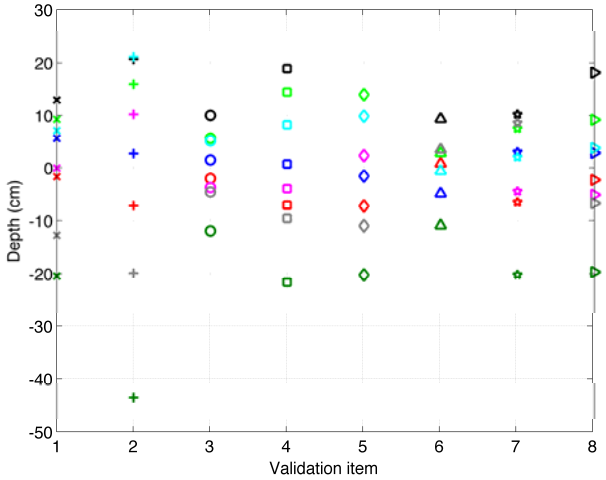

(a) Estimated depth

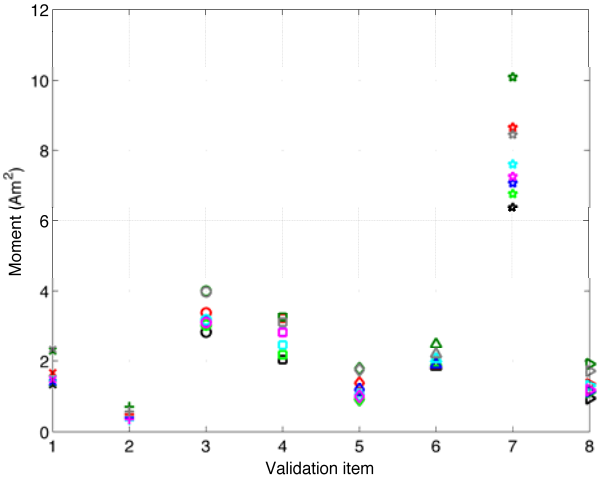

(b) Estimated dipole moment

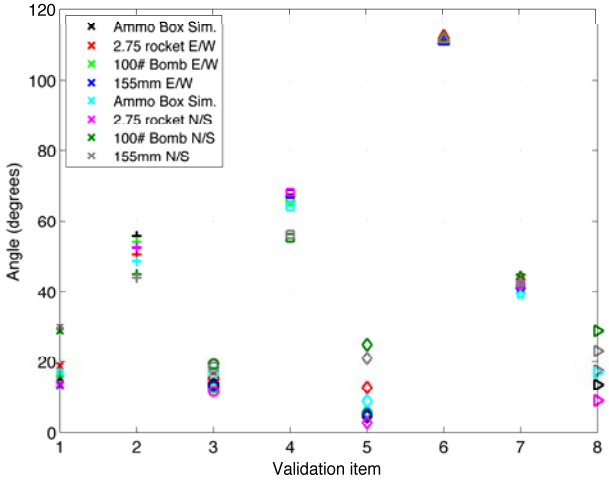

(c) Estimated angle relative to Earth's field

Figure 35. Dipole parameters estimated from the validation lane data.

Table 13: Standard deviations of dipole fit parameters on the validation lane data

	Easting (cm)	Northing (cm)	Elevation (cm)	Moment (Am^2)	Moment (% of mean)	Angle (degrees)
Ammo Box Sim.	2.1	7.6	11.5	0.41	24.5	6.5
2.75 rocket E/W	6.1	1.3	22.6	0.13	29.6	4.2
100# Bomb E/W	2.2	5.4	7.0	0.43	13.0	2.9
155mm E/W	6.9	2.4	13.4	0.47	17.1	5.3
Ammo Box Sim.	1.7	11.0	12.4	0.35	28.4	8.2
2.75 rocket N/S	2.9	0.9	6.5	0.23	11.1	0.5
100# Bomb N/S	3.1	3.1	10.1	1.22	15.7	1.6
155mm N/S	4.2	7.7	11.3	0.33	24.5	6.7

5.10 OPERATING PARAMETERS

The operating parameters include survey speed, survey altitude, and daily production rates. The daily production rate objective was 300 acres/day. Discounting reflies, down time for weather and equipment adjustments, the production rate was approximately 290 acres/day (586 acres in 2 survey days). The assessment of the survey altitude and speed was performed by extracting statistics for these parameters from the survey databases. A summary of the survey speed and altitude for each of the sites is shown in Table 14.

Aircraft speed affects the along line sample density, as well as the survey production rate. The average aircraft speed ranged from 15.8 m/s to 24.6 m/s.

Table 14. Survey altitude and speed for each area.

Area	Speed (m/s)		Altitude (m agl)	
	Mean	Standard Deviation	Mean	Standard Deviation
Central North	21.1	2.9	1.66	0.38
Seed West	18.4	4.0	1.64	0.46
West	24.6	2.4	1.90	0.42
Central South	24.4	4.0	2.15	0.35
Northeast 1	22.3	5.8	2.00	0.42
Northeast 2	15.8	2.6	2.18	0.38

Survey altitude is the parameter that has the greatest effect on the efficacy of the system for detection of discrete UXO-like ferrous objects. The lowest safe survey altitude achievable at any given time depends upon the local site conditions (vegetation, topography, and weather) as well as the skill and comfort level of the pilot. During the demonstration, the pilot was having trouble trying to keep the sensors below 2.0 m agl. Prior experience at this site indicated that it was possible to keep the sensor altitude at an average altitude of 1.5 m agl. After adjustments were

made to the boom mount, the survey altitude was reduced to between 1.6 and 1.7 m agl. Unlike the Bell 206L, the MD 530F skid gear is flexible and splays out and up when the aircraft is on the ground. Once weight is removed from the skids, they spring back in and down. Thus, when the aircraft is airborne, the skid gear hangs down about 0.2m – forcing the pilot to fly higher by this same distance. The previous survey, flown in 2005 with the Bell206L, collected data at 1.5m agl with very little emphasis placed upon flying as low as possible. On some tests the survey altitude achieved with the Bell206L was as low as 1.0m.

5.11 ROTOR NOISE SUPPRESSION ALGORITHM

In Figure 36 and Figure 37 we show data from the central sensor that were collected at high-speed over the validation line on day 078. The figures compare raw, low-pass filtered and rotor-suppressed versions of the data. The 6 Hz low-pass and rotor-suppressed data are similar at positions away from the validation lane anomalies with the 6Hz low-pass data exhibiting significant distortion over the validation lane anomalies. The helicopter is traveling fast and low to the ground which causes the signal from near-surface anomalies to overlap with that of the rotor-noise. The low-pass filter removes both the rotor-noise and some of the frequency content from the signals of interest (see Figure 37c & d in particular). In contrast, signal integrity is maintained and rotor-noise is eliminated when the rotor-noise suppression algorithm is applied to the data.

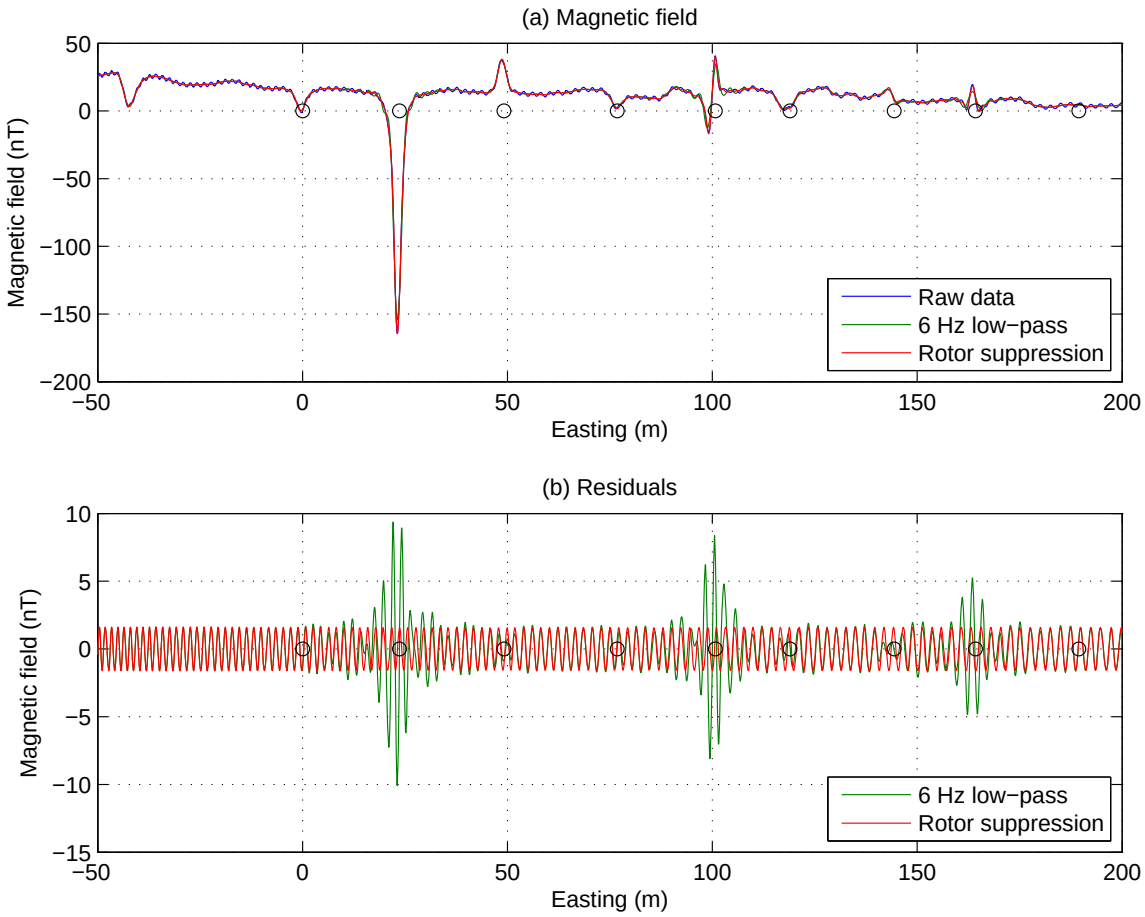

Figure 36. Data from the middle sensor (sensor 7) collected at high-speed over the validation line on day 078. (a) Compares the raw data with 6 Hz low-pass filtered and rotor suppressed versions of the data; and (b) Shows the difference between raw and low-pass filtered data, and between raw and rotor-suppressed data.

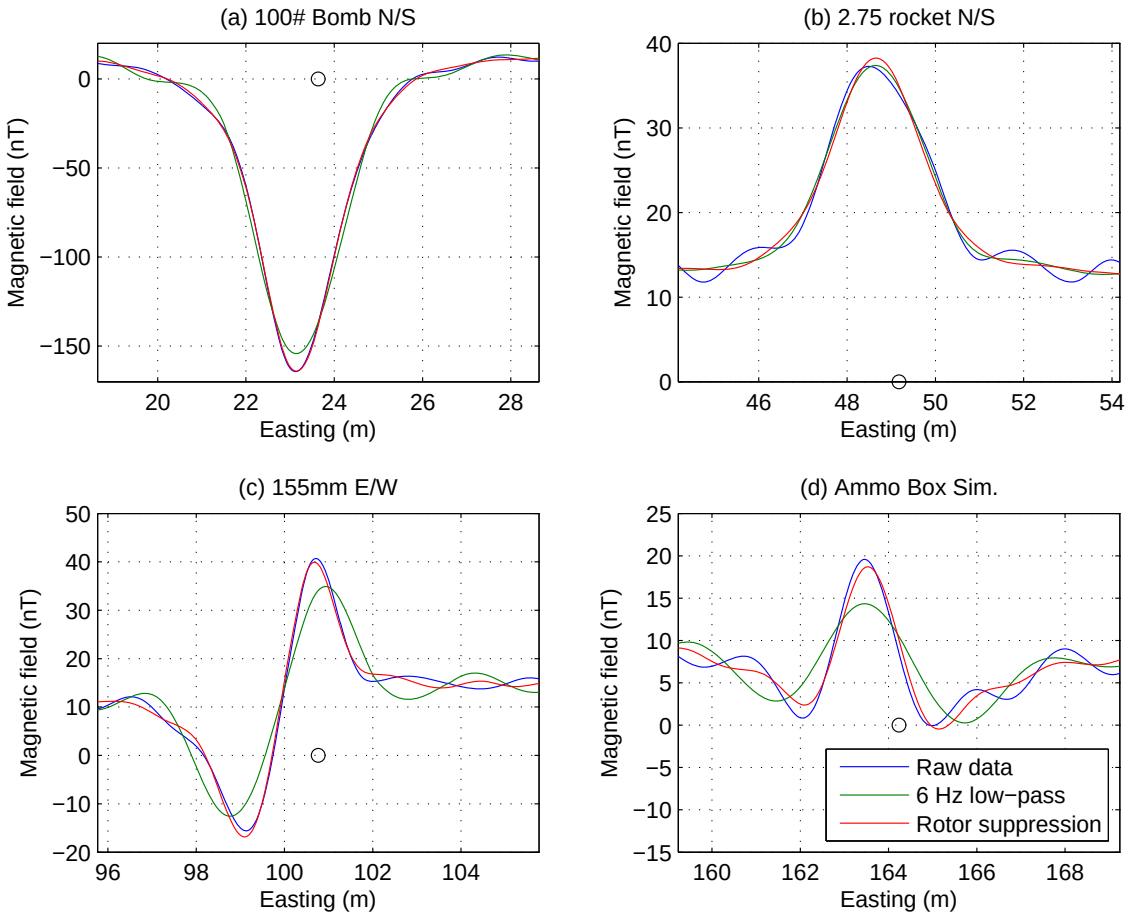

Figure 37. Close-up of validation lane anomalies from Figure 36, showing the difference between the raw data, a 6 Hz low-pass filtered version of the data and the rotor-noise corrected data.

In previous work (Foley and Wright, 2007) we have shown that the rotor-noise in a Bell 206 helicopter occurs at a lower frequency (~ 6.5 Hz) than that in the MD530F (~ 8 Hz). Without application of an intelligent noise-suppression algorithm, this places additional operational constraints on the helicopter speed versus height envelop. In Figure 38 and Figure 39 we show data from the central sensor that were collected over a validation line at Vernon, BC by the Bell 206 helicopter. We couldn't use the same rotor-noise suppression algorithm with these data because no compensation flight was flown for this survey. Instead, we used the original adaptive rotor-noise suppression algorithm described in section 2.2.1.3. The 4Hz low-pass filtered data and rotor-suppressed data are similar away from the validation lane anomalies. The low-pass filtered data are distorted around the validation lane anomalies, whereas the rotor-noise suppressed data show no such distortion. Thus, it appears that the rotor-noise suppression algorithm could be effectively applied to data from the Bell 206.

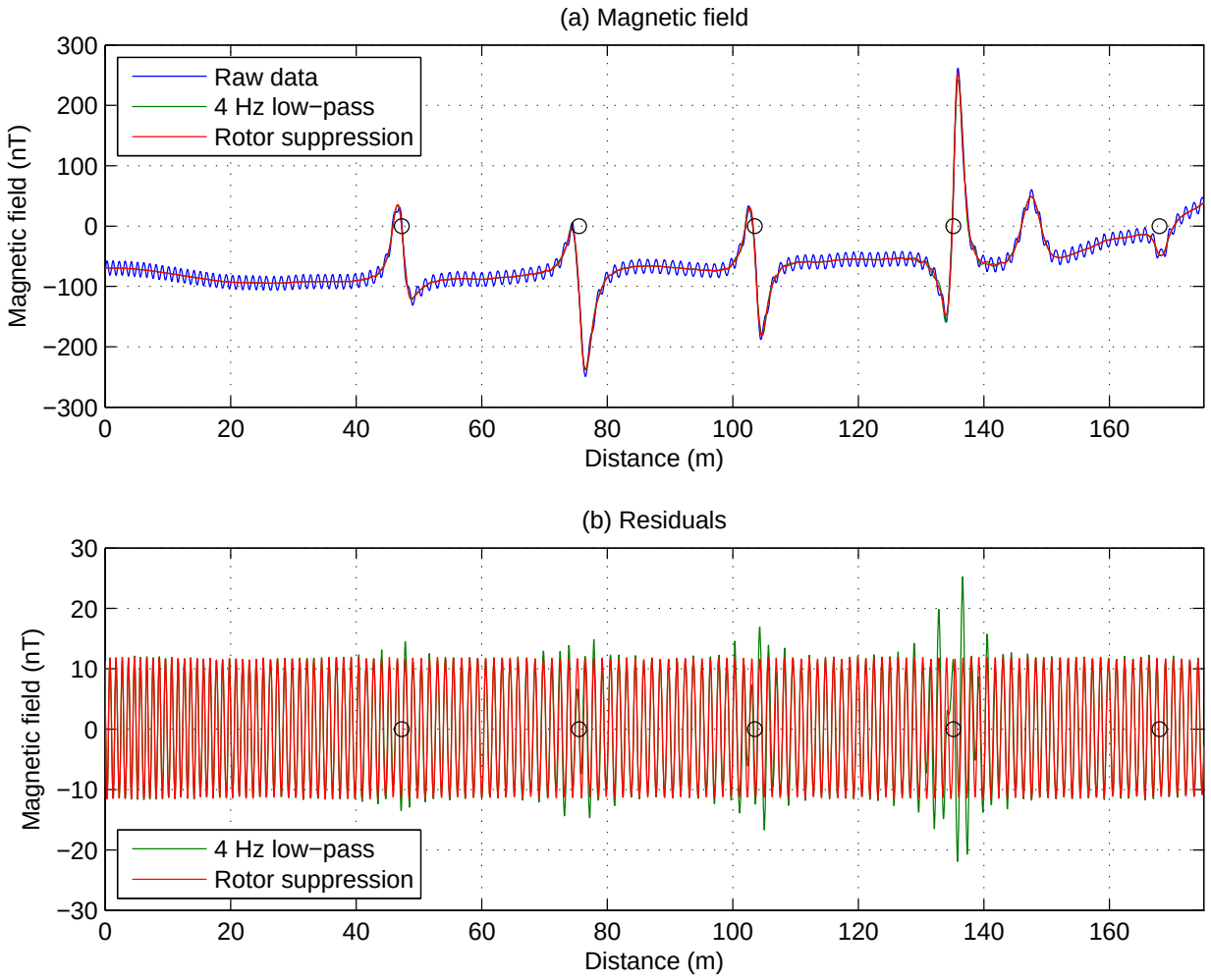

Figure 38. Validation line data collected by the Bell 206 helicopter during a survey at Vernon, BC: (a) Compares the raw data with 4 Hz low-pass filtered and rotor suppressed versions of the data; and (b) Shows the difference between raw and low-pass filtered data, and between raw and rotor-suppressed data.

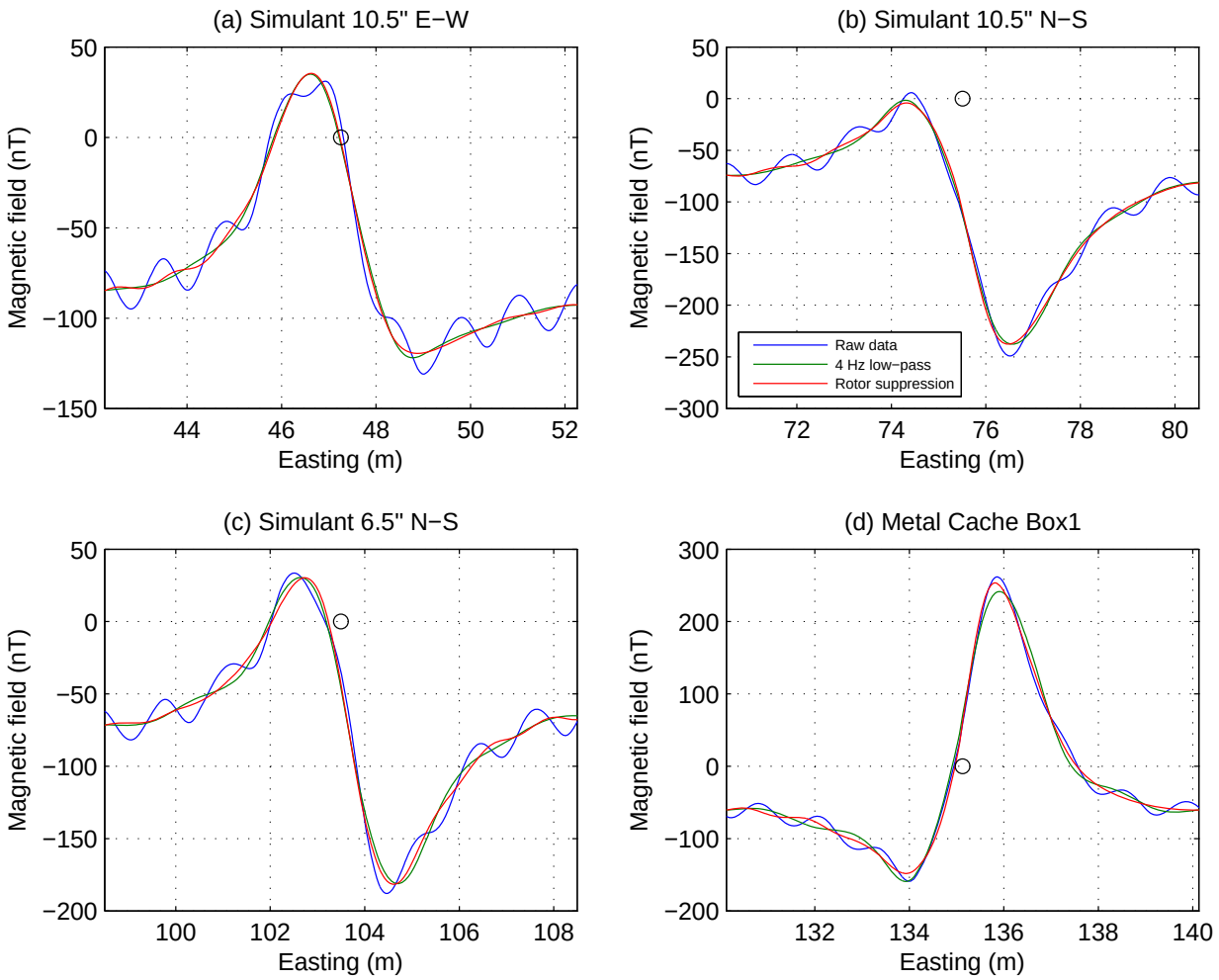

Figure 39. Close-up of validation lane anomalies from Figure 38, showing the difference between the raw data, a 4 Hz low-pass filtered version of the data and the rotor-noise corrected data.

5.12 DATA DENSITY/POINT SPACING

The cross-track data density is essentially static and is a function of the system geometry. With the exception of isolated data gaps (addressed above) the 'worst case' spacing is our sensor spacing of 0.75 m. The effective density is much higher than this due to the significant overlap required to minimize data gaps due to the inevitable cross-track variation of the helicopter flight path. However, because the density is not uniform, we quote the 'worst case' as the data density achieved. Down-track data density is much higher than the cross-track density and is a function of survey speed. At our final sample rate of 100 Hz, the survey speeds of 15 – 25 m/s (20 – 50 kts) resulted in down-line data spacing of 0.15 - 0.25 m.

5.13 SURVEY COVERAGE

As a general practice, images representing the data from each day of survey flying are created to identify areas requiring fill-in flying to cover significant gaps in coverage. Invariably there will be a number of gaps in survey coverage that cannot be practically filled. To estimate the survey

coverage performance, at each grid node (5m intervals) we search through a 1 m radius for a valid data point. We divide the number of grid nodes where valid data are found by the total number of grid nodes to derive the percentage of survey coverage. Based upon these factors and acreages, the final coverage was determined to be 99.2%.

6 COST ASSESSMENT

6.1 COST MODEL

Cost information associated with the demonstration of all airborne technology, as well as associated activities, was tracked and documented before, during, and after the demonstration to provide a basis for determination of the operational costs associated with this technology (Table 15). These costs include both operational and capital costs associated with system design and construction; salary and travel costs for support staff; subcontract costs associated with airborne services, support personnel, and any leased or rented equipment; costs associated with the processing, analysis, comparison, and interpretation of airborne results generated by this demonstration.

Table 15. Cost Tracking

Cost Category	Sub Category	Details	Costs ($)
System Modeling and Integration	Sensor configuration optimization modeling	Modeling, engineering, testing, and preparation of white papers detailing the results for sensor configuration and telemetry system. Installation and initial test flights prior to verify the entire system was operating as designed	$139,150
	Telemetry system design and testing		
	Helicopter noise measurements		
	Boom configuration development and engineering		
Start-Up Costs	Shakedown test	Includes mobilization to Denver test site, data collection, and analysis of system performance	$228,267
	Demonstration planning	Coordination w/Program Office and KPBR site, preparation of Demonstration Plan.	$24,344
Operating Costs	Demonstration at KPBR	Data acquisition and associated tasks, including helicopter operation time, mobilization and demobilization from Denver to Albuquerque	$135,532
Data Processing and Analysis	Data Processing, analysis, and reporting	Initial and secondary processing of data, analysis of airborne magnetometry datasets	$37,744

Cost Category	Sub Category	Details	Costs ($)
Management	Management and meetings	Project related management, reporting and contracting, IPRs, presentations, STC evaluation	$99,440
		Total Costs	$664,477
Total Technology Cost (demonstration preparation, operations, reporting – grey highlighted costs)			$197,620
		Acres Surveyed	586
		Unit Cost	$337

6.1.1 System Integration

System integration activities comprised several distinct areas, including:

- Modeling using existing data to identify the optimal sensor configuration. The modeling approach was more cost effective than fabricating various boom modifications and then testing different sensor configurations. Ground-based measurements were taken to characterized the helicopter noise sources to support the modeling. The results were reported in the white paper (Billings and Wright, 2007). Upon acceptance of the recommended configuration, the engineering required to accommodate the boom modifications was performed and the modified sections were fabricated. As previously arranged, SKY funded the fabrication, while the engineering costs were borne by the project.
- The telemetry system design was developed and the recommended components were purchased by SKY. Ground testing to define the equipment operational ranges was performed, and upon completion a second white paper was prepared and submitted (O'Connor and Wright, 2008).
- DAS modifications were made to accommodate the additional magnetometers and integrate the telemetry components as needed to allow the SO to monitor the operational status of the system from the ground during data collection.
- The entire system was installed on the helicopter and flight testing was conducted at the SKY facility in Ashland, OR to verify that all system components were operating as designed.

6.1.2 Start-Up Costs

Startup costs included a shakedown test that was conducted at the FLBGR site (described previously in this report and in Billings and Wright, 2008). The shakedown test included mobilization of the helicopter from Ashland, OR to Denver, CO (costs shared with other SKY projects).

The Demonstration Plan was prepared and submitted for Program Office review, and coordination with site managers for access to the KPBR survey areas was performed.

6.1.3 Operating Costs

The demonstration survey was conducted over 5 days in March, 2009. The effort included mobilization and demobilization of the helicopter and project team from Denver to Albuquerque, setup of the validation lane, compensation flights, and data collection over the selected acreage. A total of 586 acres was surveyed. The data collection was effectively completed in two days of operation. The remainder of the field effort involved some in-field modifications and adjustments (previously described), installation and removal of the boom and electronics components from the helicopter. The relatively short distance required to mobilize the helicopter and equipment for this demonstration helped kept the demonstration costs relatively low. The data collection costs on a per acre basis are similar to those for previous demonstrations of this technology.

The per acre cost to perform the demonstration is inflated relative to expected operational costs for a production survey. The actual data collection was performed over 2 days, while the total duration of the effort was 5 days. The in-field modifications and other test activities took up the remainder of the time in the field. Table 16 presents the projected operational costs for a similar production survey. The per acre cost of $193/acre is consistent with the projected costs for the existing HeliMag technology. Table 17 is taken from the WAA HeliMag Cost and Performance report (Foley and Wright, 2008d), with the estimated cost for a 1000 acre survey at $178/acre. The increased costs for the next generation system reflect the increased number of magnetometers (14 vs. 7), costs for the telemetry equipment, and a second DAS (each DAS can accommodate data for 7 magnetometers). Costs to deploy the next generation system would decrease with the size and duration of a production survey, similar to the decreasing per acre costs shown in Table 17.

Table 16. Projected Costs for 2-Day Survey Using the Next Generation HeliMag System

Cost Category	Sub Category	Details	Costs ($)
Start-up Costs	Demonstration planning	Coordination w/Program Office and KPBR site, preparation of Demonstration Plan.	$24,344
Operating Costs	Demonstration at KPBR	Data acquisition and associated tasks, including helicopter operation time, mobilization and demobilization from Denver to Albuquerque	$74,675
Data Processing and Analysis	Data Processing, analysis, and reporting	Initial and secondary processing of data, analysis of airborne magnetometry datasets	$14,348
Total Technology Cost (demonstration preparation, operations, reporting – grey highlighted costs)			$113,367
		Acres Surveyed	586
		Unit Cost	$193

Table 17. Estimated Costs Scenarios for Helicopter Magnetometry (taken from Foley and Wright, 2008d)

Cost Category	1,000 Acre Site	5,000 Acre Site	7,500 Acre Site	10,000 Acre Site
Planning, Preparation and Management	$32,000	$47,000	$55,000	$62,000
Mobilization/Demobilization	$40,000	$40,000	$40,000	$40,000
Data Acquisition Surveys	$82,000	$410,000	$612,000	$817,000
Data Processing, Analysis and GIS Products	$12,000	$40,000	$54,000	$67,000
Reporting and Documentation	$12,000	$15,000	$20,000	$30,000
Total Costs	**$178,000**	**$552,000**	**$781,000**	**$1,016,000**
Costs per Acre	**$178**	**$110**	**$104**	**$102**

6.1.4 Data Processing and Analysis, Reporting

Data processing and analysis were conducted between March and July 2009, followed by report preparation. The detailed analyses are described in Sections 4 and 5.

6.1.5 Management

Management activities have included evaluation of the requirements for obtaining a Supplemental Type Certification (STC) for the modified system on the MD530F helicopter. It was determined, in conjunction with the Program Office, that an STC for this system will be pursued in the future when the system is to be deployed for production surveys. Other management costs included presentations for Interim Progress Reviews and the SERDP/ESTCP symposia, in addition to general project management activities.

6.2 COST DRIVERS

The major cost driver for an airborne survey system is the cost of aircraft airtime. In terms of tasks, this constitutes a major percentage of the data acquisition costs–the single largest cost item. The cost analysis will be completed for the Cost and Performance Report submitted at the end of this demonstration.

6.3 COST BENEFIT

A number of factors should be considered for DoD-wide application of WAA, including data acquisition, when evaluating the appropriateness of helicopter technology and potential for cost savings. Sites must be large enough to justify the deployment of aircraft and equipment to conduct a survey. Climatic conditions and terrain can limit the results of surveys. In amenable sites, the use of helicopter magnetometry can focus the use of ground survey technology and can provide substantial cost savings through footprint reduction.

7 IMPLEMENTATION ISSUES

As a WAA technology, the Next Generation HeliMag system is subject to the same issues of regulatory acceptance of the methodology as investigated in the WAA Pilot Program. The ESTCP Program Office established a Wide Area Assessment Pilot Program Advisory Group to facilitate interactions with the regulatory community and potential end-users of this technology. Members of the Advisory Group include representatives of the USEPA, State regulators, USACE officials, and representatives from the services. The Advisory Group provided valuable feedback on the WAA methodology that is expected to facilitate its acceptance into the wider community. However, there will be a number of issues to be overcome to allow implementation of WAA technologies beyond the pilot program, including decision-making regarding areas with no indication of munitions use.

A main challenge of the Pilot Program was to collect sufficient data and perform sufficient evaluation such that the applicability of these technologies to uncontaminated land and their limitations were well understood and documented. Similarly, demonstrating that WAA data can be used to provide information on target areas regarding boundaries, density and types of munitions to be used for prioritization, cost estimation and planning requires that the error and uncertainties in these parameters are well documented.

Therefore, a successful technology demonstration of the modified HeliMag technology will piggyback on the success of ESTCP WAA Pilot Program for regulatory acceptance of the overall WAA methodology. This technology will be one more tool in the WAA “toolbox” that provides flexibility for WAA technology selection that can reduce cost of characterization.

8 REFERENCES

Billings, S. D. and Wright, D. 2008. ESTCP MM-0741, Shakedown Test Results. Prepared for ESTCP Program Office.

Billings, S. D. and Wright D. 2007. ESTCP MM-0741, Design Study: Optimal Sensor Configuration for Helicopter Magnetometry. Prepared for ESTCP Program Office.

Blakely, R. J. 1995. Potential theory in gravity and magnetic applications. Cambridge University Press.

EOD Technology, Inc. (EODT), 2007. Engineering Evaluation and Cost Analysis (EE/CA) Report for the Former Kirtland Precision Bombing Ranges West Mesa Albuquerque, New Mexico, Contract: DACA87-00-D-0037, Task Order: 0017, Project Number: K06NM044501, Prepared for: U.S. Army Engineering & Support Center, Huntsville, Alabama, Geographical Corps District: U.S. Army Corps of Engineers, Albuquerque District.

Foley, J. and Wright, D. 2007. Draft Final Report,Demonstration of Airborne Wide Area Assessment Technologies at the Toussaint River, Ohio. MM-0535 Technical Report. April.

Foley, J. and Wright, D. 2008a. Demonstration of Helicopter Multi-sensor Towed Array Detection System (MTADS) Magnetometry at Former Camp Beale, California. ESTCP Final Report, Project MM0535. October.

Foley and Wright, D. 2008b. Demonstration of Airborne Wide Area Assessment Technologies at Kirtland Precision Bombing Range, New Mexico. Final Report. October.

Foley, J. and Wright D. 2008c. Demonstration of Helicopter Multi-Sensor Towed Array Detection System (MTADS) Magnetometry at Victorville Precision Bombing Range, California. ESTCP Project MM0535 Final Report. December.

Foley, J. and Wright. D. 2008d. Demonstration of Helicopter Multi-Towed Array Detection System (MTADS) Magnetometry Technology for the ESTCP Wide Area Assessment Pilot Program Cost and Performance Report. ESTCP Final Report. October.

Leliak, P., 1961. Identification and evaluation of magnetic field sources of magnetic airborne detector equipped aircraft. IRE Trans. Aerospace Nav. Electr., 8, 95-105.

Nelson, H.H., J.R. McDonald, D. Wright. 2005. Airborne UXO Surveys Using the MTADS. ESTCP Project 200031 Final Report.

Nelson, H.H, Kaye, K., Andrews, A. 2008. ESTCP Pilot Project Wide Area Assessment for Munitions Response, Final Report. Environmental Security Technology Certification Program Office (Dod) Final Report. July.

O'Connor, D. and Wright, D. 2008. ESTCP MM-0741, Design Study: Telemetry System for Helicopter Magnetometry. Prepared for ESTCP Program Office.

Siegel, R. M. 2008. Simultaneous Magnetometer and EM61 MK2 Vehicle-Towed Array for Wide Area Assessment: Final Report, ESTCP Program Office.

Tuley, M. and Dieguez, E. 2005. Analysis of Airborne Magnetometer Data from Tests at Isleta Pueblo, New Mexico, February 2003. Technical Report, MM-0037. May.

USACE, Rock Island District and US Army Defense Ammunition Center and School. 1994. Ordnance and Explosive Waste Archives Search Report Findings for the Former Kirtland Air

Force Base Precision Bombing Ranges N-1, N-3, N-4 & "New" Demolitions (K06NM044501).

Versar. 2005. Former Kirtland Precision Bombing Range, Conceptual Site Model, V3. Prepared for ESTCP Program Office.

Wright, D.J., McDonald, J.R., Khadr, N. and Nelson, H.H. 2002. Dynamic sensor positioning in three dimensions on an airborne platform. Published in Proceedings UXO/Countermine Forum.

9 POINTS OF CONTACT

Table 18. Points of Contact

POINT OF CONTACT Name	ORGANIZATION Name Address	Phone Fax E-mail	Role in Project
Dr. Stephen Billings	Sky Research, Inc. Suite 112A 2386 East Mall Vancouver, BC, V6T 1Z3 Canada	(Tel) 541.552.5185 (Cell) 604.506.9206 Stephen.Billings@skyresearch.com	Co-Principal Investigator
David Wright	Wright Research and Design 9500 Kingsford Drive Cary, NC 27511	(Tel) 919.520.8673 david.wright@wrandd.com	Co-Principal Investigator
Ms. Joy Rogalla	Sky Research, Inc. 445 Dead Indian Road Ashland, OR 97520	(Tel) 541.552.5104 (Fax) 541.488.4606 Joy.Rogalla@skyresearch.com	Project Manager
Dr. Herbert Nelson	ESTCP Program Office 901 North Stuart St., Suite 303 Arlington, VA 32203	(Tel) 703.696.8726 (Fax) 703.696.2114 Herbert.Nelson@osd.mil	Contracting Officer's Technical Representative

APPENDIX A: FIELD NOTES

March 16 2009

Assembled the boom, testing system on ground.

Gained access to the survey area.

Established location for the Validation Lane

Seeded Validation Lane.

Set up Telemetry Command Center in HeliMag Trailer – Pictures Attached.

Conducted Test flight for compensation, seeded/unseeded Validation Lane, and collected 12 lines in NE Area 2.

Received hot refueling operation at our hangar location.

March 17 2009

Left Hotel 0620

At hangar at 0640

- Update Fluxgate HZ rate in GDCLUTS
- Remove Silicone from Pilot Nav Helmet
- Move USB multiport to provide Bob additional reach for pilot navigation helmet
- Checked Mag 4 sensor, preamp, and coax cables, changed coax T

Lift 0810

- Collect 2 Compensation flights
- Collect Validation Survey
- Recollect 6 lines in NE Area 2 that were missing fluxgate data
- HDAS crash due to flight line load, and line numbers out of sync between front ends

0930 Hot refuel Continue in NE Area 2

- Complete lines 38-50
- Land at Hangar and move sensor boom 1m fwd, add 150# ballast.

Lift again at 1210 start in NE Area 1 Lines 1001-1016

- Recollected High Altitude Compensation test with new boom Configuration.
- Conduct strobes on and off test to chase down noise
- Collected GPS location data for Validation Items.

Land 1330 for fuel and lunch

Lift 1430

- Collect lines 1017-1050

Fighting GPS RTK lock all afternoon

Land for Fuel at 1550

Collect remaining lines in NE Area 1 2001-2018

Collect Validation Survey and pitch roll yaw test

End of day tasks

Moved pilot keypad off of seat and onto RAM mount on instrument panel.

Offsite at 1745

March 18 2009

Left Hotel 0610

Arrived at Hangar 0630

Push Helicopter

Lars sets up GPS base and repeater, for coverage of Central North and Central South

Raul and Kevin setup Telemetry trailer

Bob conducts Preflight

Lift 0810

Collect Validation Lane

Problem with MS750 GPS – PDOP DIFF Error, reset GPS

Try 2 other MS750 receivers, reloaded cfg files

Retried original MS750 worked fine

Lift again 1015

Collect reflights in NE Area 1 and NE Area 2

Start Center North Area

Lunch 1200-1300

Lift 1315 continue in Center North and Begin Center South

Fuel 1500

Problem with MS750 Receiver, rest at Hangar and worked fine

Finish Central South and reflights in Central North.

Fuel 1645

Collect additional reflights in NE Area 1 and NE Area 2.

March 19 2009

0630 left hotel

0650 at Hangar

Lars left to set up GPS Base

Kevin Raul and Bob lower fwd sensor boom as much as possible

0730 Raul and Lars locate Telemetry Trailer to new location on West side North of Soil facility.

0830 Lift

Collect Compensation and Validation Test

Start West seed Area – due to wind and terrain line flown in West Direction

1000 fuel

1025 lift continue surveying West Seed Area

1320 completed West Seed Area

Lunch

1420 Begin resurvey of Central North

1600 Complete resurvey of Central North

Collect reflies in Central South

1620 fuel

Begin survey in West

1700 Complete West Survey,

Collect Validation Lane

1800 off site.

March 20 2009

0630 left hotel

0650 arrive at hangar

Lars setup GPS Base

Kevin and Raul Push Helicopter

Bob Preflights Helicopter

0720 Raul and Lars setup Telemetry station on west side of site

0750 Lift immediate problem with RTK GPS – DIFF PDOP

Bob lands at telemetry station reset GPS receivers

0810 Start Validation

Survey West Reflies

Seed Reflies

West Tie Lines

Seed Tie Lines

Central North Tie Lines

Central South Tie Lines

NE Area 1 Reflies

NE Area 1 Tie Lines

NE Area 2 Reflies

NE Area 2 Tie Lines

End Validation

1000 Land Hangar

Tear down Telemetry Station

1030 Push Data to FTP

1100 Start Demob

1245 Helicopter left Double Eagle II

1330 Truck and trailer leave Double Eagle II

2030 Truck and Trailer Arrive Centennial

Table 19: File-tracking table showing the percentage of time that the telemetry link was maintained.

Day	Survey event	Type	Lines	Telemetry Coverage
D09075	AA	Test		
	AB	Test		
	AC	Compensation	1	100%
	AD	Validation	1-2	100%
	AE	NE Area 2	1-12	90%
	AF	Validation	1-2	100%
D09076	AA	test		
	AB	Compensation	1	100%
	AC	Compensation	1	100%
	AD	Validation	1-2	100%
	AE	Test		
	AF	NE Area 2	6-24	100%
	AG	NE Area 2	25-37	100%
	AH	Compensation	1	100%
	AI	NE Area 2	38-50	100%
	AJ	NE Area 1	1	100%
	AK	NE Area 1	1001-1016	100%
	AL	NE Area 1	1017-1018	100%
	AM	Compensation	1	100%
	AN	NE Area 1	1017-1029	100%
	AO	NE Area 1	1030-1050	100%
	AP	NE Area 1	2001-2018	100%
	AQ	Validation	1-3	100%
D09077	AA	Test		

Day	Survey event	Type	Lines	Telemetry Coverage
	AB	Validation	1-3	100%
	AC	NE Area 2	1,4,5,32,38,39	100%
	AD	NE Area 2	1,4,5,32,38,39	100%
	AE	NE Area 1	1016-1049	100%
	AF	NE Area 1	2006-2016	100%
	AG	Central North	1-18	100%
	AH	Central North	19-40	100%
	AI	Central South	1001-1029	100%
	AJ	Central South	1030-1046	100%
	AK	Central South	1047	100%
	AL	Central South	1048-1050	100%
	AM	Central South	2001-2003	100%
	AN	Central South	2004-2029	100%
	AO	Central North	3	100%
	AP	Validation		100%
	AQ	NE Area 1	1045,47,49,35,37	100%
	AR	NE Area 1	2006, 11, 12,	100%
	AS	NE Area 1	2014	100%
	AT	NE Area 2	25,27,29	100%
D09078	AA	Validation	3	70%
	AB	Seed West	1001-1035	90%
	AC	Compensation	1	100%
	AD	Seed West	1036	90%
	AE	Seed West	1036-1050	90%
	AF	Seed West	2001-2006	90%
	AG	Seed West	2007-2022	90%
	AH	Seed West	2023-2034	90%
	AI	Central North	1-20	100%
	AJ	Central North	21-28	100%
	AK	Central North	27	100%
	AL	Central South	2003,2005	100%
	AM	West	1-14	80%
	AN	West	15-33	80%
	AO	Validation	3	70%

Day	Survey event	Type	Lines	Telemetry Coverage
D09079	AA	Validation	3	70%
	AB	Seed West	1013, 1024, 1034, 1044	100%
	AC	West	5, 15, 21	70%
	AD	West Tie	2	70%
	AE	Seed West Tie	2	100%
	AF	Central North Tie	2	100%
	AG	Central South Tie	2	100%
	AH	NE Area 1	1004, 1008	100%
	AI	NE Area 1	2008, 2009	100%
	AJ	NE Area 1 Tie	2	100%
	AK	NE Area 2 Tie	2	80%
	AL	Validation	3	70%